

TWO PHOTON DECAY WIDTHS OF NON-STANDARD HIGGS BOSONS

by

ROSS TAYLOR BATES

M.Sc., The University of British Columbia, 1982

B.Sc., The University of Western Ontario, 1980

A THESIS SUBMITTED IN PARTIAL FULFILLMENT OF
THE REQUIREMENTS FOR THE DEGREE OF
DOCTOR OF PHILOSOPHY

in

THE FACULTY OF GRADUATE STUDIES

Department of Physics

We accept this thesis as conforming
to the required standard

THE UNIVERSITY OF BRITISH COLUMBIA

June 1986

© Ross Taylor Bates, 1986

Abstract

This thesis examines the two photon decay widths of non-standard Higgs bosons. These widths are calculated for Two-Higgs-Doublet models in general, and for the minimal broken supersymmetry model in particular. For Two-Higgs-Doublet models a large enhancement of these widths relative to the standard model is possible. This in turn leads to larger production rates for the spin-0 bosons in ep and e^+e^- colliders. However, we find that for the minimal broken supersymmetry case, a severe upper bound on this possible enhancement is imposed by the supersymmetry features. We find that while the Higgs bosons of the Two-Higgs-Doublet model could possibly be produced at readily observable rates with the HERA collider, this will not be the case in the minimal supersymmetry model. Hence detection of these Higgs bosons could provide an experimental test of supersymmetry, which would rule out the minimal model.

Table of Contents

Abstract	ii
List of Tables	iv
List of Figures	v
Acknowledgement	vi
CHAPTER I - INTRODUCTION	1
1.1 The Standard Model	4
1.2 Why Alternative Models?	6
1.3 Fundamental Scalars	9
1.4 Supersymmetry	11
1.5 Thesis Overview	13
CHAPTER II - TWO-HIGGS-DOUBLET MODEL	18
2.1 The Model	19
2.2 Standard Model 2γ -Decay Width	28
2.3 Two-Higgs-Doublet Model 2γ -Decay Widths	29
CHAPTER III - MINIMAL BROKEN SUPERSYMMETRY MODEL	33
3.1 The Model	34
3.2 One Loop Calculation of $X^0 \rightarrow \gamma\gamma$	53
3.3 Pseudoscalar Widths of $X^0 \rightarrow \gamma\gamma$	57
3.4 Scalar Widths of $X^0 \rightarrow \gamma\gamma$	62
CHAPTER IV - NON-STANDARD SPIN-0 BOSON PRODUCTION	70
4.1 The Calculation	71
4.2 Numerical Results and Discussion	77
CHAPTER V - SUMMARY AND CONCLUSIONS	87
Bibliography	92
APPENDIX A - SOME ACCELERATOR PROPERTIES	94
APPENDIX B - EVALUATION OF FEYNMAN DIAGRAMS	95
B.1 Scalar Higgs 2γ -Decay via Fermion Loops	95
B.2 Scalar Higgs 2γ -Decay via Scalar Loops	97
B.3 Scalar Higgs 2γ -Decay via Gauge Boson Loops	98
B.4 Pseudoscalar Higgs 2γ -Decay via Fermion Loops	101
APPENDIX C - EVALUATION OF LOOP INTEGRALS	103
APPENDIX D - PROPERTIES OF THE FUNCTION $I(\lambda)$	106
APPENDIX E - FEYNMAN RULES FOR MINIMAL BROKEN SUPERSYMMETRY	108
APPENDIX F - EQUIVALENT PHOTON APPROXIMATION	113
APPENDIX G - MONTE CARLO INTEGRATION ROUTINE	116
APPENDIX H - GLOSSARY	123

List of Tables

I	Two-Higgs-Doublet Model Vertices	27
II	Supersymmetric Field Content	35
III	Accelerator Properties	94

List of Figures

1	One Loop Contributions to the 2γ -Decay of the Scalar H_j^0	52
2	One Loop Contributions to the 2γ -Decay of the Pseudoscalar H_k^0	56
3	Pseudoscalar 2γ -Decay Width for Case A	60
4	Pseudoscalar 2γ -Decay Width for Case B	61
5	Scalar 2γ -Decay Width for Case A	65
6	Scalar 2γ -Decay Width for Case B	66
7	Scalar 2γ -Decay Width for Best Case A	68
8	Feynman Diagrams for the Reaction $eq \rightarrow eqH^0$	72
9	Standard Model σ vs \sqrt{s} for $ep \rightarrow eH^0X$	78
10	Cross Sections σ vs M_H for $ep \rightarrow eH^0X$ for $\sqrt{s}=320$ GeV	79
11	Cross Sections σ vs M_H for $ep \rightarrow eH^0X$ for $\sqrt{s}=1$ TeV	80
12	Production Cross Sections for $e^+e^- \rightarrow e^+e^-H^0$	82
13	Rapidity Distributions	83
14	Fermion Loop Contribution to Scalar 2γ -Decay	96
15	Scalar Loop Contribution to Scalar 2γ -Decay	97
16	Gauge Boson Loop Contribution to Scalar 2γ -Decay	99
17	Fermion Loop Contribution to Pseudoscalar 2γ -Decay	101
18	Plot of the Function $\lambda I(\lambda)$ vs λ	107
19	Feynman Rules for Scalar H_j^0 Couplings	109
20	Feynman Rules for Photon Couplings	110
21	Feynman Rules for Chargino-Scalar H_j^0 Couplings	111
22	Feynman Rules for Chargino-Pseudoscalar H_k^0 Couplings	112
23	Photon Quark Subprocess	114

Acknowledgement

I wish to thank my research supervisor, Dr. John Ng, whose guidance made this work possible. I would also like to thank Dr. Pat Kalyniak, who collaborated with us on the supersymmetry calculations, for her contribution. Finally I would like to thank my departmental supervisor, Dr. Nathan Weiss.

Financial assistance from the Natural Sciences and Engineering Research Council and from the University of British Columbia is gratefully acknowledged.

I. INTRODUCTION

At present the basic building blocks of matter are thought to be the twelve spin-1/2 fermions known as quarks and leptons. Four fundamental forces are responsible for the interactions which describe their behaviour. These forces are the familiar gravity and electromagnetism; the strong force which binds nuclei together; and the weak force responsible for certain nuclear decays. The six leptons do not interact via the strong force. They consist of the electron, muon and tau particles which carry electric charge, along with three neutrinos which do not. The six quarks also carry electric charge, and in addition they have a "colour" charge through which the strong force acts.

The four fundamental forces can each be described by an underlying invariance or symmetry of nature. Such a symmetry implies a conserved quantity. Many of our physical laws are based on this principle. Theoretical models known as gauge theories, which are based on underlying symmetry groups, have been very successful in describing three of the basic interactions. The exception is gravity, which has not as yet been adequately described by such a gauge theory. However the effects of gravity are very small and may be neglected at the scale where elementary particle physics is currently studied.

A general feature of these gauge theories is that the forces between the basic fermions are mediated by the exchange of a new particle called a gauge boson. These gauge bosons must be massless in order to preserve the underlying symmetry of the gauge theory. The gauge theory for the electromagnetic force, known as quantum electrodynamics (QED), is the most familiar. Here the gauge boson is the massless photon, which is exchanged

between electrically charged particles. In the gauge theory of the strong force, known as quantum chromodynamics (QCD), interactions are also mediated by exchange particles. In this case massless gluons are exchanged between colour charged quarks. Early attempts to extend this highly successful approach to the weak force postulated that it must be mediated by the exchange of what are now known as W bosons. However, the existence of a massless W boson was not consistent with experiment. The observed weakness and very short range of the weak force could only be explained if the W boson was very massive. Hence these first attempts to describe the weak force by a gauge theory were unsuccessful.

The observation that the W boson must also carry electric charge suggested to some that perhaps the weak and electromagnetic forces were one and the same. The disparity in their observed strengths and ranges could be explained by the different masses of the photon and W boson exchange particles. The first models to attempt to unify these two forces also predicted the existence of another massive exchange particle, called the Z boson, which carries no electric charge. However, such neutral currents were not at that time observed. The need for massive exchange bosons in these models destroyed the underlying symmetries that one originally wished to incorporate. This led to divergent results when higher order calculations were done. Such problems frustrated these subsequent attempts at describing the weak force.

The solution to these early theoretical problems was the phenomenon of spontaneous symmetry breaking. This refers to the fact that although a theory may contain a given symmetry, the vacuum or ground state of the system described by the theory need not respect that symmetry. A simple example is that of a ferromagnet. In general its spins are randomly aligned

and the theory possesses a rotational symmetry. In the ground state however the random spins all align in one chosen direction, and hence the rotational symmetry of the theory is "spontaneously broken" by the ground state. It can be shown that whenever such a symmetry is spontaneously broken, a massless particle known as a Goldstone boson must result. For the ferromagnet the Goldstone boson corresponds to long range spin waves.

In the present gauge theory of the weak interaction, a new fundamental scalar called a Higgs particle is introduced. The ground state of this new matter field is such that the original symmetry of the theory is spontaneously broken. In this case the massless Goldstone boson appears not as a physical particle, but instead as the longitudinal component of the massless gauge boson. In this way masses can be generated for the gauge bosons without destroying the underlying symmetry of the original theory. This technique is known as the Higgs mechanism and it solves the theoretical problems of the weak model, giving finite or renormalizable results for higher order calculations.

At this point there existed a well behaved gauge theory which unified the weak and electromagnetic forces. The model predicted masses for the W and Z exchange gauge bosons, implied the existence of neutral currents, and also a new fundamental Higgs scalar. Both neutral currents and the gauge bosons themselves [1,2] have subsequently been observed, in very good agreement with prediction. Only the Higgs scalar remains to be discovered. The phenomenological successes of this electroweak theory have been such that, together with the theory of the strong force (QCD), it is now accepted as the standard model of elementary particle physics. Thus far, all the experimental tests of the standard model have proven successful, and it is now thought to be correct for energies up to at least the order of 100 GeV.

1.1 The Standard Model

The subsequent chapters of this thesis all begin with the implicit assumption that the reader is familiar with the standard model. As the currently accepted theory, it is the basis against which any new physics must necessarily be compared. A detailed description of the standard model can be found in most modern textbooks on particle physics. Consequently only a brief summary of the main features will be presented here. As the strong interaction has no direct bearing on our results, only the electroweak aspects of the model are described.

In the standard model the fundamental particles of matter consist of twelve spin-1/2 fermions. There are three massive leptons which carry electric charge $-e$. They are known as the electron, muon and tau (e^- , μ^- , τ^-) particles. Associated with each one of these charged leptons is a massive, electrically neutral lepton (ν_e , ν_μ , ν_τ) called a neutrino. The remaining six fermions are massive particles called quarks. Three of them carry electric charge $(2/3)e$, and are known as the up, charm and top (u,c,t) quarks. The other three carry electric charge $(-1/3)e$ and are called the down, strange and bottom (d,s,b) quarks. The standard model classifies these twelve fermions into three generations or families. The structure of each family is very similar, and consists of one charged lepton, one neutrino, one charge $2/3$ quark and one charge $-1/3$ quark.

Since these quarks and leptons are spin-1/2 fermions, they may be in either of two helicity states, namely left-handed or right-handed. Hence we can decompose their wave functions into left and right components. There exists a symmetry in the standard model which involves only the left-handed components of the fermions, and it is convenient to group them into pairs or doublets as shown below. Thus the three families are written as

$$\begin{pmatrix} \nu_e \\ e^- \end{pmatrix}_L \quad \begin{pmatrix} u \\ d \end{pmatrix}_L, \quad \begin{pmatrix} \nu_\mu \\ \mu^- \end{pmatrix}_L \quad \begin{pmatrix} c \\ s \end{pmatrix}_L, \quad \begin{pmatrix} \nu_\tau \\ \tau^- \end{pmatrix}_L \quad \begin{pmatrix} t \\ b \end{pmatrix}_L$$

where the subscript L denotes the left-handed component. The corresponding right-handed components are treated separately as individual singlets. Experimentally only left-handed neutrinos are observed. Hence the right-handed neutrino singlets are not included in the standard model.

Having introduced the fundamental fermions, we turn now to the spin-1 exchange bosons which mediate their electroweak interactions. There are four of these gauge bosons in the standard model. Three of them are quite massive. They consist of the electrically neutral Z boson, as well as a pair of W bosons which carry opposite charges of $\pm e$. The fourth exchange boson is the familiar massless photon. With the exception of the Higgs boson described below, this completes the description of the particle content in the standard electroweak model.

The gauge theory of the standard model is based upon what is technically known as the $SU(2) \times U(1)$ symmetry group. A requirement of any gauge theory is that its fermions and exchange bosons must be massless in order to preserve the underlying symmetry. Thus in order to generate masses for the particles described above, the basic gauge theory must be supplemented by the introduction of one or more fundamental spin-0 scalars. As described earlier, these so called Higgs fields are responsible for the spontaneous breaking of the underlying symmetry. In the case of the standard model this is done in the simplest way, through the addition of one doublet of Higgs scalars. The Higgs field is said to acquire a non-zero vacuum expectation value (VEV), meaning that its ground state does not respect the same symmetry as the theory describing it, and hence the

$SU(2) \times U(1)$ symmetry of the standard model is spontaneously broken. One neutral Higgs boson and three Goldstone bosons result from this breaking. The latter are then absorbed via the previously described Higgs mechanism as the longitudinal components of the W and Z bosons. In this way masses are generated for the exchange bosons. Through their so called Yukawa interactions with the Higgs fields, the basic fermions can also acquire a mass. Unfortunately the model makes no prediction for the mass of the physical Higgs boson itself, and it has not been found by experiment. To date however, the addition of these fundamental scalars has been the only successful method of generating masses within gauge theories. Hence the Higgs sector is a necessary and very important part of the standard model, and indeed of any gauge theory description of particle physics.

This concludes our look at the main features of the standard model. Most of the technical details have been suppressed for simplicity, and the interested reader is referred to the literature. We have introduced the particle content of the model, and stressed the importance of the Higgs sector. These should be sufficient background for a general understanding of the standard model aspects of the thesis. Other features and specific details of the standard model are discussed as they arise.

1.2 Why Alternative Models?

Despite all of its successes, there are still some untested and little understood aspects of the standard model; most notable is the all important Higgs sector needed for spontaneous symmetry breaking. The model does not predict a mass for the fundamental Higgs scalar, which has yet to be detected. Also as will be discussed, there are many technical reasons for expecting new physics beyond the standard model.

There are several arguments [3] which suggest the need for improving upon the standard model. Numerous details about the structure of the model, and the values of its roughly 20 free parameters all need to be explained. Also the standard model is not asymptotically free, meaning that it will become strongly interacting at some larger energy scale, where perturbation methods will break down. Why this breakdown occurs is discussed in more detail below.

In particle physics, calculations are performed primarily using perturbation techniques. An unknown quantity is expanded in a power series of some small parameter. In this way each successive term in the expansion serves as a small correction to the previous term. The coefficients of the expansion are then evaluated term by term to the desired accuracy of the approximation. However, it is a general property of gauge theories that the coefficients of the higher order terms in the perturbative expansion can often contain undesirable infinities. Fortunately, for what are known as renormalizable gauge theories, these troublesome infinities can be eliminated simply by a redefinition of parameters. The sources of these infinities are quantities which diverge for large energy. In general these divergences are cut off at some scale Λ , and the infinite piece absorbed into the new parameter definitions. The perturbation series is then once again convergent. This so called renormalization scheme will of course only make sense if the cutoff scale Λ is larger than the energy scale of the process we are interested in. If this is not the case, then the infinities cannot be eliminated and perturbation methods will break down.

The scale Λ used in the renormalization scheme above is not an arbitrary parameter. There must be some physical quantity in the theory which fixes the scale. In general this is taken to be the mass of the

heaviest particle in the theory, so that perturbation techniques will be valid over as large an energy range as possible. Thus for energies greater than this mass, perturbation methods break down and the gauge theory can make no quantitative predictions.

In the standard model the heaviest possible particle is the Higgs boson. Its mass M_H varies as $M_H^2 = 2\lambda v^2$. The parameter λ is a measure of the strength of the Higgs self-interaction coupling. The quantity v is the vacuum expectation value (VEV) that the Higgs field acquires from spontaneous symmetry breaking, as discussed above. In certain perturbation calculations λ is used as an expansion parameter. Therefore it must be small since otherwise the Higgs sector would become strongly interacting and perturbation theory would fail. This contradicts the many successful predictions of the standard model which are obtained perturbatively. Thus we can establish an upper bound on λ . The VEV parameter v in the expression for the Higgs mass is simply the scale at which the electroweak symmetry is broken. In other words it is the energy at which the strengths of the electromagnetic and weak forces become equal. This is established experimentally to be $v \approx 246$ GeV. Combining these results for λ and v , one finds that the mass of the Higgs boson is expected to be less than the order of 1 TeV. This then sets the scale at which the renormalization scheme, and hence perturbation methods, will break down in the standard model.

Presently the highest attainable energies which have been tested are on the order of 100 GeV, and the results have been consistent with the predictions of the standard model. Soon a new generation of particle accelerators (see appendix A) will be operating at energies up to the TeV range. This is exactly the region where we should begin to see evidence of the breakdown in the standard model, and this is one reason for expecting

new physics to be observed in these machines. Hence there is now an immediate need to develop alternative models, and establish a theoretical framework with which to describe this expected new physics.

Despite its possible breakdown at higher energies, the standard model has had great phenomenological success to date. This then suggests that it is valid only as an effective low energy description of some more fundamental theory. This new theory should be based on some larger symmetry, which when broken at low energy, results in the standard model. Evidence for such a theory would manifest itself at a higher energy scale in the form of new physics. At presently available energies however, the experimental data is consistent with the standard model. Hence any attempt to formulate a new underlying theory must at this point be guided by purely theoretical motivations. These are discussed in the next two sections. We begin by examining some of the technical problems which occur in the crucial Higgs sector.

1.3 Fundamental Scalars

The existence of a fundamental scalar Higgs particle is an essential component of the standard model, and indeed of any gauge theory with massive exchange bosons. It is the Higgs particle which induces the spontaneous symmetry breaking needed to generate the gauge boson mass. Thus the motivation for fundamental scalars is very strong. Nevertheless there are still many technical difficulties associated with these scalars.

The above 1 TeV bound on the standard model Higgs mass leads to our first problem with scalars; namely understanding why the scalar field is so light. More specifically, the question is why is the electroweak breaking scale v so small? One would wish in developing a new fundamental theory

that we could also incorporate the unification of the strong and electroweak interactions, and possibly even gravity. The scales at which the strong force (grand unification 10^{12} TeV) or gravity (Planck mass 10^{16} TeV) become comparable to the electroweak force are very large compared to the Higgs mass (<1 TeV). Understanding how to relate these very large energy scales to the much smaller scale at which the electromagnetic and weak forces are unified is known as the so called naturalness problem. The "natural" value for the scalar boson mass should be the same as the mass scale for the fundamental theory. The disparity of these scales in the theory could be understood if there were some mechanism, such as an approximate symmetry, which ensured that the scalar mass parameters are very small. However, what such a mechanism could be is very difficult to determine for these fundamental scalar particles.

The solution to the naturalness problem proposed above leads immediately to a related difficulty known as gauge hierarchy. Although originally synonymous with "naturalness", the term "gauge hierarchy" is now used in the literature to refer to the following specific aspect of the problem. Even if a mechanism could be found which ensures a small scalar mass at lowest order of perturbation theory, the higher order corrections to the scalar mass can be very large. Thus the naturalness problem reappears via these corrections. The mass parameters must be chosen at each order in perturbation theory with incredible accuracy to avoid this. Such fine tuning is not a very satisfactory way to solve the naturalness problem.

These are two of the principal difficulties associated with fundamental scalars which will arise in trying to construct alternative theories to the standard model. One approach has been to avoid these problems by eliminating fundamental scalars altogether. Composite models and

Technicolour theories [4] try to treat the scalars as extended objects constructed from more basic fermions. However, these attempts have not been very successful thus far. The other approach is to retain the fundamental scalars which work so well in the standard model, and try to solve the problems discussed above. Indeed this will prove to be possible by employing a higher symmetry which eliminates the naturalness and gauge hierarchy problems. This is the elegant supersymmetry approach. Of all the possible alternatives to the standard model, supersymmetry is now the leading candidate.

1.4 Supersymmetry

What is different about supersymmetry models is that they incorporate both fermions and bosons into the gauge theory on an equal basis. Each boson (fermion) has a superpartner fermion (boson) of equal mass, and they differ only by their spin quantum number. Gauge theories which are supersymmetric [3,5] must remain invariant under transformations between these superpartners. In order to be phenomenologically acceptable, supersymmetric gauge models must contain the usual standard model quarks, leptons and gauge bosons. The superpartners to these particles are known respectively as squarks, sleptons and gauginos. In addition it is necessary in these models that at least two Higgs fields be employed in order to generate different masses for up and down type quarks. Thus the minimal supersymmetric extension of the standard model is a two Higgs doublet model. The details of these models will be examined in later chapters. At this point we merely wish to illustrate some of the reasons why supersymmetry is the leading alternative to the standard model.

As a candidate theory for an alternative to the standard model,

supersymmetry has many desirable features. To begin with the fundamental scalars are no longer supplemental to, but rather are now a natural part of the gauge theory, on the same footing as the basic fermions. Also certain divergent quantities, which arise in the higher order corrections to the scalar masses, now cancel at each order in perturbation theory. This cancellation occurs because the divergent contribution from each particle is exactly cancelled by the contribution from its superpartner. Hence the higher order corrections remain small and do not cause a large scalar mass. This eliminates technical problems such as gauge hierarchy. Thus supersymmetry models are much better behaved. Furthermore the naturalness problem can easily be solved by supersymmetry. In general it has been difficult to identify any mechanism which could enforce a small scalar mass. However it is well known that imposing an exact chiral symmetry enforces a zero mass for fermions. In supersymmetry a massless fermion leads naturally to a massless scalar partner. Hence the naturalness problem can be solved for supersymmetric models with approximate chiral symmetries.

Perhaps the most intriguing aspect of these supersymmetry models is that local supersymmetry transformations are related to space-time transformations. There then exists the potential to couple gravity with supersymmetry, and this would allow for the possible unification of all four of nature's fundamental forces into one theory. (For a review of such supergravity models, see reference [3]). This exciting possibility, along with the solutions of the naturalness and gauge hierarchy problems, are the main reasons for examining supersymmetry in more detail.

At this point in time, it must be noted that these motivations for supersymmetry are purely theoretical. No experimental evidence has been seen to date. Indeed, if it exists then the supersymmetry must be "softly"

broken at low energies. The description softly refers to the fact that although the supersymmetry must be broken, one wants to preserve the cancellation of the various divergent quantities in the scalar mass corrections. The cancellation will no longer be exact, but if the breaking is soft enough only finite parts will remain. This breaking of the supersymmetry must occur since no superpartners have been observed for known particles. Also an exact chiral supersymmetry implies a zero mass for the Higgs scalar, which is inconsistent with the standard model. Still the potential exists for supersymmetry to be the fundamental theory which will reduce to the standard model at low energy.

The scale at which supersymmetry is broken will establish the size of the scalar mass, and hence should be related to the electroweak breaking scale of $v \approx 246$ GeV. The breaking of the supersymmetry would lift the degeneracy in the masses of superpartners, and their resulting mass differences should also be on this same scale. Thus given the masses of the known particles, one would expect to see evidence of supersymmetry at or before the TeV energy range. This is exactly the region to be studied in the new accelerators. Thus the supersymmetry hypothesis is one which can be tested in the very near future.

1.5 Thesis Overview

Regardless of whether or not supersymmetry is a correct approach, it is clear that the fundamental scalars will play a key role in constructing alternatives to the standard model. We wish to learn more about this important Higgs sector, and consequently this thesis will focus on these non-standard spin-0 Higgs bosons. Additionally we would like to know what form of new physics to expect in the new particle accelerators. The

dominant modes of producing Higgs bosons, and the rates at which they should be observed in these machines are then examined for certain models.

Given all of the motivation previously discussed, it should not be surprising that the specific model chosen for study is one of minimal broken supersymmetry. As stated earlier, this choice is a specific example of a model with two Higgs doublets. We would like to be able to distinguish between the features of this supersymmetry model which arise from either the new superparticle content, or because there are additional Higgs fields present. Hence a more general Two-Higgs-Doublet model with no supersymmetry will first be examined. Both of these models can be found in the literature. What is new in this thesis are the calculations to which the models are applied. These calculations and the various results obtained are discussed in more detail below.

In general the Higgs boson interacts with other particles with a strength proportional to their mass. Hence the dominant decay mode of the Higgs boson will be into the heaviest particles allowed by energy conservation. If its mass is greater than $160 \text{ GeV}/c^2$, the Higgs then decays into a pair of gauge bosons. This is potentially undesirable since there can be relatively large backgrounds associated with such gauge boson pairs. Also, fewer heavy Higgs bosons could be obtained to begin with. Smaller mass Higgs bosons are more likely to be produced with the limited energies available at the new colliders (see appendix A). For these reasons it was decided to study Higgs bosons in the intermediate mass range from 40 to $160 \text{ GeV}/c^2$. However, it is quite straightforward to extend the analysis for larger Higgs masses.

In the intermediate mass range the primary decay mode of the Higgs boson is into a quark-antiquark pair, which subsequently will form two

hadronic jets. Such a signal would be lost in the much larger jet backgrounds of hadronic colliders, and hence we shall only consider e^+e^- and ep machines. The discussion to follow is similar for both these types of machines, and hence for the moment we restrict ourselves to e^+e^- colliders.

If production of the Higgs boson H^0 is possible at the SLC or LEP colliders, then it would proceed via reactions such as

$$e^+ e^- \rightarrow Z^0 H^0 \quad (1.5.1)$$

$$e^+ e^- \rightarrow \ell^+ \ell^- H^0 \quad (1.5.2)$$

These are the usual processes used in standard model Higgs searches, and they produce Higgs bosons at an essentially unobservable rate. Generally, little change is found for the non-standard models studied. The exception is for a specific case of equation (1.5.2), which is the reaction

$$e^+ e^- \rightarrow e^+ e^- H^0 \quad (1.5.3)$$

Of the many processes which contribute to this reaction, one will be of particular interest. It is known as the two photon fusion mechanism [6].

This mechanism is essentially the same as the process shown in figure 8b. The Higgs boson is produced during the exchange of a photon between the colliding particles. The detailed reasons as to why this mechanism is such an important process will be given in chapter IV. The point is that although this two photon fusion mechanism is not an important one in the standard model, it can be enhanced substantially and actually dominate in models with more than one Higgs doublet. This idea is one which

has not been explored in the literature, and is the central new feature upon which the thesis is built.

For the class of models studied, the size of the Higgs boson to two photon interaction can be greatly increased over what it is in the standard model. This large enhancement is what causes the two photon fusion mechanism to dominate Higgs boson production. The actual Higgs-photon interaction is best studied by examining the two photon decay widths of the Higgs boson. Production cross sections for the two photon fusion mechanism can then be expressed directly in terms of these widths. For this reason we will initially examine only the Higgs 2γ -decay widths. Later these results are used to estimate the various production cross sections and rates. These points are all discussed in more detail as they arise in the thesis.

Finally the thesis contents are briefly outlined below. Chapter II begins with a description of the Two-Higgs-Doublet model. The two photon decay widths for the non-standard Higgs bosons of this model are then calculated. In chapter III the minimal broken supersymmetry model is introduced, and again the Higgs 2γ -decay widths are evaluated. Comparing the two models, we are able to distinguish which features of the supersymmetry model arise from the new superparticle content. The calculation of the Higgs 2γ -decay widths for these models is a new result, and in each case we discuss how large an enhancement relative to the standard model width is possible. Chapter IV examines the production cross sections for the Higgs bosons in e^+e^- and ep colliders. The details of the two photon fusion mechanism are discussed, as well as how one can relate it to the 2γ -decay widths previously calculated. The numerical procedures used are also described. Based on this analysis, we make a prediction of what rates to expect for Higgs boson production in the new particle accelerators.

A comparison with the actual experiment would then determine if the expected new physics is consistent with a supersymmetric description. Lastly the many results and conclusions are summarized in the discussion of chapter V.

II. TWO-HIGGS-DOUBLET MODEL

This model is a simple extension of the standard model, with two doublets of Higgs fields rather than one. A knowledge of this model will be important in the next chapter for comparison with the minimal broken supersymmetry model, which is a specific example of a Two-Higgs-Doublet model. This allows one to be able to distinguish between the features of the supersymmetric model which arise from either the supersymmetry or the additional Higgs field content. Although they are reviewed extensively in the literature, the details of the Two-Higgs-Doublet model will be presented below in order to familiarize the reader with the general features of the model and to establish notation.

The particle content of the Two-Higgs-Doublet model differs from the standard model only in the Higgs sector. As discussed below, instead of just one neutral scalar particle there are a pair of charged Higgs, a neutral pseudoscalar and two neutral scalars. The key result to note however, is that the Higgs to fermion couplings differ from those in the standard model by factors of $\tan\alpha$, which is the ratio of the vacuum expectation values of the two Higgs fields. If $\tan\alpha$ is very different from one, then there is the possibility of greatly enhancing these fermion couplings, with important consequences for the Higgs to 2γ decay process.

In the second section of this chapter is presented the calculation for the standard model Higgs 2γ -decay width. These results can also be found in the literature. They serve to provide some background and establish the pattern of the similar calculation for the Two-Higgs-Doublet model. The first result to note will be that in the standard model the Higgs boson decays into two photons predominantly via gauge boson loops.

More importantly the contribution of the two photon decay process is shown to be a negligible part of the total Higgs decay width.

Finally the calculation of the Higgs 2γ -decay width is presented for the Two-Higgs-Doublet model. Although the calculation is very similar to that for the standard model, the results are new and will be needed in chapter IV. Specifically the enhanced Higgs to fermion couplings in the model lead to a much larger 2γ -decay width. Maximum possible values for the enhancement factor $\tan\alpha$ are taken from the literature. Thus the 2γ -decay process is considerably more important than it was in the standard model. The consequences of this result will be discussed further in chapter IV.

2.1 The Model

Recalling the standard electroweak model [7], we see that one of the simplest extensions to it is to include an extra doublet of Higgs scalars. One need only consider the changes in the Higgs sector, since all other features in Two-Higgs-Doublet models will remain the same as in the standard model. The two Higgs scalars are described by complex field operators ϕ_a :

$$\phi_1 = \begin{pmatrix} \phi_1^+ \\ \phi_1^0 \end{pmatrix}, \quad \phi_2 = \begin{pmatrix} \phi_2^+ \\ \phi_2^0 \end{pmatrix} \quad (2.1.1)$$

which both have hypercharge +1, where the superscripts denote electric charge. The charge conjugate fields $i\tau_2\phi_a^*$, where τ_2 is the usual Pauli matrix, have the opposite hypercharge to ϕ_a . The vacuum is characterized by two vacuum expectation values (VEV's) for these field operators

$$\langle\phi_1\rangle = \begin{pmatrix} 0 \\ \frac{a}{\sqrt{2}} \end{pmatrix}, \quad \langle\phi_2\rangle = \begin{pmatrix} 0 \\ \frac{b}{\sqrt{2}} \end{pmatrix} \quad (2.1.2)$$

It is convenient to define the rotated fields

$$\phi'_1 = \phi_1 \cos\alpha + \phi_2 \sin\alpha \quad (2.1.3a)$$

$$\phi'_2 = -\phi_1 \sin\alpha + \phi_2 \cos\alpha \quad (2.1.3b)$$

so that

$$\langle \phi'_1 \rangle = \frac{1}{\sqrt{2}} \begin{pmatrix} 0 \\ (a^2+b^2)^{1/2} \end{pmatrix}, \quad \langle \phi'_2 \rangle = 0 \quad (2.1.4)$$

and

$$\tan\alpha = b/a \quad (2.1.5)$$

Then the field ϕ'_1 can be considered as the "true" Higgs doublet, as in the standard model. The gauge transformation $U(\xi)$ takes us to the unitary gauge, where the five physical fields which are mass eigenstates can be identified. Assuming the physical fields have zero VEV's, we can write

$$\phi'_1 \rightarrow U(\xi)\phi'_1 = \begin{pmatrix} 0 \\ \frac{v+\eta}{\sqrt{2}} \end{pmatrix} \quad (2.1.6a)$$

$$\phi'_2 \rightarrow U(\xi)\phi'_2 = \begin{pmatrix} \chi \\ \frac{\phi+i\psi}{\sqrt{2}} \end{pmatrix} \quad (2.1.6b)$$

where $v^2=a^2+b^2$. The two scalar fields are ϕ and η , the pseudoscalar field is ψ and the charged Higgs are χ^\pm . The three degrees of freedom not accounted for by the physical fields are the usual would-be Goldstone bosons, which have been absorbed via the Higgs mechanism as the longitudinal components of the gauge bosons W^\pm and Z^0 .

Transitions between like charged quarks of different families by so called flavour changing neutral currents are suppressed in the standard

model, in agreement with observation. The scalars of the Two-Higgs-Doublet model will in general allow such currents, and these must somehow be suppressed. Glashow and Weinberg have shown [8] that this can only be accomplished by having quarks of the same charge couple to only one Higgs field. This is done by demanding that the Lagrangian remain invariant under

$$\phi_2 \longrightarrow -\phi_2 \quad , \quad d_R \longrightarrow -d_R \quad (2.1.7a)$$

$$\phi_1 \longrightarrow -\phi_1 \quad , \quad u_R \longrightarrow -u_R \quad (2.1.7b)$$

where u_R, d_R are u,d-type right handed quarks. This symmetry will restrict the allowed Yukawa couplings, as discussed later in this section. For supersymmetry models (see chapter III), this restriction occurs automatically.

The most general renormalizable scalar potential is given by [9]

$$\begin{aligned} V(\phi_1, \phi_2) = & -\mu_1^2 \phi_1^\dagger \phi_1 - \mu_2^2 \phi_2^\dagger \phi_2 + \lambda_1 (\phi_1^\dagger \phi_1)^2 + \lambda_2 (\phi_2^\dagger \phi_2)^2 \\ & + \lambda_3 (\phi_1^\dagger \phi_1) (\phi_2^\dagger \phi_2) + \lambda_4 |\phi_1^\dagger \phi_2|^2 + (\lambda_5/2) [(\phi_1^\dagger \phi_2)^2 + (\phi_2^\dagger \phi_1)^2] \end{aligned} \quad (2.1.8)$$

with $\mu_1^2, \mu_2^2 > 0$ for spontaneous symmetry breaking. Minimizing the potential with respect to ϕ_1 and ϕ_2 leads to the conditions

$$\phi_1^\dagger [-\mu_1^2 + 2\lambda_1 |\phi_1|^2 + \lambda_3 |\phi_2|^2] + \phi_2^\dagger [\lambda_4 \phi_1^\dagger \phi_2 + \lambda_5 \phi_2^\dagger \phi_1] = 0 \quad (2.1.9a)$$

$$\phi_2^\dagger [-\mu_2^2 + 2\lambda_2 |\phi_2|^2 + \lambda_3 |\phi_1|^2] + \phi_1^\dagger [\lambda_4 \phi_2^\dagger \phi_1 + \lambda_5 \phi_1^\dagger \phi_2] = 0 \quad (2.1.9b)$$

where the fields ϕ_a are evaluated at their VEV's. These conditions can then

be solved for the VEV's

$$\frac{a^2}{2} = \frac{(2\lambda_2\mu_1^2 - \Lambda\mu_2^2)}{(4\lambda_1\lambda_2 - \Lambda^2)} \quad (2.1.10a)$$

$$\frac{b^2}{2} = \frac{(2\lambda_1\mu_2^2 - \Lambda\mu_1^2)}{(4\lambda_1\lambda_2 - \Lambda^2)} \quad (2.1.10b)$$

where $\Lambda = \lambda_3 + \lambda_4 + \lambda_5$. Expressing the potential in terms of the rotated fields of equation (2.1.3), we find that

$$\begin{aligned} V(\phi_1', \phi_2') = & - (\phi_1', \phi_1'^\dagger) [\mu_1^2 \cos^2 \alpha + \mu_2^2 \sin^2 \alpha] \\ & - (\phi_2', \phi_2'^\dagger) [\mu_1^2 \sin^2 \alpha + \mu_2^2 \cos^2 \alpha] \\ & + (1/2)(\mu_1^2 - \mu_2^2) [\phi_1', \phi_2'^\dagger + \phi_2', \phi_1'^\dagger] \\ & + (\phi_1', \phi_1'^\dagger)^2 [\lambda_1 \cos^4 \alpha + \lambda_2 \sin^4 \alpha + (\Lambda/4) \sin^2 2\alpha] \\ & + (\phi_2', \phi_2'^\dagger)^2 [\lambda_1 \sin^4 \alpha + \lambda_2 \cos^4 \alpha + (\Lambda/4) \sin^2 2\alpha] \quad (2.1.11) \\ & + [(\phi_1', \phi_2'^\dagger)^2 + (\phi_2', \phi_1'^\dagger)^2] (1/4) [(\lambda_1 + \lambda_2 - \Lambda) \sin^2 2\alpha + 2\lambda_5] \\ & + (\phi_1', \phi_1'^\dagger)(\phi_2', \phi_2'^\dagger) (1/2) [(\lambda_1 + \lambda_2 - \Lambda) \sin^2 2\alpha + 2\lambda_3] \\ & + (\phi_1', \phi_1'^\dagger)(\phi_1', \phi_2'^\dagger + \phi_2', \phi_1'^\dagger) [-\lambda_1 \cos^2 \alpha + \lambda_2 \sin^2 \alpha + (\Lambda/2) \cos 2\alpha] \sin 2\alpha \\ & + (\phi_2', \phi_2'^\dagger)(\phi_1', \phi_2'^\dagger + \phi_2', \phi_1'^\dagger) [-\lambda_1 \sin^2 \alpha + \lambda_2 \cos^2 \alpha - (\Lambda/2) \cos 2\alpha] \sin 2\alpha \\ & + |\phi_1', \phi_2'|^2 (1/2) [(\lambda_1 + \lambda_2 - \Lambda) \sin^2 2\alpha + 2\lambda_4] \end{aligned}$$

Choosing the unitary gauge and substituting from equation (2.1.6) will give the scalar potential in terms of the physical fields.

$$\begin{aligned}
V = & - (v^2/2)[\mu_1^2 \cos^2 \alpha + \mu_2^2 \sin^2 \alpha] + (v^4/4)[\lambda_1 \cos^4 \alpha + \lambda_2 \sin^4 \alpha + (\Lambda/4) \sin^2 2\alpha] \\
& + v\phi(\sin 2\alpha)[\mu_1^2 - \mu_2^2 + v^2\{-\lambda_1 \cos^2 \alpha + \lambda_2 \sin^2 \alpha + (\Lambda/2) \cos 2\alpha\}]/2 \\
& - v\eta[\mu_1 \cos^2 \alpha + \mu_2 \sin^2 \alpha - v^2\{\lambda_1 \cos^4 \alpha + \lambda_2 \sin^4 \alpha + (\Lambda/4) \sin^2 2\alpha\}] \\
& + \chi^+ \chi^- [-\mu_1^2 \sin^2 \alpha - \mu_2^2 \cos^2 \alpha + (v^2/4)\{(\lambda_1 + \lambda_2 - \Lambda) \sin^2 2\alpha + 2\lambda_3\}] \\
& - \psi^2[\mu_1^2 \sin^2 \alpha + \mu_2^2 \cos^2 \alpha - (v^2/4)\{(\lambda_1 + \lambda_2 - \Lambda) \sin^2 2\alpha + 2(\lambda_3 + \lambda_4 - \lambda_5)\}]/2 \\
& - \eta^2[\mu_1^2 \cos^2 \alpha + \mu_2^2 \sin^2 \alpha - 3v^2\{\lambda_1 \cos^4 \alpha + \lambda_2 \sin^4 \alpha + (\Lambda/4) \sin^2 2\alpha\}]/2 \quad (2.1.12) \\
& - \phi^2[\mu_1^2 \sin^2 \alpha + \mu_2^2 \cos^2 \alpha - (v^2/4)\{3(\lambda_1 + \lambda_2 - \Lambda) \sin^2 2\alpha + 2\Lambda\}] \\
& + \eta\phi[\mu_1^2 - \mu_2^2 + 3v^2\{-\lambda_1 \cos^2 \alpha + \lambda_2 \sin^2 \alpha + (\Lambda/2) \cos 2\alpha\}](\sin 2\alpha)/2 \\
& + \eta\chi^+ \chi^- v[(\lambda_1 + \lambda_2 - \Lambda) \sin^2 2\alpha + 2\lambda_3]/2 \\
& + \phi\chi^+ \chi^- v[-\lambda_1 \sin^2 \alpha + \lambda_2 \cos^2 \alpha - (\Lambda/2) \cos 2\alpha] \sin 2\alpha \\
& + (3 \text{ neutral scalar terms}) + (4 \text{ scalar terms})
\end{aligned}$$

The terms linear in η and ϕ can be eliminated using the conditions in equation (2.1.9). The actual mass eigenstates will in general be mixtures of the two neutral scalars, and the diagonalization of the η, ϕ fields is achieved through a rotation given by

$$\phi = \tilde{\phi} \cos \theta_m + \tilde{\eta} \sin \theta_m \quad (2.1.13a)$$

$$\eta = -\tilde{\phi} \sin \theta_m + \tilde{\eta} \cos \theta_m \quad (2.1.13b)$$

The mixing angle θ_m can be expressed in terms of the λ_i parameters by

$$\sin^2 \theta_m = \frac{1}{2} - \frac{[(\lambda_1 a^2 - \lambda_2 b^2)(a^2 - b^2) + 2\Lambda a^2 b^2]}{2v^2 [(\lambda_1 a^2 - \lambda_2 b^2)^2 + a^2 b^2 \Lambda^2]^{1/2}} \quad (2.1.14)$$

With θ_m as a parameter, the mass eigenstates $\tilde{\phi}$ and $\tilde{\eta}$ are now orthogonal.

The masses of the spin-0 fields simplify to

$$M_{\tilde{\phi}, \tilde{\eta}}^2 = \lambda_1 a^2 + \lambda_2 b^2 \mp [(\lambda_1 a^2 - \lambda_2 b^2)^2 + a^2 b^2 \Lambda^2]^{1/2} \quad (2.1.15a)$$

$$M_\chi^2 = -v^2(\lambda_4 + \lambda_5)/2 \quad (2.1.15b)$$

$$M_\psi^2 = -\lambda_5 v^2 \quad (2.1.15c)$$

The parameters λ_4 and λ_5 can be chosen to be negative without loss of generality and hence equations (2.1.15) do not pose a consistency problem.

The Lagrangian describing the interactions of ϕ_1 and ϕ_2 with the gauge bosons is given by

$$\mathcal{L}_g = (D_\mu \phi_1)^\dagger (D^\mu \phi_1) + (D_\mu \phi_2)^\dagger (D^\mu \phi_2) \quad (2.1.16)$$

where

$$D_\mu = -\partial_\mu - i(g'/2)B_\mu - i(g/2)\tau_a A_\mu^a \quad (2.1.17)$$

and τ_a are the Pauli matrices.

The gauge boson sector is the same as in the standard model with

$$A_\mu^1 = (W_\mu^+ + W_\mu^-)/\sqrt{2} \quad (2.1.18a)$$

$$A_\mu^2 = i(W_\mu^+ - W_\mu^-)/\sqrt{2} \quad (2.1.18b)$$

$$A_\mu^3 = \sin\theta_w A_\mu + \cos\theta_w Z_\mu \quad (2.1.18c)$$

$$B_\mu = \cos\theta_w A_\mu - \sin\theta_w Z_\mu \quad (2.1.18d)$$

One can rewrite equation (2.1.16) in terms of the fields $\tilde{\eta}, \tilde{\phi}, \chi, \psi$ via the same procedure used for the scalar potential. This gives the result

$$\begin{aligned} \mathcal{L}_g = & (g^2/2)v\cos\theta_w W_\mu^{+\mu} W_\mu^{-\mu} \tilde{\eta} - (g^2/2)v\sin\theta_w W_\mu^{+\mu} W_\mu^{-\mu} \tilde{\phi} + e^2 A_\mu^\mu A_\mu \chi^+ \chi^- \\ & - ieA^\mu [(\partial_\mu \chi^+) \chi^- - \chi^+ (\partial_\mu \chi^-)] + \text{others} \end{aligned} \quad (2.1.19)$$

where only terms in the Higgs sector which will contribute to the two photon decay width are explicitly shown.

Either one of the two Higgs doublets can be used for the lepton Yukawa term. Choosing ϕ_1 , one finds that the allowed Yukawa interactions must take the form

$$\mathcal{L}_y = y_1 (\overline{u \ d})_L i\tau_2 \phi_1^* u_R + y_2 (\overline{u \ d})_L \phi_2 d_R + y_3 (\overline{\nu \ \ell})_L \phi_1 \ell_R + \text{h.c.} \quad (2.1.20)$$

under the discrete symmetry of equation (2.1.7). Only one quark-lepton family will be important for the two photon decay width analysis. Thus the quark mixings and family labels will be omitted. As before one can express

equation (2.1.20) in terms of the physical fields, and we find that

$$\begin{aligned}
\mathcal{L}_y = & y_1 [v \cos \alpha \bar{e} e + \tilde{\eta} \bar{e} e \cos(\theta + \alpha) - \tilde{\phi} \bar{e} e \sin(\theta + \alpha) - i \psi \bar{e} \gamma_5 e \sin \alpha] / \sqrt{2} \\
& + y_2 [v \sin \alpha \bar{d}_L d_R + \tilde{\eta} \bar{d}_L d_R \sin(\theta + \alpha) + \tilde{\phi} \bar{d}_L d_R \cos(\theta + \alpha) - i \psi \bar{d}_L d_R \cos \alpha + \text{h.c.}] / \sqrt{2} \\
& + y_3 [v \cos \alpha \bar{u}_L u_R + \tilde{\eta} \bar{u}_L u_R \cos(\theta + \alpha) - \tilde{\phi} \bar{u}_L u_R \sin(\theta + \alpha) - i \psi \bar{u}_L u_R \sin \alpha + \text{h.c.}] / \sqrt{2} \\
& + \text{others} \tag{2.1.21}
\end{aligned}$$

where again only those terms which contribute to the two photon decay width are explicitly shown.

This completes the description of the Higgs sector for the Two-Higgs-Doublet model. Some of the important couplings obtained in this section are summarized in Table I. Note that the Higgs-fermion couplings differ most significantly from those in the standard model by factors of $\tan \alpha$ ($\cot \alpha$), as well as to a lesser extent due to the mixing angle θ_m . Thus for large values of $\tan \alpha$ ($\cot \alpha$) these couplings can be enhanced relative to the standard model. In section 2.3 this will be discussed further.

As a final point it should be noted that all the calculations in this section were performed in unitary gauge. It is quite straightforward to repeat the derivation for a general gauge. Indeed this is what is done for the supersymmetry models in chapter III. However, in the Two-Higgs-Doublet case, the unitary gauge results will be sufficient for the remainder of the discussion.

Table I - Two-Higgs-Doublet Model Vertices

Vertex	H^0	$\tilde{\eta}$	$\tilde{\phi}$	ψ
eeX	$y_e = \frac{-im_e}{v}$	$y_e \frac{\cos(\theta_m + \alpha)}{\cos\alpha}$	$-y_e \frac{\sin(\theta_m + \alpha)}{\cos\alpha}$	$-y_e i\gamma_5 \tan\alpha$
uuX	$y_u = \frac{-im_u}{v}$	$y_u \frac{\cos(\theta_m + \alpha)}{\cos\alpha}$	$-y_u \frac{\sin(\theta_m + \alpha)}{\cos\alpha}$	$-y_u i\gamma_5 \tan\alpha$
ddX	$y_d = \frac{-im_d}{v}$	$y_d \frac{\sin(\theta_m + \alpha)}{\sin\alpha}$	$y_d \frac{\cos(\theta_m + \alpha)}{\sin\alpha}$	$y_d i\gamma_5 \cot\alpha$
W^+W^-X	$g_w = \frac{ig^2 v}{2}$	$g_w \cos\theta_m$	$-g_w \sin\theta_m$	0

Yukawa and gauge couplings of scalars and pseudoscalar to fermions and W-bosons for the Two-Higgs-Doublet model. The mixing angle of the two VEV's is α and the mixing angle between scalars is θ_m . The standard model vertices for H^0 are shown for comparison.

2.2 Standard Model 2γ -Decay Width

The standard model's results will first be summarized, since the Two-Higgs-Doublet model is similar to it in so many ways. This serves as a benchmark for the subsequent discussions of non-standard spin-0 boson decays.

In the standard model, three classes of diagrams contribute to the 2γ -decay width of the Higgs boson; namely fermion loops, gauge boson loops and scalar loops. This separation is for later convenience since the standard model has no physical charged scalars, so the scalar loops consist only of would-be Goldstone bosons. If one writes the gauge invariant amplitude M for $H^0 \rightarrow \gamma(k_1) + \gamma(k_2)$ as

$$M = A e_1^\mu e_2^\nu [g_{\mu\nu} - (k_{1\nu} k_{2\mu}) / (k_1 \cdot k_2)] \quad (2.2.1)$$

where e_1 and e_2 are polarization vectors of the two photons, then the structure function A is given by

$$A = [ie^2 g M_{H^2} / (8\pi^2 M_w)] [A_w + A_f + A_s] \quad (2.2.2a)$$

where

$$A_w = 3\lambda_w - 2\lambda_w(2-3\lambda_w)I(\lambda_w) \quad (2.2.2b)$$

$$A_f = - \sum_f (e_f^2 c_f \lambda_f) [2 + (4\lambda_f - 1)I(\lambda_f)] \quad (2.2.2c)$$

$$A_s = (1/2) + \lambda_w I(\lambda_w) \quad (2.2.2d)$$

with $\lambda = m^2 / M_H^2$ and the function $I(\lambda)$ is given in appendix D. The subscript on λ indicates the loop particle mass, in this case either M_w or m_f .

Here the charges of the fermions are $e_f e$. The quantities A_w, A_f, A_s correspond to contributions from gauge boson loops, fermion loops and scalar

loops respectively. The sum in equation (2.2.2c) is taken over all charged fermion species with the colour factor $c_f=3$ (1) for quarks (leptons). The calculation of the results in equation (2.2.2) is presented in appendix B, and can also be found in reference [10].

The two photon decay width of the standard Higgs boson is then given by

$$\Gamma(H^0 \rightarrow \gamma\gamma) = |A|^2 / (16\pi M_H) \quad (2.2.3)$$

The gauge boson loop gives the largest amplitude and is roughly a factor 5 larger than the next contribution due to the t-quark loop. These two contributions interfere destructively. The other fermion loops and the scalar loop are unimportant. For a large range of M_H , say between 40 to 160 GeV/c², one can approximate equation (2.2.3) by

$$\Gamma(H^0 \rightarrow \gamma\gamma) \approx 10^{-5} M_H^3 \text{ keV} \quad (2.2.4)$$

with M_H measured in units of GeV/c². Hence the standard model two photon width is only about 10 keV (i.e. a branching ratio of less than 0.1%).

2.3 Two-Higgs-Doublet Model 2γ -Decay Widths

The model described in section 2.1 has one pseudoscalar and two scalar neutral Higgs bosons. This section will discuss the possibility that one or more of these non-standard spin-0 bosons has a two photon decay width which is greatly enhanced relative to the standard model.

Recall the vertices given in Table I. The magnitude and sign of the scalar coupling to charged Higgs is highly model dependent and will be discussed below. As expected the pseudoscalar ψ is not affected by the mixing parameter θ_m . It does not couple to the W-bosons or to the charged Higgs bosons, but only to fermions. Hence the pseudoscalar decay width is the least model dependent. In general the scalar couplings to the W-boson

are smaller than in the standard model. Thus one must look to the fermion loops for any possible enhancement. For simplicity we take $\theta_m=0$, which in fact produces the constraint equation

$$\lambda_2 b^2 - \lambda_1 a^2 = (b^2 - a^2)(\lambda_3 + \lambda_4 + \lambda_5)/2 \quad (2.3.1)$$

If all the λ_i 's are of the same order, this equation can be naturally satisfied. With this choice of θ_m the couplings for one of the scalars, $\tilde{\eta}$, become identical to those of the standard model Higgs boson, giving the same width as discussed in the last section. The other scalar, $\tilde{\phi}$, now does not couple at all to the W-boson, eliminating the destructive interference and leaving only the fermion loop amplitude.

There are two ways to enhance the contribution of the fermion loops. From Table I it can be seen that if $\tan\alpha$ ($\cot\alpha$) is large then the lepton and u-type quark loops will be enhanced (decreased), and the d-type quark loops decreased (enhanced). This is true for both the scalar and pseudoscalar bosons. From the standard model it was found that only the t-quark loop made a significant contribution, and thus it is the logical one to try and enhance. Hereafter the discussion will focus on the Two-Higgs-Doublet model with large $\tan\alpha$ enhancement. The results for models with large $\cot\alpha$ will be similar except that the width being enhanced is much smaller to begin with.

The dominant contribution for both the scalar $\tilde{\phi}$ and the pseudoscalar ψ now comes from the t-quark loop enhanced by $\tan\alpha$. To find the maximum enhancement allowed by the model, bounds on the magnitude of the enhancement factor can be determined by low energy phenomenology. The virtual effects of the charged Higgs in Bhabha scattering, muon decays [11,12,13] and the $K_L^0 - K_S^0$ mass difference [14] give an upper limit for $\tan\alpha$ as a function of the charged Higgs mass M_χ . The approximate bound $\tan^2\alpha < 2M_\chi/m_c$ is taken from reference [14] where m_c is the charm quark mass.

Limits on M_χ can be obtained from considering charged Higgs effects in the W and Z-boson propagators. For $M_\chi \gg M_\eta, M_\phi$ the change in the mass ratio of the gauge bosons is proportional to M_χ . Specifically $M_\chi = 1.2 \text{ TeV}/c^2$ will give a 5% change in the ρ -parameter [15] where $\rho = M_W^2/M_Z^2 \cos^2 \theta_w$. This is within the allowed experimental error [1,2]. Thus we find

$$\tan \alpha < 40 \quad (2.3.2)$$

In the Two-Higgs-Doublet model there is an additional contribution to the 2γ -decay width of the Higgs scalars coming from the charged Higgs scalar loops. The Feynman diagrams for this process are the same as those in section B.2 of appendix B, except the loop particle is a charged Higgs χ^+ rather than a would-be Goldstone boson. From equation (2.1.12) the relevant scalar coupling to charged Higgs terms of the Lagrangian are

$$\chi^+ \chi^- \tilde{\phi} \rightarrow v[-\lambda_1 \sin^2 \alpha + \lambda_2 \cos^2 \alpha - (\Lambda/2) \cos 2\alpha] \sin 2\alpha \quad (2.3.3a)$$

$$\chi^+ \chi^- \psi \rightarrow v[(\lambda_1 + \lambda_2 - \Lambda) \sin^2 2\alpha + 2\lambda_3] / 2 \quad (2.3.3b)$$

with $\theta_m = 0$. The magnitude and sign of these couplings is not determined by theory. Above it has been argued that $M_\chi < 1.2 \text{ TeV}/c^2$ which means that λ_4 and λ_5 are of the order of unity. It is natural to assume that all the λ_i 's are of the same order. This argument is by no means rigorous but is supported by partial wave unitarity plus perturbation theory [16,17] which gives a similar bound on M_χ . With these caveats it can be said that the couplings of equation (2.3.3) are not enhanced. Hence the scalar χ -loops give a negligible contribution to the two photon decay width.

For large $\tan \alpha$ the two photon decay width of the Higgs scalar is then dominated by the t-quark loop and is given by

$$\Gamma(\tilde{\phi} \rightarrow \gamma\gamma) = \tan^2\alpha |(-ie^2 g m_t^2 / 6\pi^2 M_w) [2 + (4\lambda_t - 1)I(\lambda_t)]|^2 / (16\pi M_{\tilde{\phi}}) \quad (2.3.4)$$

where $\lambda_t = m_t^2 / M_{\tilde{\phi}}^2$. This result is obtained using the same techniques, described in appendix B, as were used for the standard model calculation. The pseudoscalar fermion loop calculation is performed in section B.4 of appendix B. Again the t-quark loop dominated with the result

$$\Gamma(\psi \rightarrow \gamma\gamma) = \tan^2\alpha |(-ie^2 g m_t^2 / 6\pi^2 M_w) I(\lambda_t)|^2 / (16\pi M_{\psi}) \quad (2.3.5)$$

where $\lambda_t = m_t^2 / M_{\psi}^2$. These widths are indeed greatly enhanced over the standard model result for large $\tan\alpha$. The other scalar width $\Gamma(\tilde{\eta} \rightarrow \gamma\gamma)$ is the same as the standard model result. In general $\theta_m \neq 0$, and the 2γ -decay widths of the scalars $\tilde{\phi}$ and $\tilde{\eta}$ lie somewhere between the two extremes of the standard model result [equation (2.2.3)] and the best case result [equation (2.3.4)].

This concludes the chapter on the Two-Higgs-Doublet model. The reader has been introduced to the general features of the model, and this knowledge will be useful background for the discussion of the results to be presented in the remaining chapters. Also illustrated were the methods needed to calculate the standard model Higgs 2γ -decay width. These calculational methods can be found in the literature, and the Two-Higgs-Doublet model itself has been extensively reviewed. The only new result has been to perform the Higgs 2γ -decay width calculation for the Two-Higgs-Doublet model, obtaining equations (2.3.4) and (2.3.5) given above. For large values of the enhancement factor $\tan\alpha$, these widths are much larger than is the case for the standard model. Hence the two photon decay process is much more important in Two-Higgs-Doublet models. The consequences of this result will be discussed at length in chapter IV.

III. MINIMAL BROKEN SUPERSYMMETRY MODEL

This chapter also looks at the two photon decay widths of non-standard spin-0 bosons [18]. In this case however, the model is one of minimal broken supersymmetry, which is a specific example of a Two-Higgs-Doublet model. The motivation for supersymmetry has been discussed in the introduction. As was the case in the last chapter, the minimal broken supersymmetry model itself can be found in the literature. Again the details are presented below for the readers edification and to establish notation. The remainder of the chapter is devoted to the calculation of the Higgs 2γ -decay widths for this model. These are all new results, and their significance is further discussed in the next chapter.

The particle content of the minimal broken supersymmetry model is quite similar to that of the Two-Higgs-Doublet model, and is discussed in more detail below. The main difference is that each particle is now accompanied by a superpartner which differs by one half a unit of quantum spin. We will discover later in this chapter that these new superparticles do not significantly affect the two photon decay widths of the Higgs bosons. In fact they slightly reduce the widths through destructive interference with the usual particle contributions. Once again it is the additional Higgs field content, leading to an enhancement of the Higgs to fermion couplings, which has the largest effect on the 2γ -decay widths. However, unlike the Two-Higgs-Doublet model, we find that supersymmetry imposes a new constraint on the maximum possible value of the enhancement factor $\tan\alpha$. This new constraint has important consequences, which will be discussed in the next chapter.

3.1 The Model

Deriving the actual supersymmetry Lagrangian is too complicated to present here. The results in component field notation will be summarized below. The component field content needed for the minimal supersymmetric model is listed in table II [18]. It includes, in the gauge sector, the usual SU(2) triplet of vector bosons, V_μ^a ($a=1,2,3$), and the U(1)_y vector boson V_μ' along with their corresponding fermionic partners represented by two component spinors λ^a ($a=1,2,3$) and λ' respectively.

The matter sector contains a left-handed SU(2) lepton doublet of two component fermions L^i ($i=1,2$) along with a two component SU(2) singlet e_L^c .

Similarly, for the quark sector there is a doublet Q_L^i ($i=1,2$) and two singlets, u_L^c and d_L^c . The scalar partners of the quarks are denoted as \tilde{Q}_L^i and $\tilde{u}_R^*, \tilde{d}_R^*$ for the SU(2) doublet and singlets, respectively. The slepton SU(2) doublet and singlet are \tilde{L}^i and \tilde{e}_R^+ respectively. As in the Two-Higgs-Doublet model, only one quark lepton family will be of interest. Thus the quark mixings and family labels are omitted, although these can be included straightforwardly. The matter sector is completed with the addition of Higgs multiplets. Three sets of Higgs field, H_1 , H_2 and N are employed to break the SU(2) \times U(1) symmetry [19]. At least two scalar SU(2) doublets are necessary to give mass to both the up- and down-type quarks. With the additional constraints present in supersymmetry models, the Higgs doublets alone are no longer sufficient to break the SU(2) \times U(1) symmetry. Although not necessarily present, the addition of an extra Higgs field N is the simplest way to remedy this problem. Enlargement of the Higgs sector to include an SU(2) and U(1) singlet field N allows for discussion of the supersymmetric limit, with the gauge symmetry broken to U(1)_{em}. Finally these scalars are all accompanied by the fermionic partners $\psi_{H_1}^1$, $\psi_{H_2}^1$ and ψ_N .

Table II - Supersymmetric Field Content

Gauge Bosons	Gauginos	SU(2)	Y
V^a	λ^a	1	0
V'	λ'	0	0
Leptons	Sleptons		
$L^i = (\nu, e^-)_L$	$\tilde{L}^i = (\tilde{\nu}, \tilde{e}^-)_L$	1/2	-1
e_L^c	\tilde{e}_R^+	0	2
Quarks	Squarks		
$Q_L^i = (u, d)_L$	$\tilde{Q}_L^i = (\tilde{u}_L, \tilde{d}_L)$	1/2	1/3
u_L^c	\tilde{u}_R^*	0	-4/3
d_L^c	\tilde{d}_R^*	0	2/3
Higgs Bosons	Higgsinos		
H_1^i	$(\psi_{H_1}^1, \psi_{H_1}^2)$	1/2	-1
H_2^i	$(\psi_{H_2}^1, \psi_{H_2}^2)$	1/2	1
N	ψ_N	0	0

Field content of the minimal supersymmetric SU(2)xU(1) model with one family. SU(2) gauge bosons carry the label a=1,2,3 and the matter fields have the SU(2) index i=1,2. The last two columns give the SU(2) representations and the U(1) hypercharges of the respective fields. The superscript c indicates charge conjugation.

The component field Lagrangian has been extensively reviewed [3,5,20] and is presented below. The total interaction Lagrangian, \mathcal{L}_{int} , is divided into a supersymmetric piece, \mathcal{L}_{SS} , and a piece which softly breaks supersymmetry, \mathcal{L}_{SSB} . The supersymmetric part is invariant under transformations between bosons and fermions. Thus one has

$$\mathcal{L}_{\text{int}} = \mathcal{L}_{\text{SS}} + \mathcal{L}_{\text{SSB}} \quad (3.1.1)$$

which is constructed out of the fields listed in table II. A derivation of \mathcal{L}_{SS} from superfield formalism can be obtained in reference [21].

For clarity and completeness \mathcal{L}_{SS} will be presented in several pieces. The interactions of the gauge multiplets among themselves and the matter fields are described by $\mathcal{L}_{\text{gauge}}$. This is given by

$$\begin{aligned} \mathcal{L}_{\text{gauge}} = & ig\sqrt{2}T_{ij}^a (\lambda^a \psi_j A_i^* - \bar{\lambda}^a \bar{\psi}_i A_j) + \frac{ig'}{\sqrt{2}} (\lambda' \psi_i A_i^* - \bar{\lambda}' \bar{\psi}_i A_i) \\ & - igT_{ij}^a v_\mu^a \{ [A_i^* \partial^\mu A_j - (\partial^\mu A_i^*) A_j] - i\bar{\psi}_i \sigma^\mu \psi_j \} \\ & - \frac{ig'}{2} v_\mu' \{ y_A [A^* \partial^\mu A - (\partial^\mu A^*) A] - i y_f \bar{\psi} \sigma^\mu \psi \} \\ & + A_i^* A_j (gT_{ik}^a v_\mu^a + \frac{1}{2} g' y_A \delta_{ik} v_\mu') (gT_{kj}^b v^{\mu b} + \frac{1}{2} g' y_A \delta_{kj} v'^{\mu}) \\ & + ig\epsilon_{abc} \bar{\lambda}^a \sigma^\mu \lambda^b v_\mu^c \end{aligned} \quad (3.1.2)$$

In the above equation, A denotes the scalar fields and ψ represents generically the Majorana spinor fields of table II. The $U(1)$ hypercharge of the scalar field A is y_A and that of the matter fermion field is y_f . A sum over all scalar fields A is implicit. The $SU(2)$ generators are T_{ij}^a where $a=1,2,3$ and $i,j=1,2$. Also $\sigma^\mu=(1,\vec{\sigma})$ where $\vec{\sigma}$ denotes the three Pauli matrices.

The Yukawa interactions between the fermions and the scalar bosons are described by a second piece, \mathcal{L}_Y . Also included are the scalar-fermion Higgs field interactions since they are the supersymmetric partner interactions to the Yukawa ones. Explicitly

$$\begin{aligned}
\mathcal{L}_Y = & \epsilon_{ij} f_e H_1^{i-} \bar{L}^j e_R + \text{h.c.} + f_e^2 |H_1^i|^2 \bar{e}_R^* e_R + |f_e \epsilon_{ij} \tilde{L}^j e_R + h_d \epsilon_{ij} \tilde{Q}^j d_R|^2 \\
& + 2\text{Re}[(h_e \epsilon_{ij} H_2^j N)(f_e \epsilon_{ik} \tilde{L}^{k\sim} e_R + h_d \epsilon_{ik} \tilde{Q}^{k\sim} d_R)^*] + 2\text{Re}[(h_e \epsilon_{ij} H_1^j N)(h_u \epsilon_{ik} \tilde{Q}^{k\sim} u_R)^*] \\
& + |f_e \epsilon_{ij} H_1^{i-} \tilde{L}^j|^2 + \epsilon_{ij} h_d H_1^{i-} \tilde{Q}^j d_R + \text{h.c.} + |h_d \epsilon_{ij} H_1^{i-} \tilde{Q}^j|^2 + |h_u \epsilon_{ij} H_2^{i-} \tilde{Q}^j|^2 \\
& + \epsilon_{ij} h_u H_2^{i-} \tilde{Q}^j u_R + \text{h.c.} + |(h_d H_1^{i-} \tilde{d}_R - h_u H_2^{i-} \tilde{u}_R)|^2 + |h_u \epsilon_{ij} \tilde{Q}^j \tilde{U}_R|^2 \quad (3.1.3)
\end{aligned}$$

where f_e , h_d and h_u are the Yukawa couplings. As usual \mathcal{L}_Y gives rise to quark (squark) and lepton (slepton) masses. In the absence of supersymmetry breaking terms, the fermions and corresponding sfermions will have degenerate masses.

The third piece, \mathcal{L}_S , is the superpotential and it is given by [5]

$$\begin{aligned}
-\mathcal{L}_S &= v \\
&= h^2 (|H_1^1|^2 + |H_2^1|^2) |N|^2 + |h\epsilon_{ij} H_1^i H_2^j + s|^2 \\
&+ \frac{1}{8} g^2 \{ 4 |H_1^{1*} H_2^1|^2 - 2 |H_1^1|^2 |H_2^1|^2 + \sum_{m=1,2} [4 |H_m^{1*} \tilde{Q}_L^1|^2 - 2 |H_m^1|^2 |\tilde{Q}_L^1|^2 \\
&+ 4 |H_m^{1*} \tilde{L}^1|^2 - 2 |H_m^1|^2 |\tilde{L}^1|^2] + 4 |\tilde{Q}_1^{1*} \tilde{L}^1|^2 - 2 |\tilde{Q}_1^1|^2 |\tilde{L}^1|^2 \} \quad (3.1.4) \\
&+ |H_1^1|^2 + |H_2^1|^2 + |\tilde{Q}^1|^2 + |\tilde{L}^1|^2 \\
&+ \frac{1}{8} g'^2 [|H_2^1|^2 - |H_1^1|^2 + \frac{1}{3} |\tilde{Q}^1|^2 - \frac{4}{3} |\tilde{u}_R|^2 + \frac{2}{3} |\tilde{d}_R|^2 - |\tilde{L}^1|^2 + 2 |\tilde{e}_R|^2]^2
\end{aligned}$$

where $|A^i|^2 \equiv (A^{i*} A^i)^2$ for the scalar field A. Finally for completeness the usual gauge fixing Lagrangian

$$\begin{aligned}
\mathcal{L}_{GF} &= -\frac{1}{2\xi} [\partial_\mu \tilde{V}^\mu + ig\xi (H_{12}^{\dagger\tau} \langle H_1 \rangle - \langle H_1 \rangle^{\dagger\tau} H_1)]^2 \\
&- \frac{1}{2\xi'} [\partial_\mu V'^\mu + \frac{ig'\xi'}{2} y_1 (H_1^\dagger \langle H_1 \rangle - \langle H_1 \rangle^\dagger H_1)]^2 \quad (3.1.5)
\end{aligned}$$

and Fadeev-Popov (FP) ghost Lagrangian have to be added. The simple case of equal VEV's for the two Higgs doublets will be sufficient to illustrate the important features of the FP Lagrangian. In the expression below the ghost fields are C_\pm, C_Y, C_Z ; the would-be Goldstone bosons are G^\pm, G^0 ; the usual gauge bosons are $W^{\pm\mu}, A^\mu, Z^\mu$; and the Higgs scalar field is H. Thus

$$\begin{aligned}
\mathcal{L}_{FP} = & - C_+^\dagger \partial^2 C_+ - C_-^\dagger \partial^2 C_- - C_Y^\dagger \partial^2 C_Y - C_Z^\dagger \partial^2 C_Z - \xi M_W^2 C_Z^\dagger C_Z / \cos^2 \theta_w \\
& - \xi M_W^2 (C_+^\dagger C_+ + C_-^\dagger C_-) - (\xi g M_W / 2) [(C_+^\dagger C_+ + C_-^\dagger C_-) H + C_Z^\dagger C_Z H / \cos^2 \theta_w] \\
& + ig\xi [(\partial_\mu C_+^\dagger) W^{+\mu} - (\partial_\mu C_-^\dagger) W^{-\mu}] (C_Y \sin \theta_w + C_Z \cos \theta_w) \\
& - ig\xi [(\partial_\mu C_Y^\dagger) \sin \theta_w + (\partial_\mu C_Z^\dagger) \cos \theta_w] (C_- W^{+\mu} + C_+ W^{-\mu}) \quad (3.1.6) \\
& - (ig\xi M_W / 2) G^0 (C_+^\dagger C_+ - C_-^\dagger C_-) - g\xi M_W \sin \theta_w (C_+^\dagger G^+ + C_-^\dagger G^-) C_Y \\
& + (g\xi M_W / 2 \cos \theta_w) [C_Z^\dagger (C_+ G^- + C_- G^+) - (2 \cos^2 \theta_w - 1) (C_+^\dagger G^+ + C_-^\dagger G^-) C_Z] \\
& - ig\xi [(\partial_\mu C_+^\dagger) C_+ - (\partial_\mu C_-^\dagger) C_-] (A^\mu \sin \theta_w - Z^\mu \cos \theta_w)
\end{aligned}$$

The 't Hooft-Feynman gauge will be chosen. Combining all the pieces together, the supersymmetric standard model Lagrangian is just

$$\mathcal{L}_{SS} = \mathcal{L}_{\text{gauge}} + \mathcal{L}_Y + \mathcal{L}_S + \mathcal{L}_{GF} + \mathcal{L}_{FP} \quad (3.1.7)$$

The above interaction Lagrangian is globally supersymmetric. To be phenomenologically realistic, the supersymmetry must be broken. This can be achieved by soft breaking terms [22] which are thought to be induced by supergravity at the scale of the Planck mass, M_p . The effective low energy (i.e. below the Planck mass) Lagrangian that breaks supersymmetry can be written as [23,24]

$$\begin{aligned} \mathcal{L}_{SSB} = & -\frac{1}{2}\tilde{m}'(\lambda'\lambda' + \bar{\lambda}'\bar{\lambda}') - \frac{1}{2}\tilde{m}(\lambda^a\lambda^a + \bar{\lambda}^a\bar{\lambda}^a) \\ & - \sum_A m_A^2 A^* A - m_{3/2}(h(Z) + \text{h.c.}) \end{aligned} \quad (3.1.8)$$

where

$$h(Z) = (A-3)g(Z) + \sum_A \frac{\partial g}{\partial Z_A} Z_A \quad (3.1.9a)$$

and

$$\begin{aligned} g = & (h\epsilon_{ij} H_1^i H_2^j N + sN) + f_e \epsilon_{ij} H_1^i \tilde{L}^j \tilde{e}_R \\ & + h_d \epsilon_{ij} H_1^i \tilde{Q}_L^j \tilde{d}_R + h_u \epsilon_{ij} H_2^i \tilde{Q}_L^j \tilde{u}_R + \text{h.c.} \end{aligned} \quad (3.1.9b)$$

As before the sum over A represents a sum over all scalar fields. The gaugino masses \tilde{m}' and \tilde{m} as well as the gravitino mass $m_{3/2}$ are free parameters. Equation (3.1.9a) contains terms that split the degeneracy in the masses of the sfermions and fermions. Because of the simplicity and the added attraction of having a structure close to the unbroken supersymmetric model, it is usual [23] to take the parameter in equation (3.1.9a) to be $A=3$.

It is often argued that the gaugino and the scalar masses can be taken to be all equal to the $m_{3/2}$ at the Planck scale. However, there are many uncalculable effects involving gravitons in the high energy theory and it is not clear that a common mass can still be maintained at low energies. Hence the m_A 's are different in general. Hereafter, these parameters will

carry subscripts denoting their particle species. Thus m_N , m_{H_1} , m_{H_2} , etc. will be the bare mass terms of the scalar fields N , H_1 , H_2 , etc. respectively.

The gauge symmetry breaking is achieved by letting the three sets of Higgs fields, H_1 , H_2 and N develop vacuum expectation values (VEV's), given by

$$\langle H_1 \rangle = \begin{pmatrix} \frac{v_1}{\sqrt{2}} \\ 0 \end{pmatrix} \quad (3.1.10a)$$

$$\langle H_2 \rangle = \begin{pmatrix} 0 \\ \frac{v_2}{\sqrt{2}} \end{pmatrix} \quad (3.1.10b)$$

$$\langle N \rangle = \frac{v_3}{\sqrt{2}} \quad (3.1.10c)$$

As was done in the Two-Higgs-Doublet model, a set of constraint equations on the VEV's can then be obtained by minimizing the scalar potential contained in equations (3.1.4) and (3.1.8). They are

$$m_{3/2} \left(\frac{3}{2} h v_1 v_2 + s \right) + \frac{v_3}{\sqrt{2}} \left(m_N^2 + \frac{h^2}{2} v^2 \right) = 0 \quad (3.1.11a)$$

$$\frac{3}{\sqrt{2}} m_{3/2} h v_2 v_3 + m_{H_1}^2 v_1 + \frac{h}{2} [h v_1 (v_2^2 + v_3^2) + 2s v_2] + \frac{1}{8} g^2 v_1 (v_1^2 - v_2^2) = 0 \quad (3.1.11b)$$

$$\frac{3}{\sqrt{2}} m_{3/2} h v_1 v_3 + m_{H_2}^2 v_2 + \frac{h}{2} [h v_2 (v_1^2 + v_3^2) + 2s v_1] - \frac{1}{8} g^2 v_2 (v_1^2 - v_2^2) = 0 \quad (3.1.11c)$$

where

$$v^2 = v_1^2 + v_2^2 \quad (3.1.12)$$

and

$$\bar{g}^2 = g^2 + g'^2 \quad (3.1.13)$$

In the limit that $v_1=v_2 \neq 0$, taking the difference of equations (3.1.11b) and (3.1.11c) gives

$$(m_{H_1}^2 - m_{H_2}^2)v_1 = 0 \quad (3.1.14)$$

Hence it is necessary for the 'bare' masses of H_1 and H_2 to be equal if they are to develop the same VEV. The special case where $v_1=v_2=a$ and $m_{H_1}=m_{H_2}=m_N=m_{3/2}$ is solved in reference [23]. A particularly simple solution in this limit is given by

$$v_3 = - \frac{\sqrt{2}}{h} m_{3/2} \quad (3.1.15a)$$

$$a = \sqrt{2} \frac{m_{3/2}}{h} \left(1 - \frac{sh}{m_{3/2}^2} \right)^{1/2} \quad (3.1.15b)$$

Next the phenomenologically more interesting case of $v_1 \neq v_2$ is investigated. For this case, the constraint equations can be recast into the following forms

$$\frac{3}{\sqrt{2}} m_{3/2} h v_3 - \frac{1}{4} \overrightarrow{g^2} v_1 v_2 + \frac{h}{2} (h v_1 v_2 + 2s) = \frac{m_{H_2}^2 - m_{H_1}^2}{v_2 - v_1} v_1 v_2 \quad (3.1.16a)$$

$$\frac{1}{2} (h^2 v_3^2 + \frac{1}{4} \overrightarrow{g^2} v^2) (v_1^2 - v_2^2) + \frac{m_{H_1}^2}{2} v_1^2 - \frac{m_{H_2}^2}{2} v_2^2 = 0 \quad (3.1.16b)$$

$$\frac{3}{\sqrt{2}} m_{3/2} h v_3 + \frac{1}{2} h (h v_1 v_2 + 2s) + \frac{v_1 v_2}{v^2} (m_{H_1}^2 + m_{H_2}^2 + h^2 v_3^2) = 0 \quad (3.1.16c)$$

which are useful in simplifying the mass matrix for the Higgs bosons.

Equations (3.1.16) simplify for the case $m_{H_1} = m_{H_2} = m$ in the non-degenerate VEV region. In particular equation (3.1.16b) becomes

$$h^2 v_3^2 + 2m^2 = -\frac{1}{4} \overrightarrow{g^2} v^2 \quad (3.1.16b')$$

The three Higgs fields H_1 , H_2 and N are not the physical mass eigenstates and a diagonalization has to be performed. There are six neutral spin-0 fields given by the real and imaginary parts of the three

Higgs fields; explicitly they are given by

$$H_1 = \left(\frac{v_1 + \text{Re}H_1^0 + i\text{Im}H_1^0}{\sqrt{2}}, H_1^2 \right) \quad (3.1.17a)$$

$$H_2 = \left(H_2^1, \frac{v_2 + \text{Re}H_2^0 + i\text{Im}H_2^0}{\sqrt{2}} \right) \quad (3.1.17b)$$

$$N = \frac{1}{\sqrt{2}} (v_3 + \text{Re}N + i\text{Im}N) \quad (3.1.17c)$$

The superscripts on the H-fields are SU(2) indices. Two charged scalars form the following combinations

$$H^+ \equiv \frac{1}{v} (v_1 H_2^1 + v_2 H_1^{2*}) \quad (3.1.18)$$

$$G^+ \equiv \frac{1}{v} (v_2 H_2^1 - v_1 H_1^{2*}) \quad (3.1.19)$$

with H^- and G^- given by the conjugates of equations (3.1.18) and (3.1.19).

The physical charged Higgs fields are H^\pm . The G^\pm are the would-be Goldstone bosons which enter in the gauge-fixing conditions for the W-bosons given by

$$\partial_\mu W^{\mu+} = \frac{ig}{2\xi} v G^+ \quad (3.1.20a)$$

$$\partial_\mu W^{\mu-} = \frac{ig}{2\xi} v G^- \quad (3.1.20b)$$

where ξ is the gauge fixing parameter. Noting that $M_W^2 = g^2 v^2 / 4$, equations (3.1.20) are seen to be the usual gauge conditions for the standard model.

For the 't Hooft-Feynman gauge $\xi=1$. The combinations in equations (3.1.18-19) can be shown to diagonalize the charged scalar mass matrix when the constraint equations (3.1.16) are used. The unphysical bosons G^\pm have mass M_w in the 't Hooft-Feynman gauge as expected. The mass of the physical charged scalars is given by

$$M_{H^\pm}^2 = h^2 v_3^2 + m_{H_1}^2 + m_{H_2}^2 + M_w^2 \quad (3.1.21)$$

for the general case of $v_1 \neq v_2$. This equation further limits the allowed values for m_{H_1} and m_{H_2} . One example is the case where $v_1 \neq v_2$ and $m_{H_1} = m_{H_2}$.

Using equation (3.1.16b') gives

$$M_{H^\pm}^2 = -\frac{1}{4} g'^2 v^2 \quad (3.1.21')$$

and hence if the effective Lagrangian is not to give unphysical masses to the charged Higgs bosons, then $m_{H_1} \neq m_{H_2}$ in the region where $v_1 \neq v_2$.

It is instructive to consider the case of degenerate VEV's, i.e. $v_1 = v_2$. Further simplification is made by the choice of

$$M_{H_1} = M_{H_2} = m_{3/2} \quad (3.1.22)$$

and the solution of equation (3.1.15a). Then we obtain

$$M_{H^\pm}^2 = 4m_{3/2}^2 + M_w^2 \quad (3.1.23)$$

Thus the simplest solutions lead to the conclusion that the charged Higgs boson is heavier than the W-boson quite independent of the coupling parameters in the scalar potential. It must be emphasized that this need not be true in general for $v_1 \neq v_2$ and $m_{H_1} \neq m_{H_2}$.

The six neutral spin-0 bosons consist of three scalars and three pseudoscalars. One of the pseudoscalars is the would-be Goldstone boson which gives mass to the Z^0 , and it is given by

$$G^0 = \frac{1}{v} (v_2 \text{Im}H_2^0 - v_1 \text{Im}H_1^0) \quad (3.1.24a)$$

Orthogonal to G^0 is a pseudoscalar h_4^0 ; explicitly written as

$$h_4^0 = \frac{1}{v} (v_1 \text{Im}H_2^0 + v_2 \text{Im}H_1^0) \quad (3.1.24b)$$

and a third pseudoscalar $\text{Im}N$. In this basis G^0 decouples from the other two and only plays the role in Z^0 gauge fixing, i.e. terms like $G^0 h_4^0$ and $G^0 \text{Im}N$ are rotated away. However, the mass matrix of the two remaining 0^- bosons is still not diagonal. As usual the diagonalization is achieved by a rotation, leading to the two physical pseudoscalars, H_4^0 and H_5^0 , below.

$$H_4^0 = h_4^0 \cos x - \text{Im}N \sin x \quad (3.1.25a)$$

$$H_5^0 = h_4^0 \sin x + \text{Im}N \cos x \quad (3.1.25b)$$

The mixing angle x can be obtained in terms of the scalar potential parameters via

$$\tan 2x = \frac{6h m_{3/2} v}{\sqrt{2} \{h^2 v_3^2 + (m_{H_1}^2 + m_{H_2}^2 - m_N^2)\}} \quad (3.1.26)$$

In the degenerate VEV case with $m_{H_1} = m_{H_2} = m_N = m_{3/2}$ and solution (3.1.15a), this reduces to

$$\tan 2x = \frac{\sqrt{2} h M_W}{g m_{3/2}} \quad (3.1.26')$$

The pseudoscalar masses are given by

$$M_4^2 = (h^2 v_3^2 + m_{H_1}^2 + m_{H_2}^2 + \frac{1}{2} h^2 v^2) \cos^2 x + (\frac{1}{2} h^2 v^2 + m_N^2) \sin^2 x + \frac{6}{\sqrt{2}} h m_{3/2} v \cos x \sin x \quad (3.1.27a)$$

$$M_5^2 = (h^2 v_3^2 + m_{H_1}^2 + m_{H_2}^2 + \frac{1}{2} h^2 v^2) \sin^2 x + (\frac{1}{2} h^2 v^2 + m_N^2) \cos^2 x - \frac{6}{\sqrt{2}} h m_{3/2} v \cos x \sin x \quad (3.1.27b)$$

which satisfy the sum rule

$$M_4^2 + M_5^2 = h^2 (v_3^2 + v^2) + m_{H_1}^2 + m_{H_2}^2 + m_N^2 \quad (3.1.28)$$

The remaining degrees of freedom are the scalar (0^+) fields $\text{Re}H_1^0$, $\text{Re}H_2^0$ and $\text{Re}N$ which again have a non-diagonal mass matrix. The physical mass eigenstates shall be denoted by H_i^0 with eigenvalues M_i (where $i=1,2,3$), and they are obtained from the above by a unitary transformation

$$H_i = U_{ij} \text{Re}H_j^0 \quad (3.1.29)$$

In equation (3.1.29) it is understood that $\text{Re}N$ is to be substituted for $j=3$. In general the elements of U are complicated functions of the VEV's and the bare scalar masses. These will not be examined here as they are not particularly illuminating. However, the interesting sum rule

$$\sum_{i=1}^3 M_i^2 = M_4^2 + M_5^2 \quad (3.1.30)$$

should be noted. Phenomenologically the U_{1j} can be treated as free parameters. From the above discussion one would expect that these spin-0 bosons have masses of the order of M_w or $m_{3/2}$, unless the transformation parameters are wildly different.

In addition to the mixing in the Higgs sector, the scalar fermions will also mix to a certain extent. Attention is focused in particular on the scalar t-quarks, since they will be the only relevant ones contributing to the 2γ -decay width calculation. A mixing between the distinct states \tilde{t}_L and \tilde{t}_R arises from the last term in equation (3.1.9b) when H_2 develops a VEV. The mass matrix for \tilde{t}_L and \tilde{t}_R is given by

$$\begin{pmatrix} m_R^2 & m_t(m_{3/2} + \frac{hv_1}{v_2} v_3) \\ m_t(m_{3/2} + \frac{hv_1}{v_2} v_3) & m_L^2 \end{pmatrix} \quad (3.1.31a)$$

where

$$m_R^2 = \frac{1}{6} g'^2 (v_1^2 - v_2^2) + m_{BR}^2 \quad (3.1.31b)$$

and

$$m_L^2 = \frac{1}{24} g'^2 (v_1^2 - v_2^2) + m_{BL}^2 \quad (3.1.31c)$$

with m_t being the fermion t-quark mass and $m_{B,R(L)}$ the bare mass appearing in \mathcal{L}_{SSB} . In general $m_{BR} \neq m_{BL}$. The mixing angle $\tilde{\theta}$ between \tilde{t}_L and \tilde{t}_R can be deduced from equation (3.1.31) giving

$$\tan 2\tilde{\theta} = \frac{16m_{3/2}m_t}{8(m_{BR}^2 - m_{BL}^2) + (g'^2 - g^2)(v_1^2 - v_2^2)} \quad (3.1.32)$$

In the symmetrical case of $v_1 = v_2$ and $m_{BR}^2 = m_{BL}^2$ then $\tilde{\theta} = \pi/4$. In general however $v_1 \neq v_2$ and $m_{BR}^2 \neq m_{BL}^2$. If one takes $m_{BR} = m_{3/2}$ then $\tilde{\theta}$ is of the order of $\tan^{-1} [m_t / m_{3/2}]$. Preliminary data from CERN [25] indicates that $20 < m_t < 50 \text{ GeV}/c^2$ and it is possible that $m_{3/2}$ can be a few times heavier than M_W . Thus $\tilde{\theta}$ is generally quite small even for the scalar t-quarks. For simplicity this small mixing is neglected, and the scalar quarks \tilde{t}_L and \tilde{t}_R are treated as mass eigenstates.

There is yet a third set of mixed states that are important in the 2γ -decay width calculation. These are the states formed from the mixing of the W-gauginos and charged Higgsinos. In the Lagrangian [see eq. (3.1.2)] the charged gauginos and Higgsinos are represented by Majorana spinors λ^\pm and $\psi_{H_1}^1$ and $\psi_{H_2}^2$, respectively with

$$\lambda^\pm = (\lambda^1 \mp i\lambda^2)/\sqrt{2} \quad (3.1.33)$$

Again they are not the physical mass eigenstates. These physical states are

constructed explicitly as follows:

$$\chi_1 = \begin{pmatrix} -i\lambda^+ \cos\phi_+ + \psi_{H_2}^1 \sin\phi_+ \\ i\lambda^- \cos\phi_- + \bar{\psi}_{H_1}^2 \sin\phi_- \end{pmatrix} \quad (3.1.34a)$$

$$\chi_2 = \begin{pmatrix} -i\lambda^+ \sin\phi_+ - \psi_{H_2}^1 \cos\phi_+ \\ -i\lambda^- \sin\phi_- + \bar{\psi}_{H_1}^2 \cos\phi_- \end{pmatrix} \quad (3.1.34b)$$

Notice that there are two separate mixing angles ϕ_+ and ϕ_- .

One can read off directly from equations (3.1.2) and (3.1.8) the mass terms involving the W-gauginos and charged Higgsinos. Diagonalization is achieved using equation (3.1.34), which then gives the mixing angles ϕ_{\pm} and the masses $\tilde{M}_{1,2}$ of the two physical chargino states χ_1 and χ_2 respectively. In terms of the parameters appearing in the Lagrangian, these angles are given by

$$\sin 2\phi_{\pm} = \frac{\tilde{m}}{\sqrt{2M_w}} \frac{[(1+\sin 2\alpha)^{1/2} \pm (1-\sin 2\alpha)^{1/2}]}{\left\{ \left(1 + \frac{\tilde{m}^2}{2M_w^2}\right)^2 - \sin^2 2\alpha \right\}^{1/2}} \quad (3.1.35)$$

where

$$\tan \alpha \equiv v_1 / v_2 \quad (3.1.35')$$

This result agrees with that presented in a different form in reference [19]. For $v_1 \gg v_2$ or $v_2 \gg v_1$ the angles become

$$\sin 2\phi_+ = \frac{\sqrt{2} \tilde{m}}{M_w \left(1 + \frac{\tilde{m}^2}{2M_w^2}\right)} \quad (3.1.36a)$$

and

$$\phi_- \approx 0 \quad (3.1.36b)$$

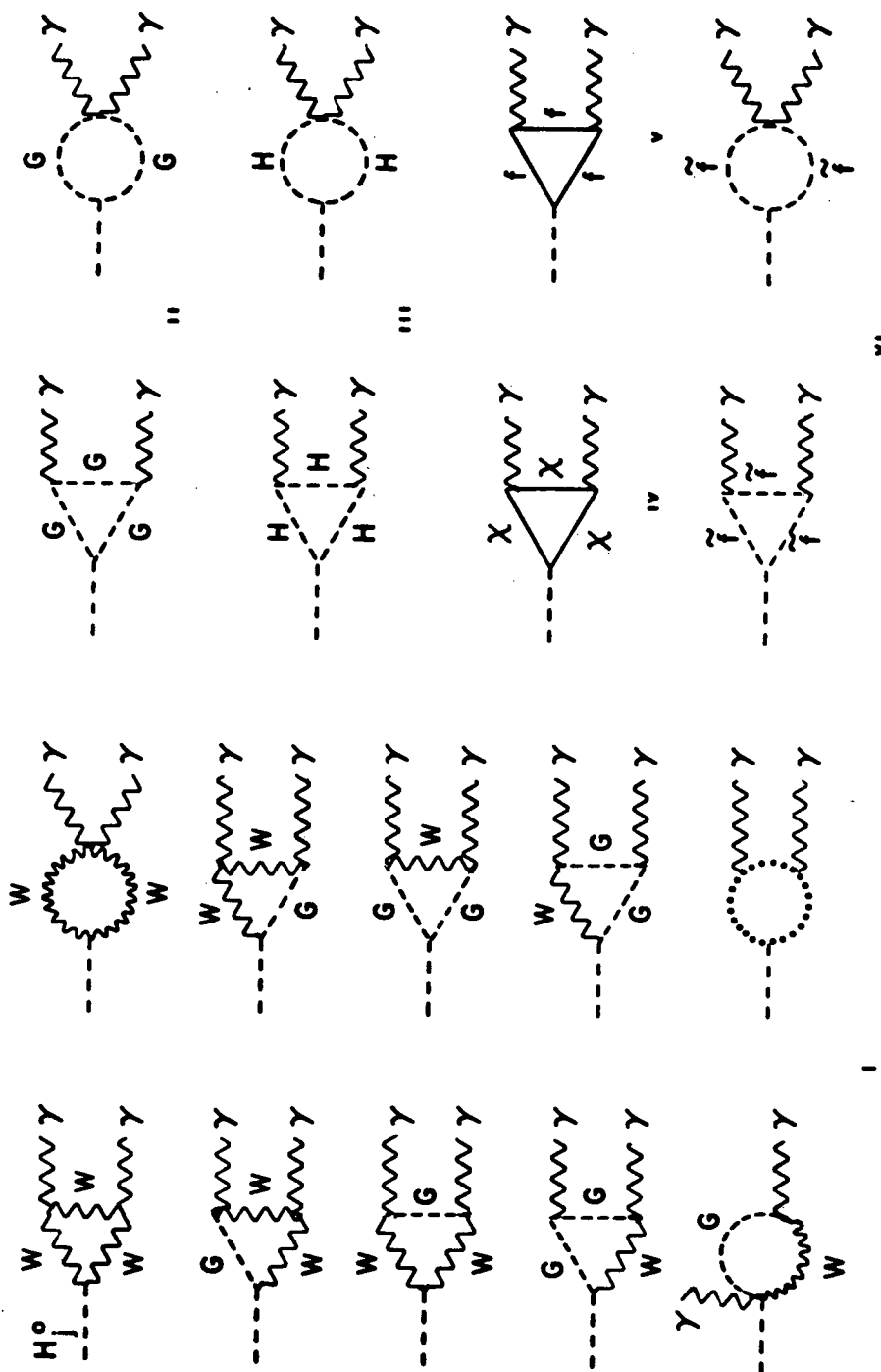
On the other hand with equal VEV's the angles become equal $\phi_+ = \phi_- = \phi$ and equation (3.1.35) reduces to

$$\sin^2 2\phi = \left(1 + \frac{\tilde{m}^2}{4M_w^2}\right)^{-1} \quad (3.1.37)$$

The calculation also yields the masses \tilde{M}_1 and \tilde{M}_2 . These are written explicitly as

$$\tilde{M}_{1,2} = \frac{1}{\sqrt{2}} M_w \left[\left(1 + \sin 2\alpha + \frac{\tilde{m}^2}{2M_w^2}\right)^{1/2} \pm \left(1 - \sin 2\alpha + \frac{\tilde{m}^2}{2M_w^2}\right)^{1/2} \right] \quad (3.1.38)$$

This completes the discussion on the physical states which will appear in the 2γ -decay width calculation for the minimal broken supersymmetric model. The detailed Feynman rules which are obtained from the Lagrangian are given in appendix E.

Figure 1 - One Loop Contributions to the 2γ -Decay of the Scalar H_j^0 

The diagrams are grouped into separately gauge invariant sets. (I) gauge boson, would-be Goldstone boson, and ghost loops (II) would-be Goldstone boson loops (III) physical charged Higgs boson loops (IV) charginos loops (V) fermion loops (VI) scalar-fermion loops

3.2 One Loop Calculation of $X^0 \rightarrow \gamma\gamma$

The Feynman rules listed in Appendix E are used to calculate the matrix elements which contribute to the two photon decay widths of the spin-0 bosons, denoted by X^0 , in the one-loop approximation. The internal loops for all of the scalar H_j^0 decays consist of fermion and scalar fermions, gauge bosons and gauginos, and physical charged Higgs bosons. The would-be Goldstone boson and Fadeev-Popov ghost loops are also included. The one-loop contribution to the two photon decays of the scalar H_j^0 are displayed in six sets of diagrams in figure 1. Each set is separately gauge invariant. Set 1 is the gauge boson loop contribution, denoted by a_{jw} , and includes mixed would-be Goldstone bosons-gauge bosons and Fadeev-Popov ghosts. Set 2 is denoted by a_{jG} and consists only of full would-be Goldstone boson loops. Both of these sets have the same structure as in standard model Higgs boson to two photon decays [6]. In addition there are contributions from loops containing the physical charged Higgs boson, H^\pm , and the charginos, χ_i^\pm ($i=1,2$). These are sets 3 and 4, contributing amounts a_{jH} and $a_{j\chi_{1,2}}$ respectively. If the Yukawa couplings are non-vanishing then the fermion loops of set 5 will give the a_{jf} . Finally set 6 shows the scalar-fermion contribution $a_{j\tilde{f}}$, which contains both gauge and Yukawa pieces. As noted in the previous section, the small mixing between left and right types of scalar-fermions has been neglected for simplicity. Combining all the contributions, the matrix elements for the scalar H_j^0 ($j=1,2,3$) decays into two photons with polarization vectors e_μ^1 and e_ν^2 are presented below. The details of the calculation are given by combining the Feynman rules of appendix E with the calculational techniques of appendix B. The results are

$$a_j = (a_{j_w} + a_{j_G} + a_{j_{\chi_1}} + a_{j_{\chi_2}} + a_{j_H} + a_{j_f} + a_{j_{\tilde{f}}}) N^{\mu\nu} e_\mu^1 e_\nu^2 \quad (3.2.1)$$

$$\text{with } a_{j_w} = \frac{ie^2 g M_w}{(4\pi)^2} [6 + (-8 + 12\lambda_w) I(\lambda_w)] \left[\frac{v_1 U_{1j} + v_2 U_{2j}}{v} \right] \quad (3.2.2)$$

$$a_{j_G} = \frac{ie^2 g M_j^2}{(4\pi)^2 M_w} [1 + 2\lambda_w I(\lambda_w)] \left[\frac{v_1 U_{1j} + v_2 U_{2j}}{v} \right] \quad (3.2.3)$$

$$a_{j_{\chi_{1/2}}} = - \frac{2\sqrt{2} ie^2 g \tilde{M}_{1/2}}{(4\pi)^2} [2 + (4\lambda_{1/2} - 1) I(\lambda_{1/2})] [s_{\mp} c_{\pm} U_{1j} + s_{\pm} c_{\mp} U_{2j}] \quad (3.2.4)$$

$$a_{j_H} = \frac{2ie^2 g M_w}{(4\pi)^2} [1 + 2\lambda_H I(\lambda_H)] \left\{ \left(1 - \frac{1}{2}\lambda_w^{-1}\right) \left(\frac{v_1 U_{1j} + v_2 U_{2j}}{v}\right) + \frac{2h^2 v_3 U_{3j}}{g M_w} \right\} \quad (3.2.5)$$

$$a_{j_f} = - \sum_f \frac{2ige^2 e_f^2 m_f^2 c_f v}{(4\pi)^2 M_w} [2 + (4\lambda_f - 1) I(\lambda_f)] v^f \quad (3.2.6)$$

$$a_{j_{\tilde{f}}} = - \sum_f \frac{2ie^2 e_f^2 c_f}{(4\pi)^2} [1 + 2\lambda_{\tilde{f}} I(\lambda_{\tilde{f}})] \left\{ \frac{g^2 (v_2 U_{2j} - v_1 U_{1j})}{2\cos^2\theta_w} N_{L(R)}^{\tilde{f}} - 2m_f^2 v_{\tilde{f}} \right\} \quad (3.2.7)$$

$$\text{where } v^{f(\tilde{f})} = \frac{1}{v_1} U_{1j} \text{ for } f=d\text{-fermions (sfermions)} \quad (3.2.8a)$$

$$= \frac{1}{v_2} U_{2j} \text{ for } f=u\text{-fermions (sfermions)} \quad (3.2.8b)$$

Furthermore,

$$N_L^{\tilde{f}} = \frac{1}{2} \eta_f - e_f \sin^2\theta_w, \quad N_R^{\tilde{f}} = e_f \sin^2\theta_w \quad (3.2.9)$$

and

$$\lambda = m^2/M_j^2 \quad (3.2.10)$$

The subscript of the λ 's corresponds to the mass of the internal loop particle. Here η_f is +1 (-1) for up (down) type sfermions. Also s_{\pm} , c_{\pm} denote $\sin\phi_{\pm}$, $\cos\phi_{\pm}$ respectively [see eq. (3.1.34)]. The colour factor c_f is 3 for quarks and 1 for leptons. The gauge invariant quantity $N_{\mu\nu}$ is

$$N_{\mu\nu} = \left[g_{\mu\nu} - \frac{p_{\nu} q_{\mu}}{p \cdot q} \right] \quad (3.2.11)$$

where p and q are the photon momenta, of the first and second photon respectively, and

$$I(\lambda) = \int_0^1 dx \frac{1}{x} \ln \left[1 - \frac{1}{\lambda} x(1-x) \right] \quad (3.2.12)$$

The function $\lambda I(\lambda)$ has a very weak dependence on λ for values of $\lambda \gg 1/4$. This dependence is shown in appendix D.

Similarly the matrix elements for the two photon decays of the pseudoscalars H_4^0 and H_5^0 are computed. The diagrams which contribute are displayed in figure 2, and consist only of fermion and gaugino loops. The matrix elements for the pseudoscalar H_k^0 ($k=4,5$) are

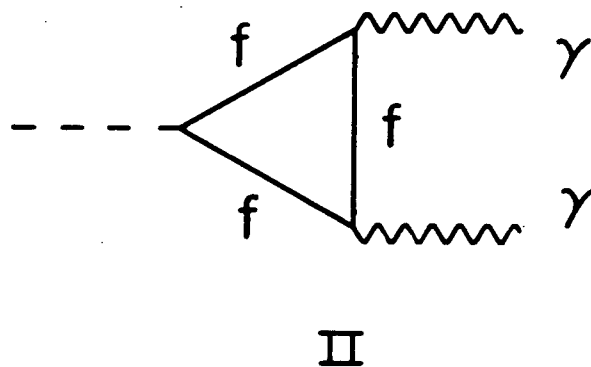
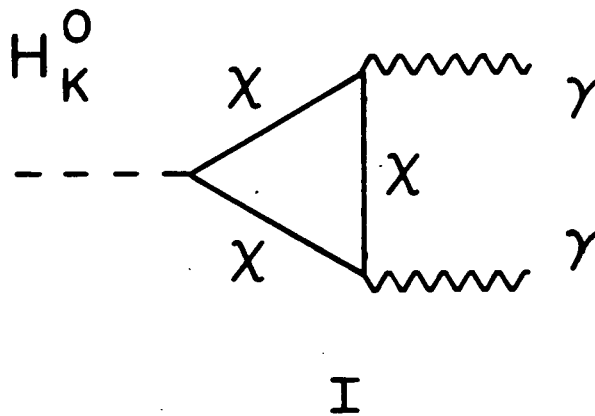
$$a_k = (a_{k\chi_1} + a_{k\chi_2} + a_{kf}) N_{ps}^{\mu\nu} e_1^1 e_2^2 \quad (3.2.13)$$

$$\text{with } a_{k\chi_2} = \frac{4\sqrt{2} e^2 g \tilde{M}_2}{(4\pi)^2 v} (v_2 s_{\mp} c_{\pm} + v_1 s_{\pm} c_{\mp}) I(\lambda_2) \eta_k \quad (3.2.14)$$

$$a_{kf} = - \sum_f \frac{4e^2 e_f^2 g m_f^2 c_f}{(4\pi)^2 M_w} \left(\frac{v_1}{v_2} \right)^{\eta_f} I(\lambda_f) \eta_k \quad (3.2.15)$$

$$\text{where } N_{ps}^{\mu\nu} = \epsilon^{\mu\nu\rho\omega} \frac{p_{\rho} q_{\omega}}{2p \cdot q} \quad (3.2.16)$$

and η_k is $\cos x$ ($\sin x$) for $k=4$ (5).

Figure 2 - One Loop Contributions to the 2γ -Decay of the Pseudoscalar H_k^0 

(I) chargino loops (II) fermion loops

The above gives the general amplitudes for scalar or pseudoscalar Higgs boson to two photon decays in broken supersymmetric theory, calculated with component field techniques. (Note that these remain non-vanishing in the supersymmetric limit [21]). Obviously these amplitudes contain many unknown parameters such as mixing angles and masses of unseen particles. In the next two sections are some reasonable simplifying assumptions, and an estimate of the widths. Also examined carefully is the allowed enhancement of these widths in broken supersymmetric gauge theories.

3.3 Pseudoscalar Widths of $X^0 \rightarrow \gamma\gamma$

The pseudoscalar widths of $X^0 \rightarrow \gamma\gamma$ can now be calculated from the results presented in the last section. However, first one must establish a range for the many parameters appearing in the amplitudes. The two extreme cases for the ratio of the two VEV's, v_1 and v_2 , are denoted as case A for $v_1 \gg v_2$ and case B for $v_1 = v_2$.

In case A, the mixings of the charginos are given by equation (3.1.35). Substituting into equations (3.2.15) and (3.2.16) one finds the dominant contributions come from χ_1 and the t-quark; thus for H_4^0 decays

$$a_{\chi_1} = \frac{\sqrt{2} e^2 g \tilde{M}_1}{4\pi^2} I(\lambda_{\chi_1}) \cos\alpha \sin\phi_+ \quad (3.3.1)$$

$$a_t = -\frac{e^2 g}{3\pi^2} M_W \tan\alpha \frac{m_t^2}{M_W^2} I(\lambda_t) \cos\alpha \quad (3.3.2)$$

From equation (3.1.26) there is no apparent reason why the mixing between the pseudoscalars should be small. Hence, one expects $\cos\alpha \approx 1/\sqrt{2}$. Notice that the relative phases of a_t and a_{χ_1} are destructive since ϕ_+ is in the

first quadrant. The width for H_4^0 decays is then obtained to be

$$\Gamma(H_4^0 \rightarrow \gamma\gamma) = \frac{\alpha^3 M_W^2 \cos^2 x}{(4\pi)^2 \sin^2 \theta_w M_4} \left[\sqrt{2} \frac{\tilde{M}_1}{M_W} I(\lambda_{\chi_1}) \sin \phi + \frac{4}{3} \tan \alpha \frac{m_t^2}{M_W^2} I(\lambda_t) \right]^2 \quad (3.3.3)$$

The width of the H_5^0 decay is obtained from the above by substituting $\sin x$ for $\cos x$ and M_4 by M_5 .

At first sight, bounds on the magnitude of $\tan \alpha$ can be determined by low energy phenomenology just as in the Two-Higgs-Doublet model. Again this is achieved by examining constraints from Bhabha scattering, muon decays [11,12,13] and the $K_L^0 - K_S^0$ mass difference [14]. Taken together these gave

$$\tan \alpha < 40 \quad (3.3.4a)$$

Moreover, one could also argue for the much more stringent bound of

$$\tan \alpha < 12 \quad (3.3.4b)$$

from theoretical reasons which take into account partial wave unitarity plus perturbation theory [26].

In supersymmetry there is a further constraint on $\tan \alpha$. This is due to the relation between the masses, \tilde{M}_1 and \tilde{M}_2 , and $\tan \alpha$. Now recall from equation (3.1.37) that

$$\tilde{M}_2 = \frac{M_W}{\sqrt{2}} \left[\left(1 + \sin 2\alpha + \frac{\tilde{m}^2}{2M_W^2} \right)^{1/2} \pm \left(1 - \sin 2\alpha + \frac{\tilde{m}^2}{2M_W^2} \right)^{1/2} \right] \quad (3.3.5)$$

For the case of interest, it is easily proven that

$$\tan\alpha = 2M_W^2 / \tilde{M}_1 \tilde{M}_2 \quad (3.3.6)$$

As can be seen in equation (3.3.5), χ_2 is the lighter of the two charginos. It must have a mass greater than 20 GeV/c² in order to agree with e⁺e⁻ experimental data [27]. This then puts

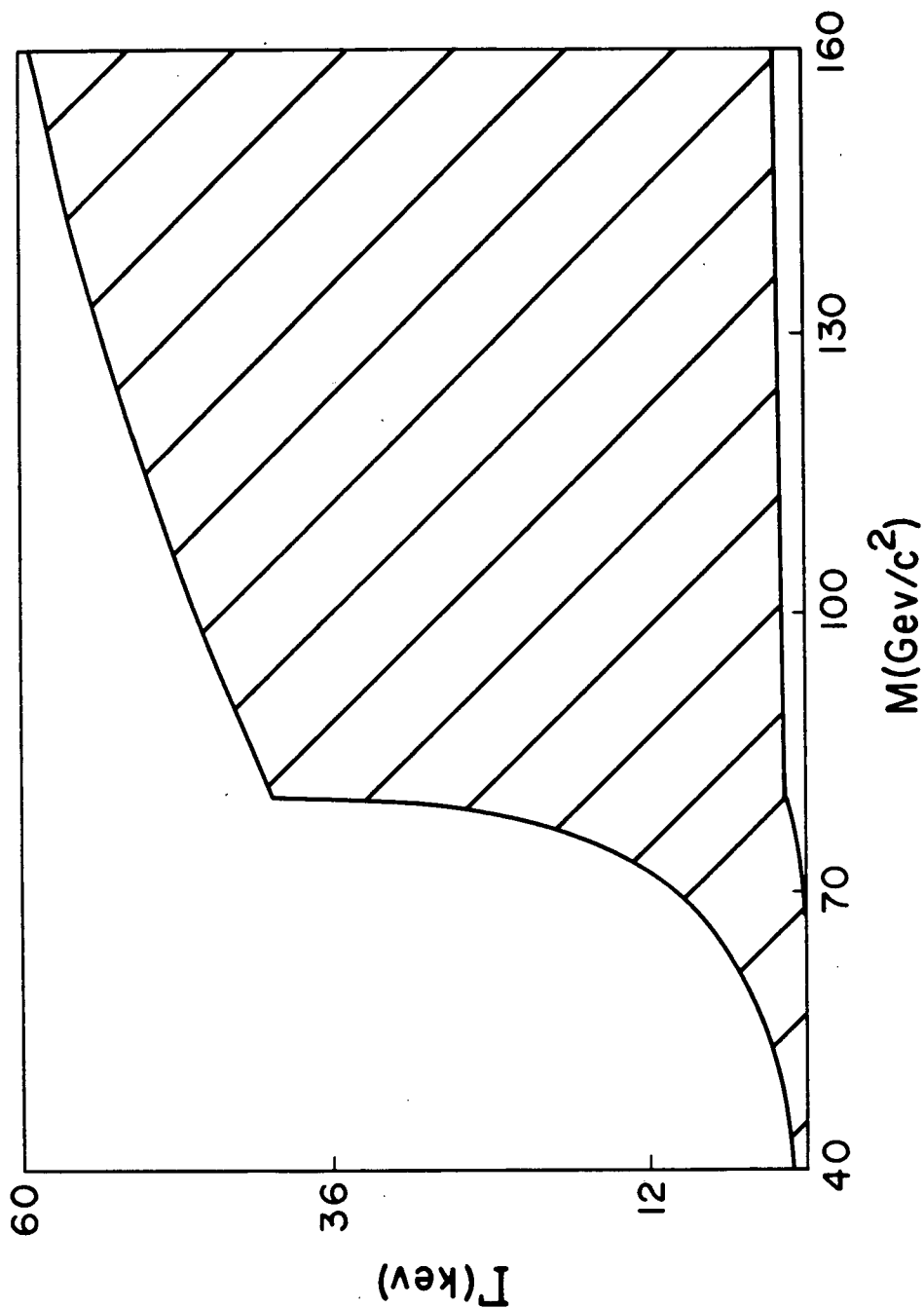
$$\tan\alpha < 8M_W / \tilde{M}_1 \quad (3.3.4c)$$

for $M_W=80$ GeV/c² and $\tilde{M}_2 > 20$ GeV/c². Hence in order to remain in case A, χ_1 must have a mass no more than ~7 times M_W . The consistent range for \tilde{M}_1 would be $\sqrt{2} M_W < \tilde{M}_1 < 7 M_W$. Thus the upper bound becomes

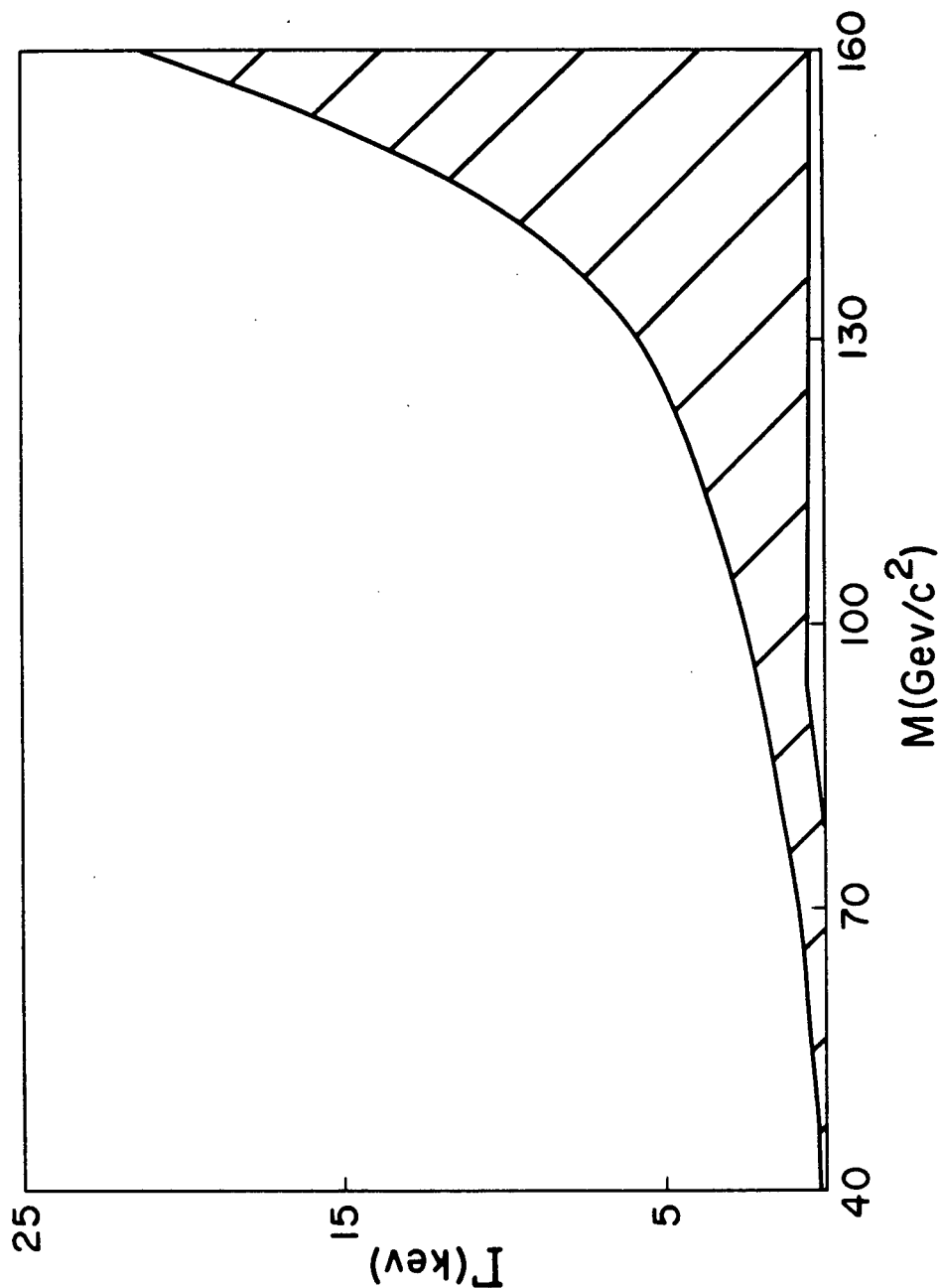
$$\tan\alpha < 5.7 \quad (3.3.4d)$$

Figure 3 displays the width of H_4^0 decaying into two photons as a function of its mass, for the range of allowed χ_1 masses, with the mixing angle α chosen to be $\pi/4$. It is seen that this width is typically of the order of 60 keV or less for an intermediate mass pseudoscalar.

The width is dominated in this case by the t-quark loop contribution. The dependence of $\tan\alpha$ via equation (3.3.4c) on the χ_1 mass is the reason for the large range of possible widths for a given pseudoscalar mass. As the pseudoscalar mass approaches and then crosses the threshold for decay into a pair of real t-quarks ($m_t=40$ GeV/c²), the rise in the width respectively increases sharply and then slows abruptly. In general this type of behaviour will occur whenever the threshold for pair production of a particle which makes an important loop contribution to the decay width is crossed. Similar results hold for H_5^0 decays.

Figure 3 - Pseudoscalar 2γ -Decay Width for Case A

Case A ($v_1 \gg v_2$): two photon decay width as a function of mass for the pseudoscalar H_k^0 ($k=4,5$) with mixing angle $\alpha=\pi/4$, for the range of allowed χ_1 masses.

Figure 4 - Pseudoscalar 2γ -Decay Width for Case B

Case B ($\nu_1 = \nu_2$): two photon decay width as a function of mass for the pseudoscalar H_k^0 ($k=4,5$) with mixing angle $\alpha = \pi/4$, for the range of allowed χ_1 masses.

Next examine case B. With $\alpha = \pi/4$ one obtains again $\phi_+ = \phi_- = \phi$ and explicitly

$$\phi = \frac{1}{2} \sin^{-1} \left[\frac{1}{\left(1 + \frac{\tilde{m}^2}{4M_w^2}\right)^{1/2}} \right] \quad (3.3.7)$$

The masses of the charginos are given by

$$\tilde{M}_{\frac{1}{2}} = M_w \left[\left(1 + \frac{\tilde{m}^2}{4M_w^2}\right)^{1/2} \pm \frac{\tilde{m}}{2M_w} \right] \quad (3.3.8)$$

and they are the order of M_w . Now the two photon widths of H_4^0 and H_5^0 are easily obtained to be

$$\Gamma(H_4^0 \rightarrow \gamma\gamma) = \frac{\alpha^3 M_w^2 \cos^2 x}{(4\pi)^2 \sin^2 \theta_w M_4} \left[\frac{\tilde{M}_1}{M_w} I(\lambda_{\chi_1}) + \frac{\tilde{M}_2}{M_w} I(\lambda_{\chi_2}) \sin 2\phi - \frac{4}{3} \frac{m_t^2}{M_w^2} I(\lambda_t) \right]^2 \quad (3.3.9)$$

and similarly substituting $\sin^2 x$ for $\cos^2 x$ and M_5 for M_4 to get $\Gamma(H_5^0 \rightarrow \gamma\gamma)$.

These widths as a function of their mass, for the range of allowed chargino masses, are plotted in figure 4. Neither χ_1 , χ_2 nor the t-quark loop contributions dominate, since there is no $\tan\alpha$ enhancement.

Consequently the width is much smaller than in case A, i.e. less than 25 keV. The upper bound curve in figure 4 corresponds to both charginos having mass M_w , and hence is sharply peaked near the threshold at $2M_w$.

3.4 Scalar Widths of $X^0 \rightarrow \gamma\gamma$

It is now straightforward to carry out the same analysis for the two photon widths of the scalar Higgs bosons H_j^0 ($j=1,2,3$). For definiteness consider only H_1^0 decays. It is clear that the same analysis can be pushed through almost verbatim for H_2^0 and H_3^0 . Just as in the case of the

pseudoscalars there is no apparent reason for the mixing U_{ij} between these scalars to be small. For simplicity, assume that they are all approximately equal, i.e. $U_{1j} \approx U_{2j} \approx U_{3j} = U = 1/\sqrt{3}$ for $j=1,2,3$.

As seen in figure 1 there are many more internal loop contributions compared to pseudoscalars; hence, more free parameters in the form of internal masses appear. It has already been noted that the combination $\lambda I(\lambda)$ does not vary a great deal over a wide range of values for λ . Thus, one does not expect the two photon widths to be too sensitive to the values chosen for these masses.

Observe that the amplitude due to fermion loops of equation (3.2.6) is dominated by the t-quark for both cases A and B. This is due to the mass of the t-quark being much larger than other fermions in the minimal 3 quark lepton families universe. For case A further enhancement is due to the presence of the V^f factor. Notice that the scalar-fermion loop contribution of equation (3.2.7) is dominated by the scalar-top for both cases A and B. To the extent that $\lambda_f I(\lambda_f)$ is insensitive to the choice of scalar fermion mass, the term involving $N_{L(R)}^{\tilde{f}}$ will give zero when summed over all scalar fermion types. The remaining Yukawa term is proportional to the square of the corresponding fermion mass, and hence the scalar-top dominates. Again in case A there is further enhancement by the $V^{\tilde{f}}$ factor.

Incorporating the above considerations, one finds that for case A the scalar decays have

$$\Gamma(H^0 \rightarrow \gamma\gamma) = \frac{1}{16\pi M} |a_w + a_G + a_{\chi_1} + a_{\chi_2} + a_H + a_t + a_{\tilde{t}}|^2 \quad (3.4.1)$$

where

$$a_w = \frac{ie^2 gM_w}{(4\pi)^2} [6 + (-8+12\lambda_w)I(\lambda_w)]U \quad (3.4.2)$$

$$a_G = \frac{ie^2 gM_w}{(4\pi)^2} [\lambda_w^{-1} + 2I(\lambda_w)]U \quad (3.4.3)$$

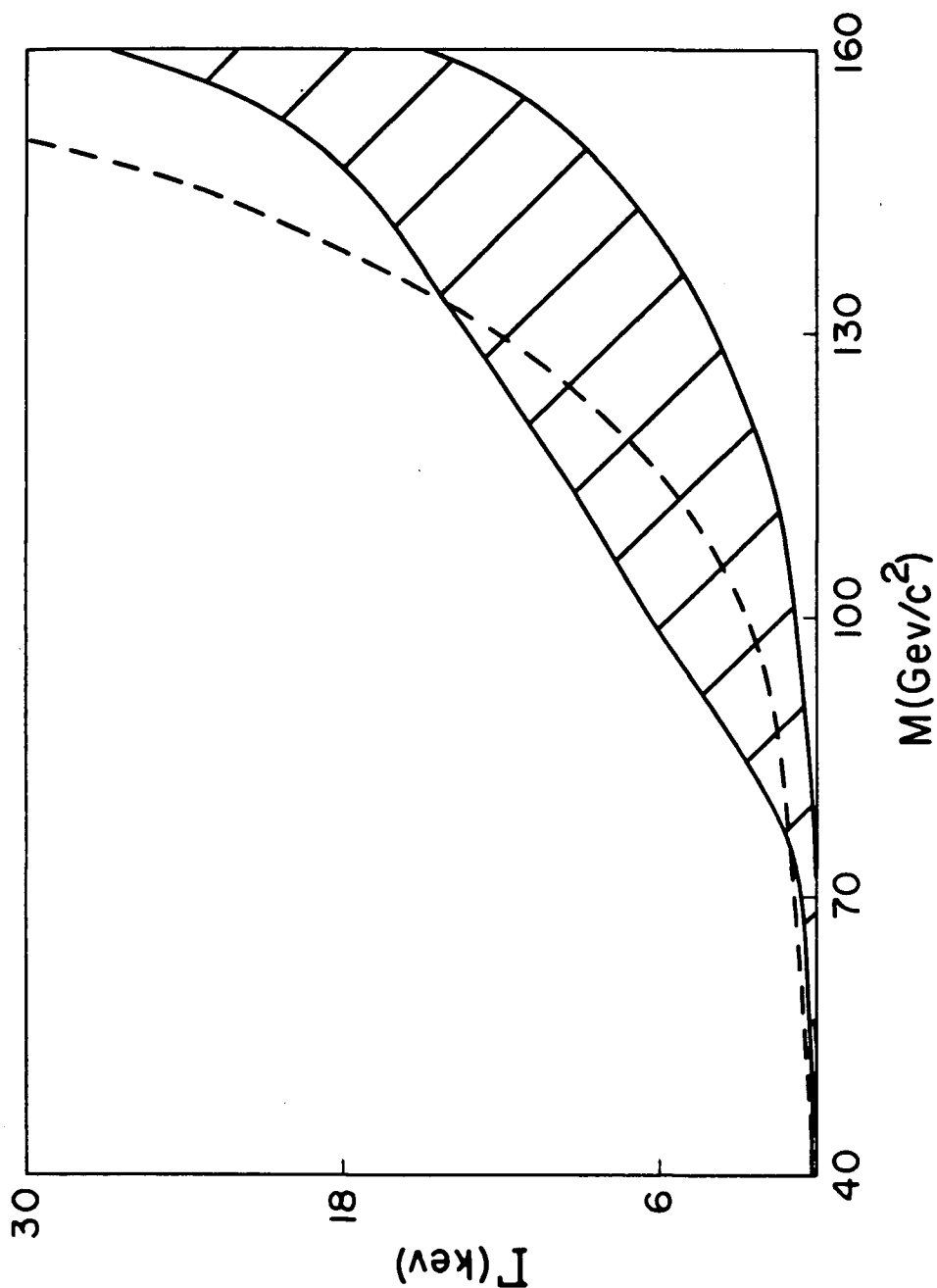
$$a_{\chi_{1/2}} = \frac{-2\sqrt{2}ie^2 g\tilde{M}_{1/2}}{(4\pi)^2} [2 + (4\lambda_{1/2}-1)I(\lambda_{1/2})]U \sin\phi_+ \quad (3.4.4)$$

$$a_H = \frac{2ie^2 M_w}{(4\pi)^2} [1 + 2\lambda_H I(\lambda_H)] \left\{ \left(1 - \frac{1}{2}\lambda_w^{-1}\right) + \frac{2h^2 v_3}{gM_w} \right\} U \quad (3.4.5)$$

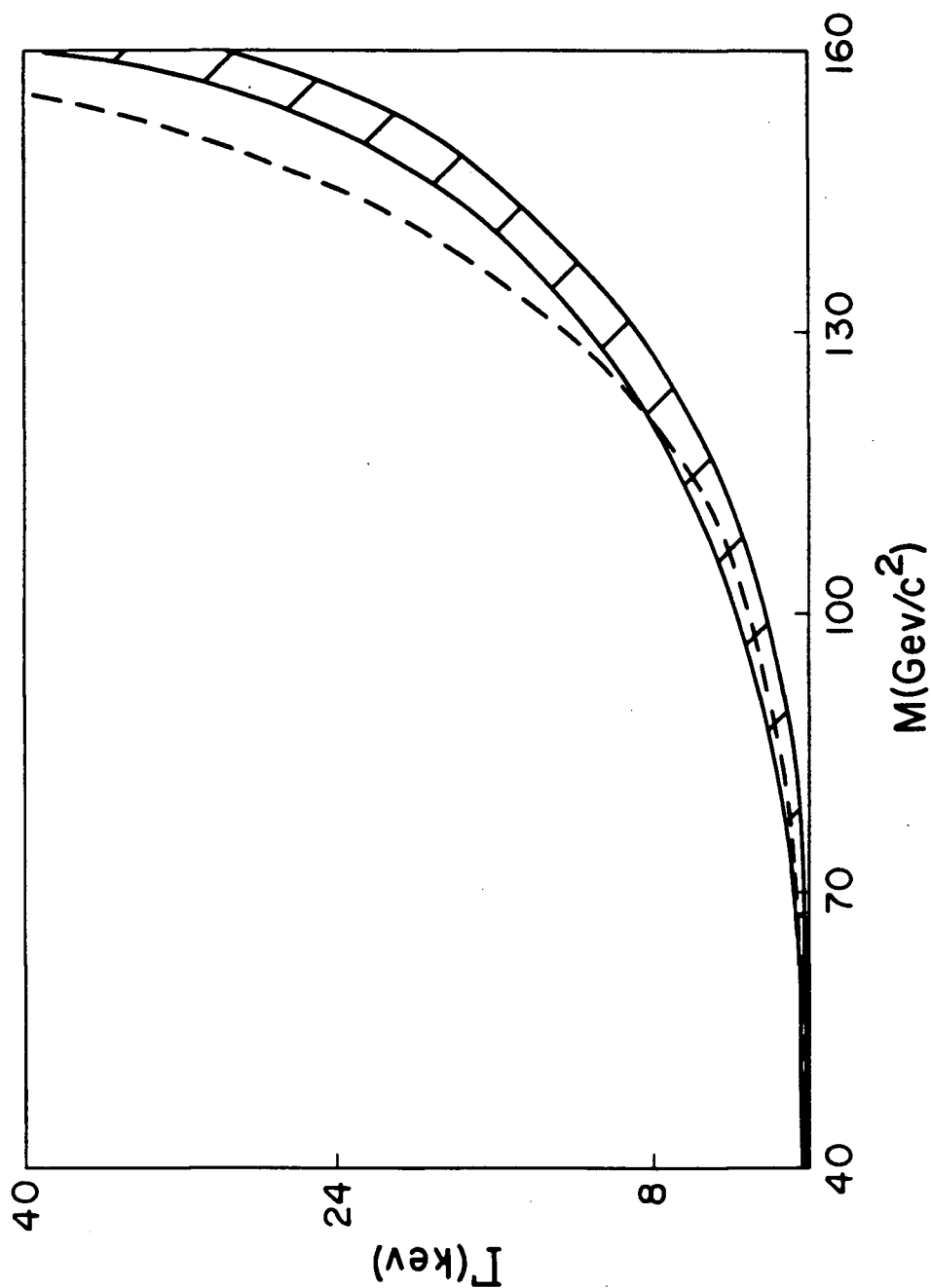
$$a_t = -\frac{8ige^2 m_t^2}{3(4\pi)^2 M_w} [2 + (4\lambda_t-1)I(\lambda_t)]U \tan\alpha \quad (3.4.6)$$

$$a_{\tilde{t}} = \frac{16ie^2 g m_t^2}{3(4\pi)^2 M_w} [1 + 2\lambda_{\tilde{t}} I(\lambda_{\tilde{t}})]U \tan\alpha \quad (3.4.7)$$

This width as a function of the scalar mass is displayed in figure 5. The standard model scalar width is also shown for comparison. The major contributions to the scalar width in this mass range are the t-quark loop, W-gauge boson loop, and to a smaller extent the chargino loops. For larger scalar masses, the scalar-top and charged Higgs loops will also contribute, but only near or above their thresholds. Destructive interference between the t-quark and W-gauge boson loops results in a generally smaller width than in the standard model which by comparison is dominated only by the W-gauge boson loop. All the curves in figure 5 rise sharply near 160 GeV/c², which corresponds to the threshold for W-gauge boson pairs.

Figure 5 - Scalar 2γ -Decay Width for Case A

Case A ($v_1 \gg v_2$): Two photon decay width as a function of mass for the scalar H_j^0 ($j=1,2,3$) with mixing angles $U_{1j}=U_{2j}=U_{3j}=1/\sqrt{3}$, for the range of allowed χ_1 masses. The broken curve shows the standard model Higgs boson width for comparison.

Figure 6 - Scalar 2γ -Decay Width for Case B

Case B ($v_1=v_2$): Two photon decay width as a function of mass for the scalar H_j^0 ($j=1,2,3$) with mixing angles $U_{1j}=U_{2j}=U_{3j}=1/\sqrt{3}$, for the range of allowed χ_1 masses. The broken curve shows the standard model Higgs boson width for comparison.

Similarly for case B one has

$$a_w = \frac{ie^2 gM_w}{(4\pi)^2} [6 + (-8+12\lambda_w)I(\lambda_w)]U\sqrt{2} \quad (3.4.8)$$

$$a_G = \frac{ie^2 gM_w}{(4\pi)^2} [\lambda_w^{-1} + 2I(\lambda_w)]U\sqrt{2} \quad (3.4.9)$$

$$a_{\chi_2} = \frac{-2\sqrt{2}ie^2 g\tilde{M}_2}{(4\pi)^2} [2 + (4\lambda_2^{-1}-1)I(\lambda_2)]U \sin 2\phi \quad (3.4.10)$$

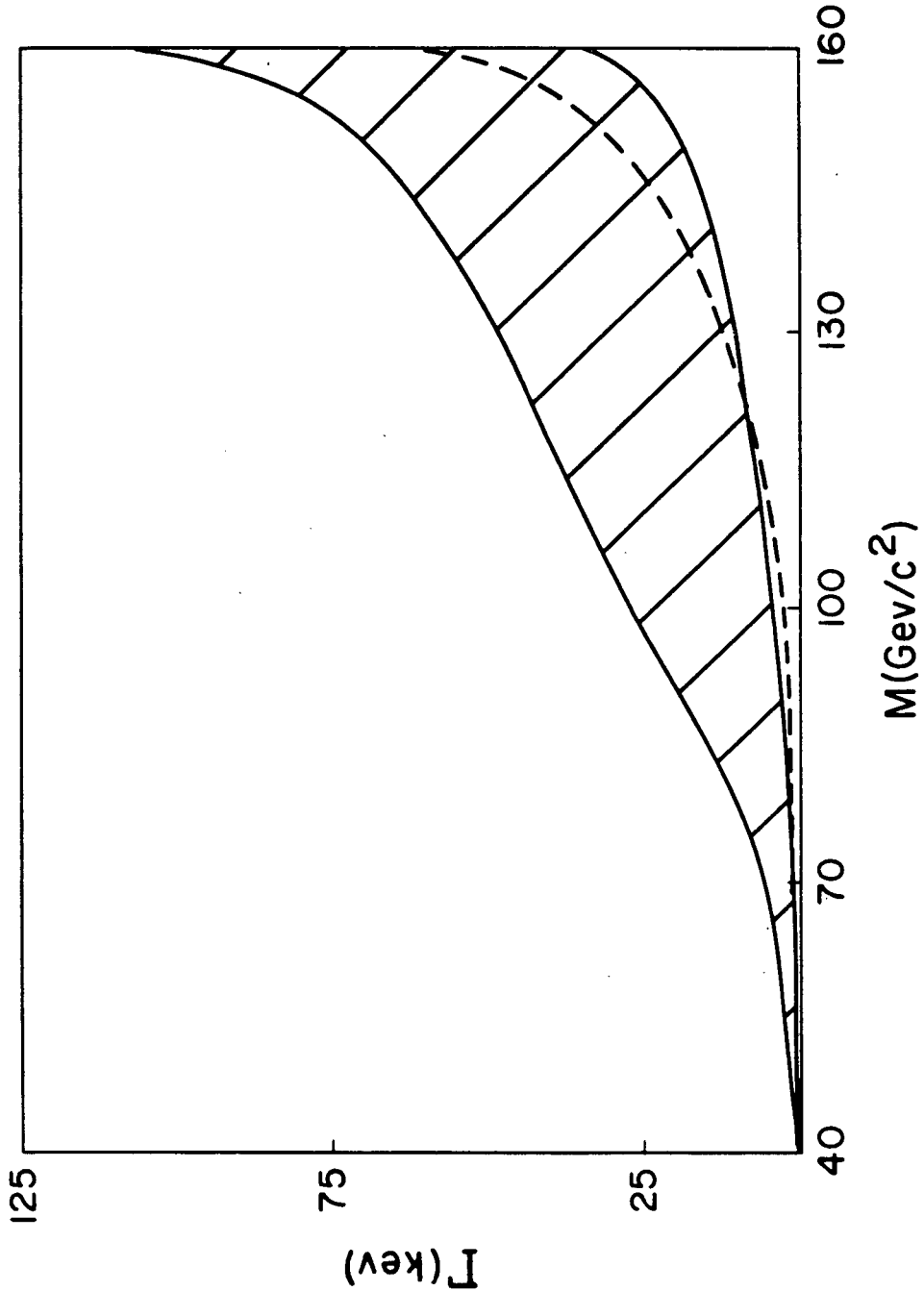
$$a_H = \frac{2ie^2 M_w}{(4\pi)^2} [1 + 2\lambda_H I(\lambda_H)] \left\{ \left(1 - \frac{1}{2}\lambda_w^{-1}\right)\sqrt{2} + \frac{2h^2 v_3}{gM_w} \right\} U \quad (3.4.11)$$

$$a_t = -\frac{8ige^2 m_t^2}{3(4\pi)^2 M_w} [2 + (4\lambda_t^{-1}-1)I(\lambda_t)]U\sqrt{2} \quad (3.4.12)$$

$$a_{\tilde{t}} = \frac{16ie^2 g m_t^2}{3(4\pi)^2 M_w} [1 + 2\lambda_{\tilde{t}} I(\lambda_{\tilde{t}})]U\sqrt{2} \quad (3.4.13)$$

Substituting these into equation (3.4.1) gives the width $\Gamma(H^0 \rightarrow \gamma\gamma)$ which is again displayed as a function of scalar mass in figure 6. Once again the standard model width is shown for comparison. The discussion is similar to that for case A, except that the t-quark loop is not an important contribution here, since there is no $\tan\alpha$ enhancement. Consequently the width is a bit larger, and dominated mostly by the W-gauge boson loop. The gaugino loops interfere destructively with the W-gauge boson loop and hence the scalar width is still smaller than in the standard model.

Finally note that thus far only the example where the mixings U_{ij} are all approximately equal has been used. Now consider the best case possibility, where the relative phases between mixings is such that the

Figure 7 - Scalar 2γ -Decay Width for Best Case A

Case A ($v_1 \gg v_2$): Two photon decay width as a function of mass for the scalar H_j^0 ($j=1,2,3$) with mixing angles $U_{1j} = -U_{2j} = U_{3j} = 1/\sqrt{3}$, for the range of allowed χ_1 masses. The broken curve shows the standard model Higgs boson width for comparison.

dominant loop contributions interfere constructively. This is not possible in case B since the gauge boson and gaugino loops contain the same combinations of U_{ij} with an overall relative minus sign. However, for case A one can greatly increase the width if $U_{1j} \approx -U_{2j}$. This will give constructive rather than destructive interference between the two main contributors, namely the gauge boson and t-quark loops. The scalar width for this best case scenario is plotted in figure 7 and it is indeed now enhanced relative to the standard model width, although not by a great amount.

This concludes chapter III on the minimal broken supersymmetry model. The model, which is also described in the literature, was first introduced and then applied to the calculation of the 2γ -decay widths of the Higgs bosons. The results of this calculation are all new, and we remind the reader of some important highlights. First the additional superparticle content did not significantly alter the Higgs 2γ -decay widths, generally causing a small decline through destructive interference effects. Once again it was the enhancement of the Higgs to fermion couplings, due to the additional Higgs doublet, which led to a greatly increased Higgs 2γ -decay width. Unlike the case for the Two-Higgs-Doublet model however, supersymmetry imposes a much more severe bound on this possible enhancement. The next chapter will discuss the effects of this new constraint, as well as the significance of the other results obtained thus far.

IV. NON-STANDARD SPIN-0 BOSON PRODUCTION

The results of the last two chapters will now be used to determine production cross sections for the spin-0 bosons in ep and e^+e^- colliders. These cross sections can be expressed in terms of the Higgs boson to two photon decay widths previously calculated. If its 2γ -decay width is large enough, the dominant production mode in these colliders for the Higgs boson will be via the two photon fusion mechanism. This mechanism and the specifics of how to calculate the production cross sections are discussed in detail below. The point is that the Higgs boson production rates can be directly related to their 2γ -decay widths, if the widths are large enough. This is indeed the case for the supersymmetry and Two-Higgs-Doublet models previously introduced, if the enhancement factor $\tan\alpha$ is large. Spin-0 boson production rates are calculated for each of these models in ep and e^+e^- colliders. These new results are presented for discussion and comparison below.

Detection of the Higgs bosons in these colliders is achieved by observing a peak in the invariant mass distribution of their decay products. For the Higgs mass range studied, these decay products will consist of two hadronic jets of particles, which form from the original pair of quarks that the Higgs predominantly decays into. Hence the cleanest signal will be for e^+e^- machines. Unfortunately we will find that the production rates at the SLC collider will be too low for observation even in the most optimistic scenario. Thus we must turn to the higher luminosity ep machines, at the expense of larger backgrounds and potential problems in distinguishing decay jets from the initial beam jets. Nevertheless we will find promising results for the Two-Higgs-Doublet model, with production rates in the best

case which are readily observable at the HERA collider. For the minimal broken supersymmetry model however, we will find that once again the rates are unobservable, as a result of the more severe constraints on the enhancement factor $\tan\alpha$. The significance of these results is discussed below.

4.1 The Calculation

This section studies the production of scalar (S^0) and pseudoscalar (P^0) spin-0 bosons in electron-proton and e^+e^- colliders. The ep semi-inclusive reactions studied are

$$e + p \longrightarrow e + S^0 + X \quad (4.1.1a)$$

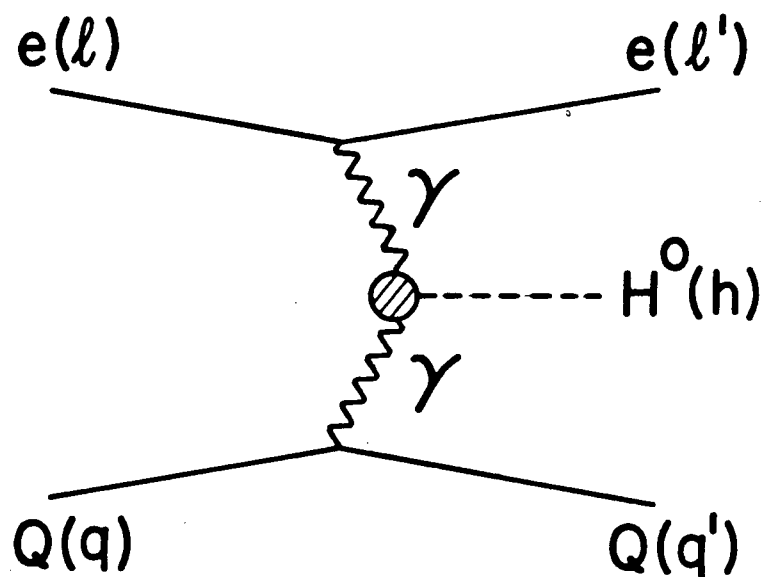
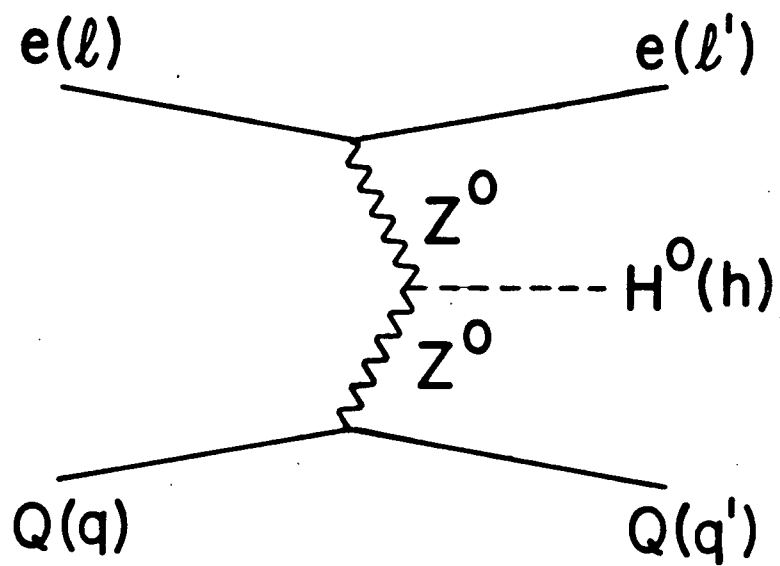
$$e + p \longrightarrow e + P^0 + X \quad (4.1.1b)$$

where X denotes any hadronic states. The quark-parton model is assumed for the collision in equation (4.1.1). The electron-quark scattering subprocesses are

$$e(\ell) + Q(q) \longrightarrow e(\ell') + S^0(h) + Q(q') \quad (4.2.2a)$$

$$e(\ell) + Q(q) \longrightarrow e(\ell') + P^0(h) + Q(q') \quad (4.2.2b)$$

where Q denotes either the u-type or d-type quark in the proton. In equation (4.2.2) the 4-momenta of the various particles are given in their respective parentheses.

Figure 8 - Feynman Diagrams for the Reaction $e q \rightarrow e q H^0$ 

(a) t-channel Z-boson exchange (b) t-channel photon exchange

It is well known that the production rate for the standard model Higgs boson is very small [28] for an ep collider such as HERA. This can be understood by examining the production mechanism for reaction (4.2.2). In ep collisions, Higgs boson production proceeds via the t-channel diagrams depicted in figure 8. The process of figure 8a is suppressed by the two Z-propagators, although this is partly compensated by the large H^0ZZ coupling. On the other hand the process in figure 8b has no such suppression but is enhanced by the double photon exchange poles. However, the $H^0\gamma\gamma$ vertex is of higher order thereby rendering this amplitude small. In most cases the standard model amplitude of figure 8a is larger than that of figure 8b, but it still results in an extremely small production rate as discussed below.

The situation is more optimistic for Two-Higgs-Doublet models. As seen in the previous chapters, both the $S^0\gamma\gamma$ and $P^0\gamma\gamma$ vertices can be enhanced substantially. For the scalar this makes the photon exchange amplitude dominate over the Z-exchange one since the S^0ZZ coupling remains unchanged to lowest order. The pseudoscalar will be produced only through the photon exchange amplitude. Thus one can express the production cross sections of these spin-0 bosons in terms of their 2γ -decay widths.

In the same view one should also consider the production of S^0 and P^0 in e^+e^- scattering. The purpose is to compare the relative strengths of the above two types of colliders for scalar and pseudoscalar production. The reactions studied here are ones similar to equation (4.1.1); namely

$$e^+ + e^- \longrightarrow e^+ + e^- + S^0 \quad (4.1.3a)$$

$$e^+ + e^- \longrightarrow e^+ + e^- + P^0 \quad (4.1.3b)$$

Being interested in cases where the $S^0\gamma\gamma$ and/or $P^0\gamma\gamma$ vertices are enhanced, one again concentrates on the two photon production mechanism. This is the same as figure 8b with quark lines being replaced by e^+ lines. There is an added complication for the e^+e^- reaction not present for the ep case. The s-channel equivalent of the diagram in figure 8b should be included. The resulting destructive interference with the more dominant t-channel exchange graph causes a small correction. This correction can be neglected for the purposes of obtaining order of magnitude estimates for the production cross section. Hence only the dominant t-channel process will be retained. Otherwise the calculation is the same as for the ep case, except that one does not need to convolute over parton distributions.

The production cross sections for the processes in equation (4.1.1) were calculated using the equivalent photon approximation (EPA) [29 30]. The photon spectrum used is given by [31]

$$\sigma_{eq}(s) = \frac{\alpha}{\pi} \ln \frac{s}{m_e^2} \int_{M_H^2}^s \frac{ds'}{s'} \left[1 - \frac{s'}{s} + \frac{s'^2}{2s^2} \right] \sigma_{\gamma q}(s') \quad (4.1.4)$$

This method relates the photon-quark cross section (see figure 8b) to the electron-quark cross section for the subprocesses in equation (4.1.2). Details of the calculation are described in appendix F. The approximation is useful in that equation (4.1.4) can be solved analytically. The EPA has been demonstrated to be good to within ten percent in resonance production in e^+e^- collisions, and it is expected to be of the same accuracy in ep collisions. As a check the production cross sections were also calculated directly using the Monte-Carlo method (see appendix G), which evaluates the integrals numerically. The convergence of the Monte-Carlo routine is very slow in ep collisions due to the Lorentz boost between the lab and the

cm frames. This boost prevents the use of importance sampling techniques, which concentrate the effort of the Monte-Carlo routine near the important photon poles. Nevertheless the results agree to within the accuracy of the two methods.

The results of the EPA calculation for the cross sections of the subprocess equation (4.1.2) are given below. For the scalar one obtains

$$\begin{aligned} \sigma_{eq}(\hat{s}) = & 4\alpha^2 e_q^2 M_{S0}^{-3} \Gamma(S^0 + \gamma\gamma) \ln\left(\frac{\hat{s}}{m_e^2}\right) \left\{ \ln\left(\frac{M_{S0}^2}{m_q^2}\right) [\rho^2 + 2\rho - 3 - (2 + 2\rho + \rho^2/2) \ln\rho] \right. \\ & + (\rho^2/4) \ln^2\rho + (2\rho^2 + 4\rho - 6) \ln(1-\rho) - (2.5\rho^2 + 4\rho - 5) \ln\rho \\ & \left. + (25 - 24\rho - \rho^2)/4 + (\rho^2 + 4\rho + 4) [-\text{Li}(1) + \text{Li}(\rho) + (\ln^2\rho)/2] \right\} \end{aligned} \quad (4.1.5)$$

where $\rho \equiv M_{S0}^2/\hat{s}$, and $\hat{s} \equiv (1+q)^2$ is the (cm energy)² for the subprocess. The quark charges are given by ee_q and $\text{Li}(x) \equiv -\int_0^x dt \ln(1-t)/t$ is the dilogarithm function. For the pseudoscalar one obtains the slightly different form given by

$$\begin{aligned} \sigma_{eq}(\hat{s}) = & 4\alpha^2 e_q^2 M_{P0}^{-3} \Gamma(P^0 + \gamma\gamma) \ln\left(\frac{\hat{s}}{m_e^2}\right) \left\{ \ln\left(\frac{M_{P0}^2}{m_q^2}\right) [\rho^2 + 2\rho - 3 - (2 + 2\rho + \rho^2/2) \ln\rho] \right. \\ & + (1 + \rho + \rho^2/4) \ln^2\rho + (2\rho^2 + 4\rho - 6) \ln(1-\rho) + (6 - 4\rho - 7\rho^2/4) \ln\rho \\ & \left. + (47 - 28\rho - 19\rho^2)/8 + (\rho^2 + 4\rho + 4) [-\text{Li}(1) + \text{Li}(\rho) + (\ln^2\rho)/2] \right\} \end{aligned} \quad (4.1.6)$$

The 2γ -decay widths in equations (4.1.5) and (4.1.6) were calculated in the previous chapters. The quark-parton model is then used to estimate the cross section for the physical processes of equation (4.1.1) by convoluting over the quark distribution functions $f_q(x)$. Explicitly

$$\sigma_{ep}(s) = \int_{M_H^2}^1 dx \sum_q f_q(x) \sigma_{eq}(xs) \quad (4.1.7)$$

where this last integration is done numerically. The specific quark distributions used were

$$f_u(x) = 2.2x^{-.49}(1-x)^{2.8} \quad (4.1.8a)$$

$$f_d(x) = 1.25x^{-.49}(1-x)^{3.8} \quad (4.1.8b)$$

$$f_u(x) = f_d(x) = 0.27x^{-1}(1-x)^{8.1} \quad (4.1.8c)$$

which are taken from reference [32].

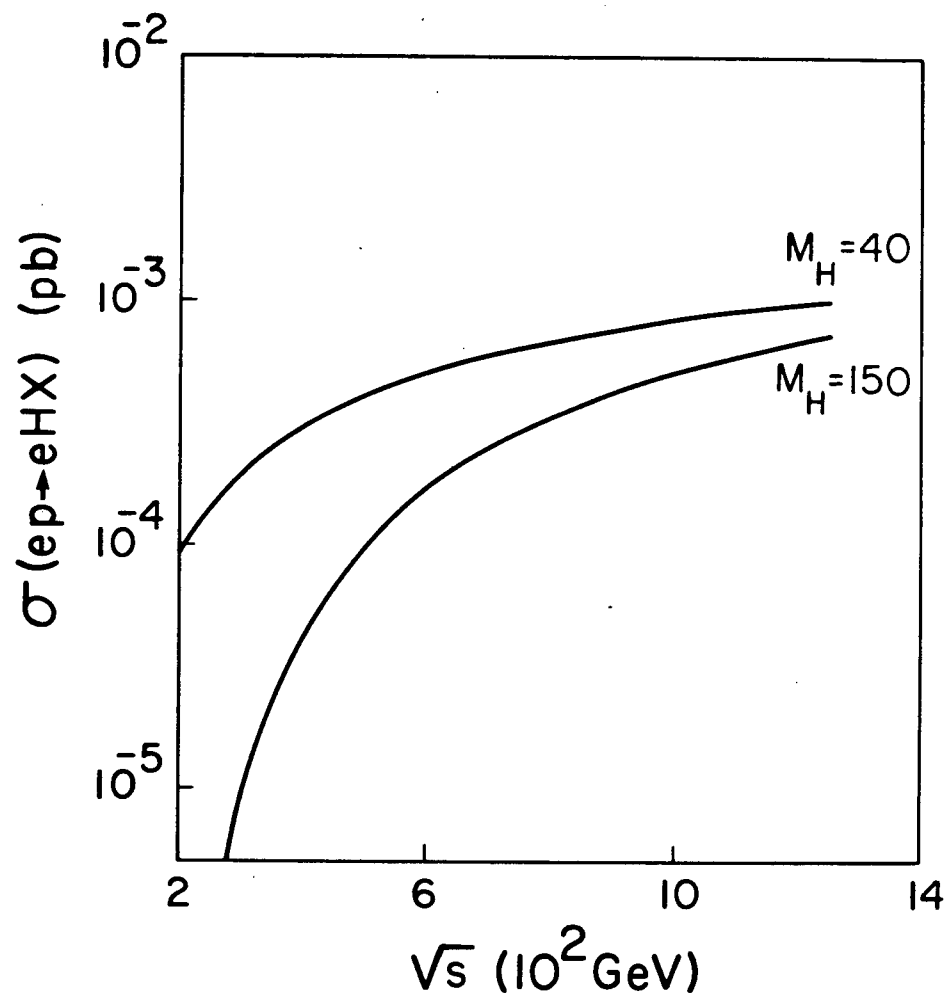
Similarly the results for the e^+e^- collisions of equation (4.1.3) are easily obtained. They are simply given by equations (4.1.5) and (4.1.6) with \hat{s} replaced by s , the (cm energy)² of the e^+e^- system. Of course there is no need to convolute over parton distribution functions, as the result is already in its final form. Again the results agree with the numerical Monte-Carlo check. For this case the lab and cm frames are the same. The importance sampling techniques mentioned above can therefore be used, and convergence of the Monte-Carlo routine is quite rapid.

Thus the production cross sections of the spin-0 bosons are now expressed in terms of their 2γ -decay widths for both ep and e^+e^- colliders.

4.2 Numerical Results and Discussion

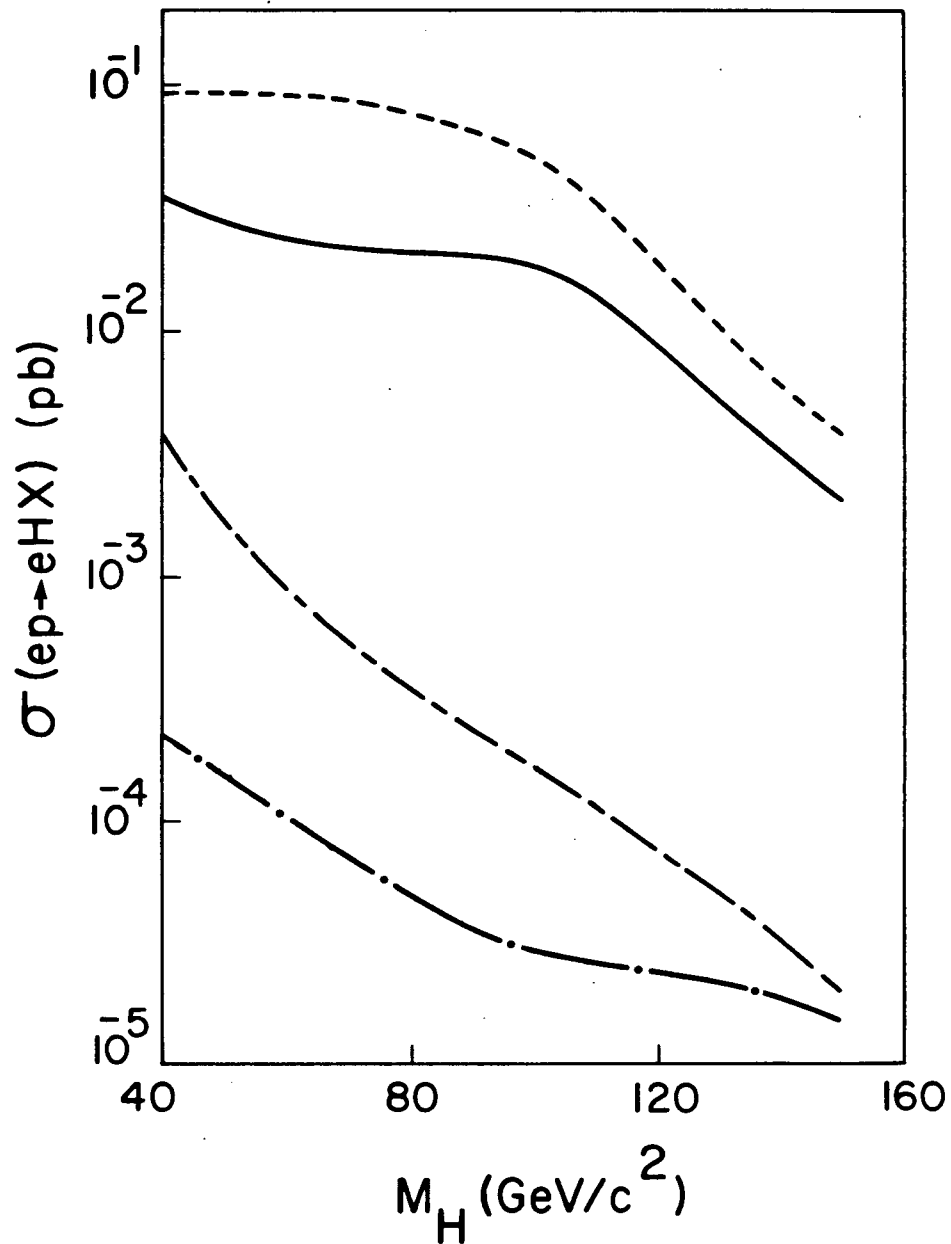
The photon-exchange production cross section as a function of \sqrt{s} is given in figure 9 for the standard model Higgs boson in an ep collider. In accordance with previous calculations [28] this cross section is distressingly small, typically on the order of 10^{-40} cm² for collider energies. The lower curve in figure 10 depicts the same cross section as a function of the Higgs boson mass for $\sqrt{s}=320$ GeV, appropriate for HERA. Also indicated is the cross section due to the two Z-boson fusion mechanism alone. Similar curves for $\sqrt{s}=1$ TeV are shown in figure 11. Although obscured somewhat in figure 10 by the effects of phase space, there is a rise in the photon exchange cross section for large M_H , which is very apparent in figure 11. This rise is due to the behaviour of the function $I(\lambda)$ as discussed in appendix D. The biggest standard model contribution comes from the W-boson loop, and hence the cross section rises near the threshold at $M_H=2M_W$. Standard model Higgs boson production in ep collision is dominated by the two Z mechanism. At $\sqrt{s}=320$ GeV the cross section is at least one order of magnitude too small for observation even for light Higgs. For $\sqrt{s}=1$ TeV the two Z mechanism becomes just large enough if the same luminosity can be maintained, and the production rate for the two photon process is too low. Thus for the standard model, the prediction for the production of Higgs bosons is that ep colliders will not be able to observe them. Similar results hold in e^+e^- machines. These conclusions are well known and the standard model results have only been shown for comparison with the more interesting Two-Higgs-Doublet model.

Plots of the enhanced cross sections as a function of mass, using $\tan\alpha=40$, are given for the spin-0 bosons of the Two-Higgs-Doublet model in figures 10 and 11. Again there is a peak in the cross sections of figure 11

Figure 9 - Standard Model σ vs \sqrt{s} for $ep \rightarrow eH^0X$ 

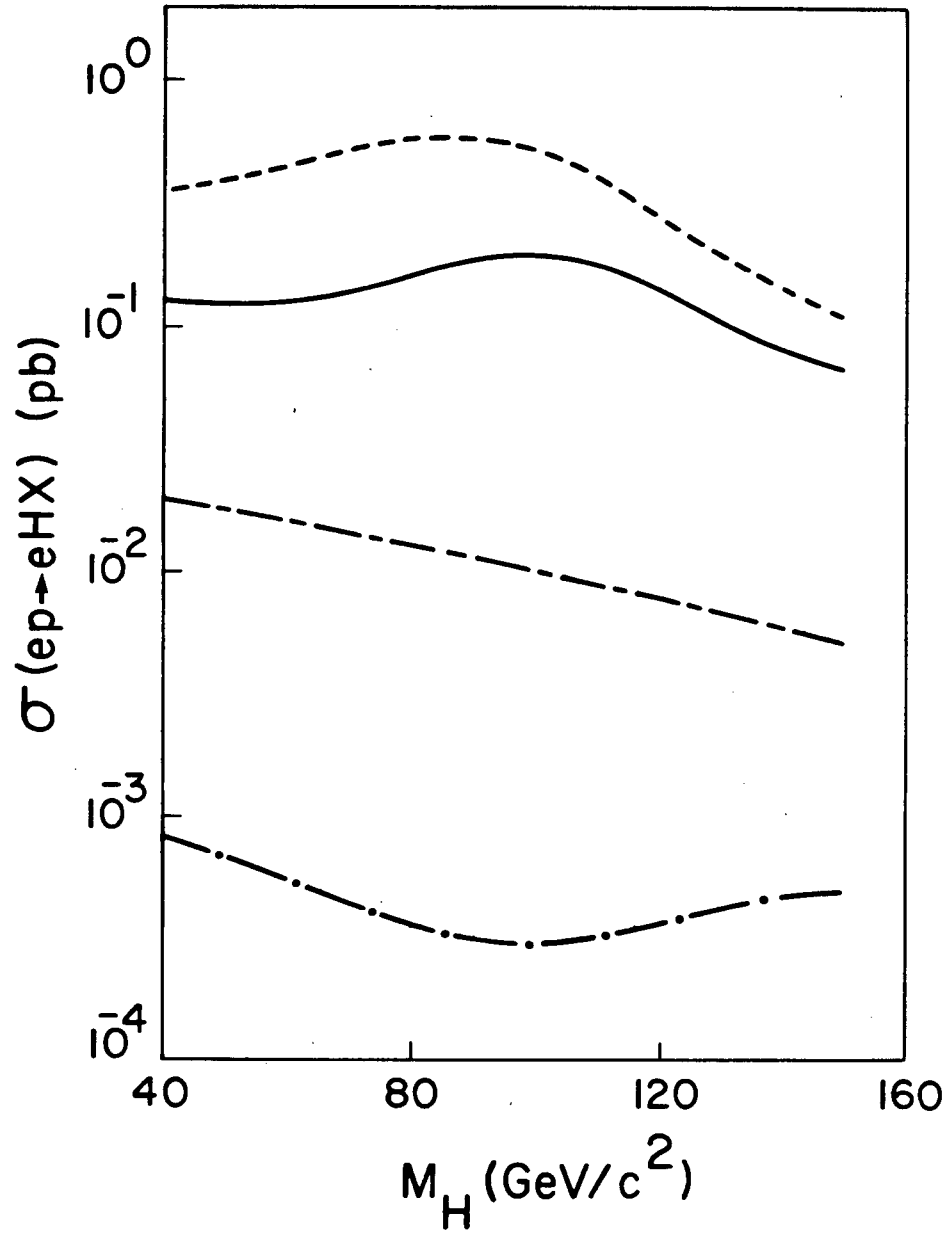
Photon exchange production cross section with $M_H = 40, 150$ GeV/c².

Figure 10 - Cross Sections σ vs M_H for $ep \rightarrow eH^0 X$ for $\sqrt{s}=320$ GeV



The dash-dot (dashed) line is for standard model photon (Z-boson) exchange. The solid (broken) line is for Two-Higgs-Doublet model photon exchange scalar (pseudoscalar) production with $\tan\alpha=40$.

Figure 11 - Cross Sections σ vs M_H for $ep \rightarrow eH^0 X$ for $\sqrt{s}=1$ TeV

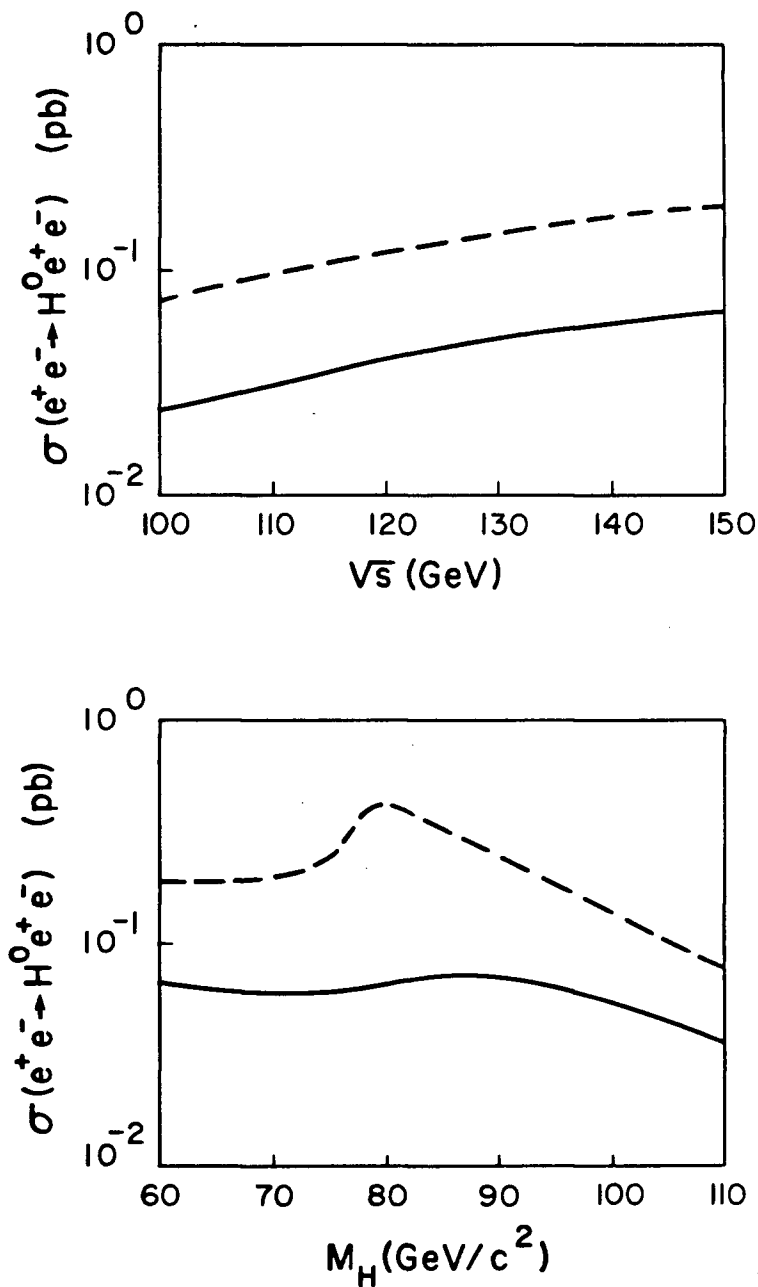


The dash-dot (dashed) line is for standard model photon (Z-boson) exchange. The solid (broken) line is for Two-Higgs-Doublet model photon exchange scalar (pseudoscalar) production with $\tan\alpha=40$.

due to the behaviour of $I(\lambda)$. However in this case the t-quark loop dominates so that the threshold occurs for $M_H=2m_t$. In the scalar case the peak is less pronounced and is displaced at larger M_H due to the factor $(4\lambda-1)$ which multiplies $I(\lambda)$ in equation (2.3.4). Similar behaviour in figure 10 is somewhat obscured since the more restrictive phase space dominates the shape of the cross section. For a range of Higgs mass, the enhanced photon exchange cross sections are much larger than the unchanged Z-boson fusion mechanism by roughly an order of magnitude. The pseudoscalar rate is about three times that of the scalar. Although the actual cross sections for a Two-Higgs-Doublet model may fall below the bounds shown, reasonably large cross sections (up to 10^{-37} cm²) are possible even at HERA energies. Hence one may be able to observe Higgs boson production in ep collisions within the context of the Two-Higgs-Doublet model.

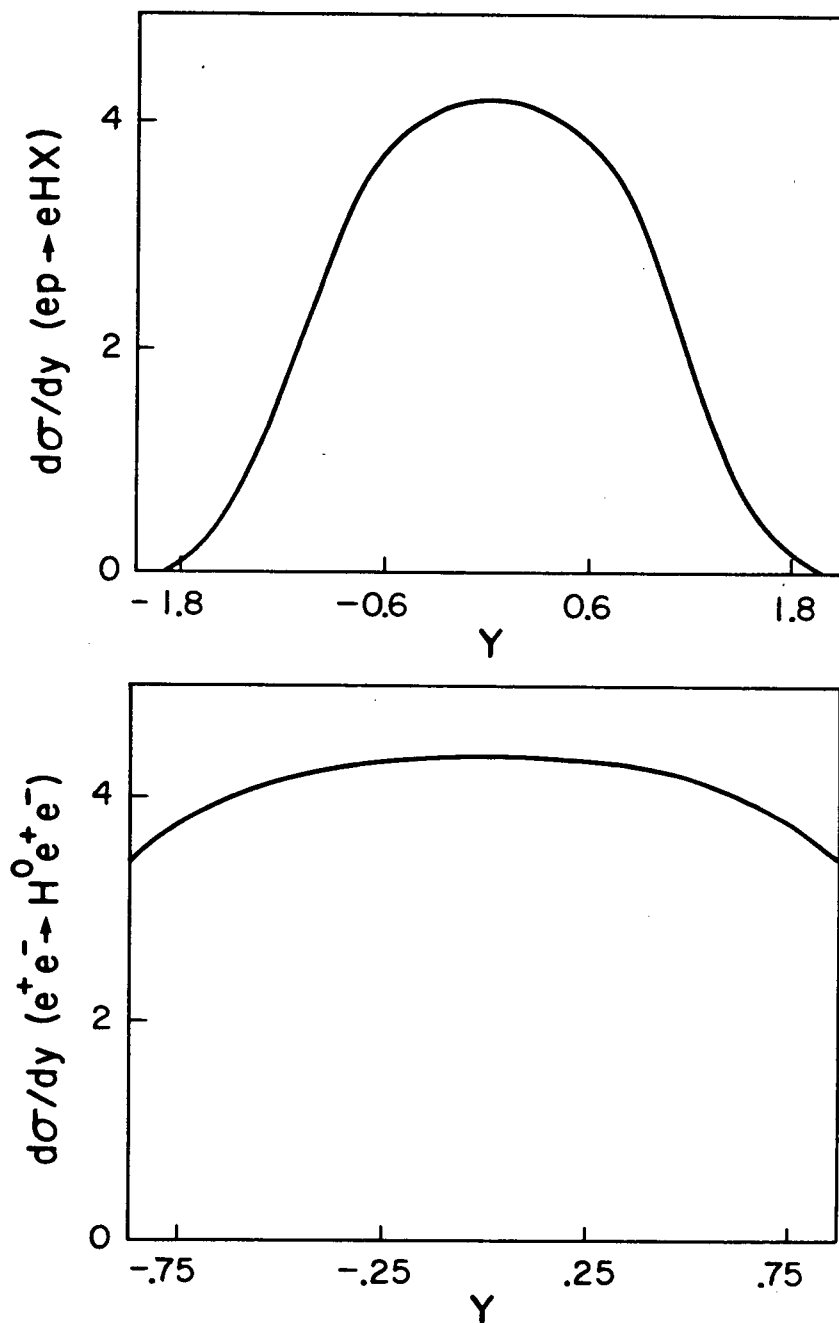
Plots of the enhanced ($\tan\alpha=40$) photon exchange cross sections are given in figure 12 for the Two-Higgs-Doublet model bosons produced in e^+e^- collisions. The variation of cross section with \sqrt{s} for $M_H=60$ GeV/c², and the cross section versus M_H for $\sqrt{s}=150$ GeV are displayed. These values were chosen to facilitate comparison with the standard model graphs given in reference [33]. The behaviour is similar to that found for ep scattering above. The peak in the σ vs. M_H distribution is sharper since there is no smearing by the parton distributions. The enhanced cross section is roughly an order of magnitude larger than for the standard model one [33] which makes it just observable as discussed below.

As in the standard model, the intermediate mass scalar or pseudoscalar bosons will decay primarily into a pair of heavy quarks, leading to a signal of two jets. In figure 13 the rapidity distributions of the Higgs scalar $\tilde{\phi}$ for ep and e^+e^- photon exchange mechanisms are given. The pseudoscalar

Figure 12 - Production Cross Sections for $e^+e^- \rightarrow e^+e^-H^0$ 

Production cross sections as a function of (a) \sqrt{s} for $M_H=60 \text{ GeV}/c^2$ (b) M_H for $\sqrt{s}=150 \text{ GeV}$. The solid (broken) line is for Two-Higgs-Doublet model photon exchange scalar (pseudoscalar) production with $\tan\alpha=40$.

Figure 13 - Rapidity Distributions



Scalar boson rapidity distribution in the cm frame for (a) $ep \rightarrow eH^0X$ with $\sqrt{s}=320$ GeV and $M_H=40$ GeV/c² (b) $e^+e^- \rightarrow e^+e^-H^0$ with $\sqrt{s}=150$ GeV and $M_H=60$ GeV. The normalization is arbitrary.

rapidity distributions are very similar. In both cases the cm frame rapidity is broadly peaked about zero. It is straightforward to obtain these distributions from the EPA calculation of appendix F, or directly from the Monte-Carlo calculation. For the $e^+e^- \rightarrow e^+e^-H^0$ process, the lab frame and the cm frame coincide. The two Higgs decay jets should therefore stand out well away from the beam axis, providing a good signal. However in the $ep \rightarrow eH^0X$ process, the cm frame has a large velocity in the lab frame. The resulting Lorentz boost will shift the scale on the rapidity distribution in figure 13a by roughly -1.6 at HERA. Hence in the laboratory frame the Higgs rapidity will peak at less than 10° from the beam axis, and at least one of the decay jets may be difficult to distinguish from the beam jets. In order to resolve this problem, much higher event rates may be needed for ep colliders than for e^+e^- machines.

The ep event rates discussed below are for HERA assuming $\sqrt{s}=320$ GeV and an integrated luminosity over one year's running of 1.89×10^{39} cm^{-2} . The e^+e^- rates are for SLC assuming $\sqrt{s}=100$ GeV and an integrated luminosity over one year of 9.45×10^{37} cm^{-2} . In the standard model, Higgs boson production is dominated by the Z-boson exchange mechanism and the event rates of <3 per year are too small to be observed. On the other hand the cross sections for the Two-Higgs-Doublet model can be quite substantial. This is due to the possibility of enhancing the Yukawa coupling of the t-quark in this model. Without folding in detection efficiency, the upper bound estimates on the event rates in ep colliders are calculated to be <65 for the scalar boson and <176 for the pseudoscalar. In e^+e^- colliders the corresponding event rates are <2 for the scalar and <13 for the pseudoscalar.

Although the cleaner signal may be found with e^+e^- machines, the upper bound production rates for SLC are not large enough. A higher luminosity

e^+e^- machine, perhaps LEP II, would be useful in providing both larger rates and a clean signal. On the other hand the ep production rates are already quite large, especially for the pseudoscalar boson. Hence it can be concluded that it may be possible to detect non-standard spin-0 bosons in ep colliders such as HERA.

The results for the minimal broken supersymmetry model are not as promising as for Two-Higgs-Doublet models in general. The qualitative results are similar, but the more stringent bound on $\tan\alpha$ in equation (3.3.4d) gives a reduction in the production cross sections by roughly a factor of 50. Thus the best possible event rates for one year running will be <3 for the pseudoscalar in ep collisions, and even smaller rates occur for the other cases. These rates are much too low, and hence it will not be possible to detect the non-standard Higgs bosons of the minimal broken supersymmetry model with this method.

This concludes chapter IV. The new results obtained were the production rates of Higgs bosons in ep and e^+e^- colliders for the Two-Higgs-Doublet and minimal broken supersymmetry models. It was found that e^+e^- machines could not produce observable quantities of the Higgs bosons and hence the emphasis shifted to ep colliders. Here it was found that for the Two-Higgs-Doublet model, readily observable rates on the order of 100 events per year were possible for the HERA collider. For the minimal broken supersymmetry model however, production rates were once again unobservable due to the smaller $\tan\alpha$ enhancement factor. From these results we may conclude that the production of Higgs bosons in supersymmetry models is as difficult as in the standard model. More importantly we now have a potential experimental test of supersymmetry. If Higgs bosons are detected at HERA as allowed by Two-Higgs-Doublet models, then we can rule out the

minimal broken supersymmetry model. How general a supersymmetry model could be ruled out is discussed in the next chapter.

V. SUMMARY AND CONCLUSIONS

The two photon decay widths of non-standard spin-0 bosons were calculated for the two doublets extension of the standard $SU(2) \times U(1)$ electroweak model, and for the minimal broken supersymmetry model. The results were then used to obtain production rates for these spin-0 bosons in ep and e^+e^- colliders, for the intermediate mass range (40-160 GeV/c²) studied.

Features of the Two-Higgs-Doublet model include the scalar and pseudoscalar bosons which are present in addition to the usual standard model Higgs scalar. Also there is the possibility of enhanced fermion couplings to these bosons relative to the standard model, if the ratio of the two VEV's, $\tan\alpha$, is large. The largest uncertainty of the calculation lies in the charged Higgs boson loops (see figure 15), but fortunately their contribution is negligible if the parameters in the scalar potential are not large. If not, one encounters either strongly interacting scalars or vacuum instability. Larger 2γ -decay widths than in the standard model are possible by enhancing the fermion loops (see figure 14). In the best case the t -quark loop is enhanced by the upper bound value of $\tan\alpha=40$, and it dominates the other processes. This occurs for both the pseudoscalar and one of the scalar Higgs bosons. The other scalar would behave as in the standard model but with the gauge boson loop suppressed, and hence its smaller width is of little interest. The bound of $\tan\alpha < 40$ was obtained using only phenomenological constraints on the mixing of the two VEV's. Perturbative partial wave unitarity constraints [26], which would lead to the more stringent bound of $\tan\alpha < 12$, were not used. If one adopts this then the numerical results discussed should be scaled accordingly.

The minimal broken supersymmetry model is a specific example of a Two-Higgs-Doublet model, with some added theoretical motivation. Consequently it too has all of the features just described. In addition there are new features associated with the underlying albeit broken supersymmetry. Specifically the charged gauginos and scalar-fermions will give additional loop contributions to the two photon decay widths. In the intermediate mass range studied (40-160 GeV/c²), it was found that these additional contributions are not very large and in fact they in general reduce the width by interfering destructively with the usual contributions. One important new feature arising from the supersymmetry is the upper bound imposed on $\tan\alpha$ by the allowed range of the gaugino masses. The upper limit of $\tan\alpha < 5.7$ in the minimal broken supersymmetry model is less than half of the most restrictive bound for a general Two-Higgs-Doublet model, and much smaller than the phenomenological bound. The width varies as $\tan^2\alpha$ for large $\tan\alpha$, so that the largest possible width for this model is from 4 to 50 times smaller than one might have hoped for. A more optimistic situation can arise if the mixings between the scalars, coming from the breaking of the supersymmetry, have phases such that constructive interference occurs between the W-gauge boson and t-quark loops. In this case the scalar width is enhanced to partially compensate for the smaller $\tan\alpha$ factor. Even this best case possibility allows an enhancement of the scalar width of less than an order of magnitude over the standard model width. For the pseudoscalar this best case possibility does not occur since the relative phases are fixed, and hence the pseudoscalar width is definitely smaller. Hence, it can be concluded that the supersymmetry imposes a much lower upper bound on the possible $\tan\alpha$ enhancement of the two photon decay widths than do Two-Higgs-Doublet models in general. Widths of the order of 100 keV are the

best one can hope for, for both scalars and pseudoscalars, in the minimal broken supersymmetric gauge theory.

The production cross sections in ep and e^+e^- colliders were calculated for the non-standard spin-0 bosons in terms of their two photon decay widths. From the rapidity distributions it was found that the cleanest signal will occur for e^+e^- colliders. Unfortunately the production rates were too low to be observed at the SLC collider for all cases studied. Therefore one must concentrate on the ep results.

The ep upper bound production rates for the Two-Higgs-Doublet model are very large, being of the order of 100 events per year at HERA. Hence one concludes that it may be possible to detect these non-standard Higgs bosons in ep colliders. The ep results for the minimal broken supersymmetry model are more disappointing. The much stricter upper bound on the possible enhancement in this model leads to very low production rates for the non-standard spin-0 bosons, which again are not observable. Thus the observable production of non-standard Higgs bosons for minimal supersymmetry models will not be possible at HERA. The two photon decay widths of these Higgs particles in supersymmetry models are of little more importance than is the case for the standard model. This negative conclusion for the two photon process does not of course prevent supersymmetry from manifesting itself in other processes.

It should be noted that if non-standard spin-0 Higgs bosons are produced at HERA by this mechanism, as allowed by general Two-Higgs-Doublet models, then the minimal broken supersymmetry model would definitely be ruled out. Thus we have a possible experimental test of supersymmetry. Such an occurrence would not however completely rule out supersymmetry. We have only considered the minimal model with three families of quarks and

leptons. If there are more than three families, some of the additional heavy fermions could contribute to the 2γ -decay width as much as the t-quark does. Thus the predicted production rates could be much larger. This will not occur in the standard model unless incredibly large numbers of additional families (>35) are used. However, for supersymmetry models the addition of only one extra family leads to an increased rate by a factor of nine. This is because the t-quark, the new heavy u-type quark, and the new heavy lepton would each contribute roughly the same to the 2γ -decay width. Thus we could still have a supersymmetric model, although a more complicated one than the minimal model.

This concludes the presentation of this thesis. We have examined the two photon decay widths of non-standard spin-0 bosons for Two-Higgs-Doublet models in general, and the minimal broken supersymmetry model in particular. While the models themselves are established in the literature, their application to the Higgs 2γ -decay width and the subsequent calculation of the various Higgs production rates all represent new results. In these models with additional Higgs doublets, there is the possibility for enhanced spin-0 boson to fermion couplings if the ratio of the two vacuum expectation values ($\tan\alpha$) is large. This in turn leads to enhanced production of these bosons via the two photon fusion mechanism at rates which could readily be observed at the HERA collider. In supersymmetry models the new superparticle content will give rise to additional contributions to the 2γ -decay process. We found that these are not very large and that their effect is to slightly reduce the width via destructive interference with the usual contributions. The important new result arising from supersymmetry is that it imposes a much smaller upper bound on the possible $\tan\alpha$ enhancement of the fermion couplings than do Two-Higgs-Doublet models in general. The

origin of this additional constraint lies in the experimentally established lower limits for the mass of the supersymmetric gaugino particles. Hence even for the best case possibility, the Higgs bosons of the minimal 3-family supersymmetry model cannot be produced at observable rates. Only supersymmetry models with additional generations of heavy fermions can produce Higgs bosons at rates which could be observable at HERA. Therefore we have a possible experimental test of supersymmetry in that the detection of Higgs bosons at HERA could rule out the minimal model.

BIBLIOGRAPHY

1. G. Arnison et al., UA1 Collaboration, Phys. Lett. 122B, 103 (1983);
ibid, 126B, 398 (1983).
2. M. Banner et al., UA2 Collaboration, Phys. Lett. 122B, 476 (1983);
ibid, 129B, 130 (1983).
3. N.P. Nilles, Phys. Rept. 110C, 1 (1984).
4. E. Farhi and L. Susskind, Phys. Rept. 74C, 277 (1981).
5. H.E. Haber and G. Kane, Phys. Rept. 117C, 76 (1985).
6. R. Bates and J.N. Ng, Phys. Rev. D33, 657 (1986).
7. S.M. Bilenky and J. Hosek, Phys. Rept. 90C, 73 (1982).
8. S. Glashow and S. Weinberg, Phys. Rev. D15, 1958 (1977).
9. R.A. Flores and M. Sher, Annals of Phys. 148, 95 (1981).
10. J. Ellis, M.K. Gaillard and D.V. Nanopoulos, Nucl. Phys. B106, 292
(1976).
11. H.E. Haber, G.L. Kane and T. Sterling, Nucl. Phys. B161, 493 (1979).
12. J.N. Ng, Phys. Rev. D31, 464 (1985).
13. Y.P. Nikitin, D.V. Pikhterev and S.G. Rubin, Sov. J. Nucl. Phys. 36,
106 (1982).
14. L.F. Abbott, P. Sikivie and M.B. Wise, Phys. Rev. D21, 1393 (1980).
15. D. Toussiant, Phys. Rev. D18, 1626 (1978).
16. B.W. Lee, C. Quigg and H.B. Thacker, Phys. Rev. D16, 1519 (1977).
17. H. Huffel and G. Pocsik, Z. Phys. C8, 13 (1981).
18. R. Bates, J.N. Ng and P. Kalyniak, TRIUMF preprint TRI-PP-108-85,
To be published in Phys. Rev. D34, (1986).
19. P. Fayet, Nucl. Phys. B90, 104 (1975).
20. J.F. Gunion and H.E. Haber, SLAC-PUB-3404 (1984).
21. P. Kalyniak, R. Bates and J.N. Ng, Phys. Rev. D33, 755 (1986).

22. L. Girardello and M.T. Grisaru, Nucl. Phys. B194, 65 (1982).
23. E. Cremmer, P. Fayet and L. Girardello, Phys. Lett. 122B, 41 (1983).
24. R. Barbieri, S. Ferrara and C.A. Savoy, Phys. Lett. 119B, 343 (1982).
25. G. Arnison et al., UAl Collaboration, Phys. Lett. 147B, 493 (1984).
26. M.S. Chanowitz, M.A. Furman and I. Hinchliffe, Nucl. Phys. B153, 402 (1979).
27. V. Barger, R.W. Robinett, W.Y. Keung and R.J.N. Phillips, Phys. Rev. D28, 2912 (1983).
28. R.J. Cashmore, Proceedings of the Study of an ep Facility for Europe, edited by U. Amaldi, DESY Report No. 79/48 (1979), unpublished.
29. K.F. Weizsacker, Z. Phys. 88, 612 (1934).
30. E.J. Williams, Phys. Rev. 45, 729 (1934).
31. A.N. Kamal, J.N. Ng and H.C. Lee, Phys. Rev. D24, 2842 (1981).
32. R. Baier, J. Engels and B. Peterson, Z. Phys. C6, 309 (1980).
33. R. Bates and J.N. Ng, Phys. Rev. D32, 51 (1985).
34. J. Wess and B. Zumino, Phys. Lett. 49B, 52 (1974).
35. B. deWit and D.Z. Freedman, Phys. Rev. D12, 2286 (1975).
36. P. Zakarauskas, Ph.D. Thesis, University of British Columbia, (1984), unpublished.
37. I.M. Sobol, The Monte Carlo Method, MIR Publishers, Moscow (1975).

APPENDIX A - SOME ACCELERATOR PROPERTIESTable III - Accelerator Properties

Location	Collider	Type	Luminosity ($\text{cm}^{-2} \text{s}^{-1}$)	\sqrt{s} (GeV)
SLAC	SLC	e^+e^-	3×10^{30}	100
CERN	LEP I	e^+e^-	6×10^{31}	100
CERN	LEP II	e^+e^-	2×10^{32}	170
DESY	HERA	ep	6×10^{31}	320
U.S.A.	SSC	pp	10^{33}	40,000

APPENDIX B - EVALUATION OF FEYNMAN DIAGRAMS

Consider a spin-0 Higgs particle decaying into two photons with 4-momenta k_1, k_2 and polarization vectors $e^\mu(k_1), e^\nu(k_2)$ respectively. One would a priori expect the matrix element for this process to have the gauge invariant forms

$$M^{\mu\nu} = A [g^{\mu\nu} - k_1^\nu k_2^\mu / k_1 \cdot k_2] \quad (\text{B.1a})$$

$$M^{\mu\nu} = B \epsilon^{\mu\nu\alpha\beta} k_{1\alpha} k_{2\beta} / k_1 \cdot k_2 \quad (\text{B.1b})$$

for a scalar or pseudoscalar Higgs particle respectively. These terms are the only tensors one can make from the two independent momenta (k_1, k_2) which do not vanish when the scalar product is taken with the polarization vectors. The contributions of the different Feynman diagrams to this matrix element are shown below.

Each set is separately gauge invariant as is demonstrated. Although the details of the coupling strengths will depend on the model studied, the methods of calculation illustrated are the same for the standard model, Two-Higgs-Doublet models and supersymmetric models. Consequently only one representative example is evaluated for each set of Feynman diagrams. The standard model Feynman rules needed can be found in reference [10].

B.1 Scalar Higgs 2γ -Decay via Fermion Loops

The contribution of the fermion loop in figure 14 is demonstrated for the standard model. Such a contribution will arise from quarks and leptons in all the models studied, as well as from chargino loops for supersymmetry.

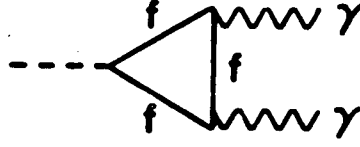


Figure 14 - Fermion Loop Contribution to Scalar 2γ -Decay

The matrix element, obtained using the standard model Feynman rules, is

$$M_f^{\mu\nu} = (-1) \int \frac{d^4 q}{(2\pi)^4} \text{Tr} \left[\left(\frac{-igm_f}{2M_W} \right) \left(\frac{i}{q-m_f} \right) (-iee_f \gamma^\mu) \left(\frac{i}{q-k_1-m_f} \right) \right. \\ \left. \times (-iee_f \gamma^\nu) \left(\frac{i}{q-h-m_f} \right) \right] \quad (\text{B.1.1})$$

where $h=k_1+k_2$ is the Higgs 4-momentum and k_1, k_2 are the photon 4-momenta.

Evaluating the trace results in

$$M_f^{\mu\nu} = \frac{-2ge^2 e_f^2 m_f^2}{M_W} \left\{ 4C_2^{\mu\nu} - 2C_1^\mu (h+k_1)^\nu - 2k_1^\mu C_1^\nu + (k_1^\mu h^\nu + h^\mu k_1^\nu) C_0 \right. \\ \left. + g^{\mu\nu} [-C_{2\alpha}^\alpha + 2C_1 \cdot k_1 + (m_f^2 - k_1 \cdot h) C_0] \right\} \quad (\text{B.1.2})$$

where the loop integrals C_0, C_1, C_2 are given in appendix C. Substituting the results from appendix C, and retaining only those terms consistent with the form of equation (B.1) gives

$$M_f^{\mu\nu} = \frac{2ige^2 e_f^2 m_f^2}{16\pi^2 M_W} \left[-2 - (4\lambda-1)I_{-1} \right] \left[g^{\mu\nu} - \frac{k_1^\nu k_2^\mu}{k_1 \cdot k_2} \right] \quad (\text{B.1.3})$$

where $\lambda = m_f^2/M_H^2$ and I_{-1} is given by equation (C.1). An additional factor of 2

is included in equation (B.1.3), arising from the crossed diagram where identical photons are interchanged. Note that the coefficients of both the $g^{\mu\nu}$ and $k_1^\nu k_2^\mu / k_1 \cdot k_2$ terms are identical, explicitly demonstrating the gauge invariance of the matrix element.

B.2 Scalar Higgs 2γ -Decay via Scalar Loops

The contribution of the scalar loops in figure 15 is demonstrated for the standard model in the 't Hooft-Feynman gauge. In this case the scalar loop particle is the would-be Goldstone boson. In Two-Higgs-Doublet models this set of Feynman diagrams arises for both would-be Goldstone bosons and physical charged Higgs bosons. Similar contributions occur for supersymmetry models, along with scalar-fermion loops.

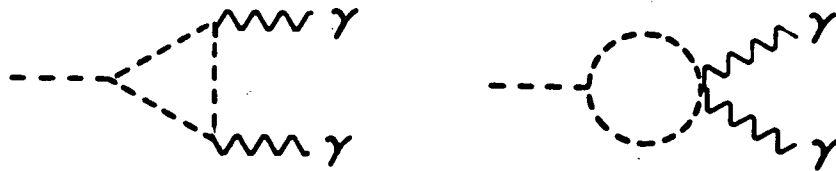


Figure 15 - Scalar Loop Contribution to Scalar 2γ -Decay

The matrix elements, obtained from the standard model Feynman rules, are

$$M_{s(a)}^{\mu\nu} = \int \frac{d^4q}{(2\pi)^4} \left[(-ie(k_1 - 2q)^\mu) \left(\frac{1}{(q - k_1)^2 - M_W^2} \right) (-ie(h - 2q + k_1)^\nu) \right. \\ \left. \times \left(\frac{1}{(q - h)^2 - M_W^2} \right) \left(\frac{-igM_H^2}{2M_W} \right) \left(\frac{1}{q^2 - M_W^2} \right) \right] \quad (\text{B.2.1a})$$

$$M_{s(b)}^{\mu\nu} = \frac{1}{2} \int \frac{d^4q}{(2\pi)^4} (2ie^2 g^{\mu\nu}) \left(\frac{1}{(q - h)^2 - M_W^2} \right) \left(\frac{-igM_H^2}{2M_W} \right) \left(\frac{1}{q^2 - M_W^2} \right) \quad (\text{B.2.1b})$$

Rewriting in terms of the loop integrals C_0, C_1, C_2, C' from appendix C gives

$$M_{s(a)}^{\mu\nu} = \frac{e^2 g M_H^2}{2M_W} [4C_2^{\mu\nu} - 4C_1^\mu k_1^\nu - 2C_1^\mu k_2^\nu - 2C_1^\nu k_1^\mu + k_1^\mu (2k_1 + k_2)^\nu C_0] \quad (\text{B.2.2a})$$

$$M_{s(b)}^{\mu\nu} = -\frac{e^2 g M_H^2}{2M_W} g^{\mu\nu} C' \quad (\text{B.2.2b})$$

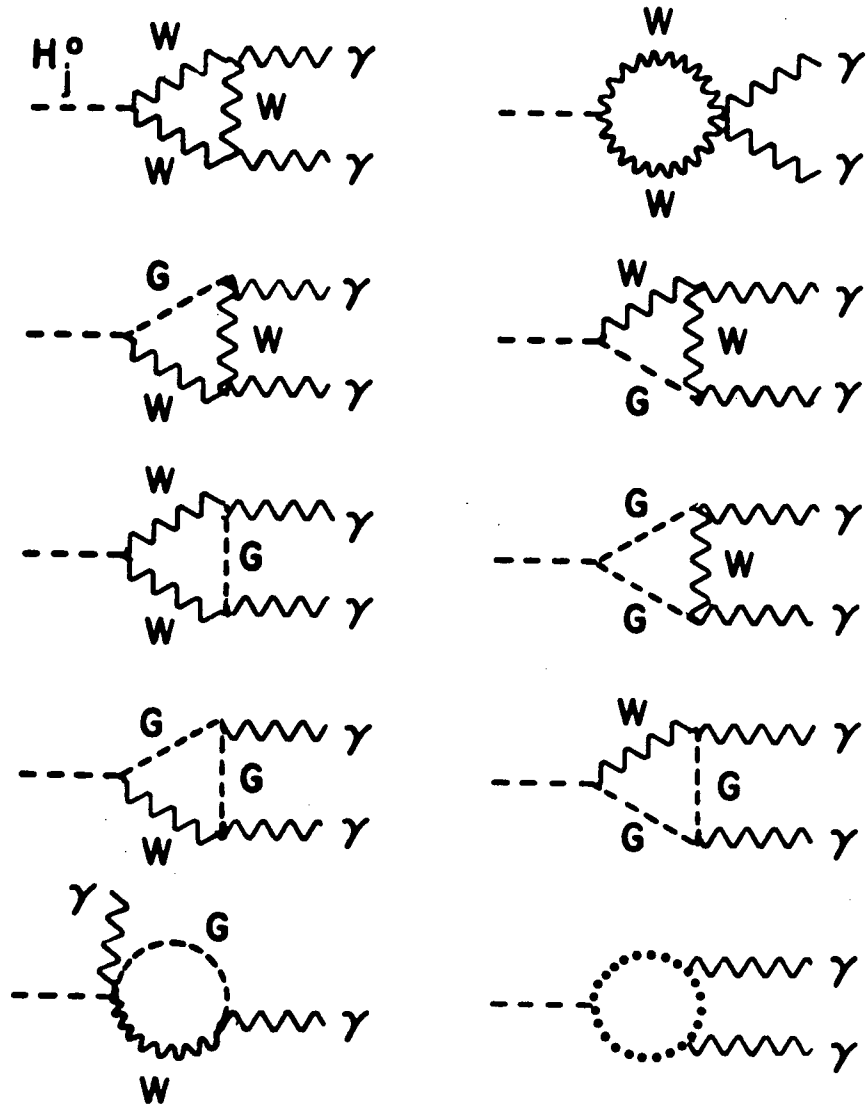
Combining these two matrix elements with the results of appendix C, retaining terms of the form in equation (B.1) and including a factor of 2 for the identical photons gives

$$M_s^{\mu\nu} = \frac{ie^2 g M_H^2}{16\pi^2 M_W} (1 + 2\lambda I_{-1}) \left(g^{\mu\nu} - \frac{k_1^\nu k_2^\mu}{k_1 \cdot k_2} \right) \quad (\text{B.2.3})$$

where $\lambda = M_W^2/M_H^2$. Again note the explicit gauge invariant form of eq. (B.2.3). As discussed in appendix D, the factor $(1 + 2\lambda I_{-1})$ is small for $\lambda \gg 1/4$ and consequently the scalar loop contribution is usually small as well.

B.3 Scalar Higgs 2γ -Decay via Gauge Boson Loops

The diagrams in figure 16 are the largest set to contribute to the scalar Higgs decay width. The loop particles include W-gauge bosons,

Figure 16 - Gauge Boson Loop Contribution to Scalar 2γ -Decay

would-be Goldstone bosons and the Fadeev-Popov ghosts. Such a contribution arises in all the models studied, and is demonstrated for the standard model in 't Hooft-Feynman gauge. As was done in the previous sections, one obtains the matrix elements given by

$$M_{(a)}^{\mu\nu} = e^2 g_M^w [10C_2^{\mu\nu} - 9C_1^\mu k_1^\nu - k_2^\mu C_1^\nu + 5C_0 k_2^\mu k_1^\nu + g^{\mu\nu}(2C_{2\alpha}^\alpha - C_1 \cdot (k_1 + k_2) - 2C_1 \cdot k_1 - 4k_1 \cdot k_2 C_0)] \quad (\text{B.3.1a})$$

$$M_{(b)}^{\mu\nu} = -3e^2 g_M^w g^{\mu\nu} C' \quad (\text{B.3.1b})$$

$$M_{(c)}^{\mu\nu} = -\frac{e^2 g_M^w}{2} [-C_2^{\mu\nu} + 3C_1^\mu k_1^\nu - 4C_1^\nu k_2^\mu + g^{\mu\nu}(C_{2\alpha}^\alpha + 2C_1 \cdot k_2)] \quad (\text{B.3.1c})$$

$$M_{(d)}^{\mu\nu} = \frac{e^2 g_M^w}{2} [C_2^{\mu\nu} - 5C_1^\mu k_1^\nu + C_1^\nu k_2^\mu + 2k_2^\mu k_1^\nu C_0 + g^{\mu\nu}(-C_{2\alpha}^\alpha + (4k_1 + 2k_2) \cdot C_1 - 4k_1 \cdot k_2 C_0)] \quad (\text{B.3.1d})$$

$$M_{(e)}^{\mu\nu} = -e^2 g_M^3 g^{\mu\nu} C_0 \quad (\text{B.3.1e})$$

$$M_{(f)}^{\mu\nu} = -\frac{e^2 g_M^w M_H^2}{2} g^{\mu\nu} C_0 \quad (\text{B.3.1f})$$

$$M_{(g)}^{\mu\nu} = -\frac{e^2 g_M^w}{2} [-2C_2^{\mu\nu} - 2C_1^\mu k_1^\nu] \quad (\text{B.3.1g})$$

$$M_{(h)}^{\mu\nu} = \frac{e^2 g_M^w}{2} [2C_2^{\mu\nu} - 2C_1^\mu k_1^\nu - 4C_1^\nu k_2^\mu + 4k_1^\nu k_2^\mu C_0] \quad (\text{B.3.1h})$$

$$M_{(i)}^{\mu\nu} = -e^2 g_M^w g^{\mu\nu} C'' \quad (\text{B.3.1i})$$

$$M_{(j)}^{\mu\nu} = -e^2 g_M^w [C_2^{\mu\nu} - C_1^\mu k_1^\nu] \quad (\text{B.3.1j})$$

where only terms of the form in equation (B.1) have been kept. Substituting from appendix C gives the expected gauge invariant form, with $\lambda = M_w^2/M_H^2$, as

$$M^{\mu\nu} = \frac{ie^2 g_M^w}{16\pi^2} [6 + (-8+12\lambda)I_{-1}] [g^{\mu\nu} - \frac{k_1^\nu k_2^\mu}{k_1 \cdot k_2}] \quad (\text{B.3.2})$$

B.4 Pseudoscalar Higgs 2γ -Decay via Fermion Loops

The fermion loop contribution of figure 17 is demonstrated for the Two-Higgs-Doublet model. Similar contributions arise in supersymmetry models.

The matrix element is given by

$$M_{f'}^{\mu\nu} = (-1) \int \frac{d^4q}{(2\pi)^4} \text{Tr} \left[\left(\frac{1}{q-m_f} \right) (-ie e_f \gamma^\mu) \left(\frac{1}{q-k_1-m_f} \right) (-ie e_f \gamma^\nu) \right. \\ \left. \times \left(\frac{1}{q-h-m_f} \right) (-y_f \gamma_5) \right] \quad (\text{B.4.1})$$

where y_f is the coupling strength of the pseudoscalar to two fermions.

Evaluating the trace results in

$$M_{f'}^{\mu\nu} = 4ie^2 e_f^2 y_f m_f \epsilon^{\mu\nu\alpha\beta} [C_{2\alpha\beta} + k_{1\alpha} (k_1+k_2)_\beta C_0] \quad (\text{B.4.2})$$

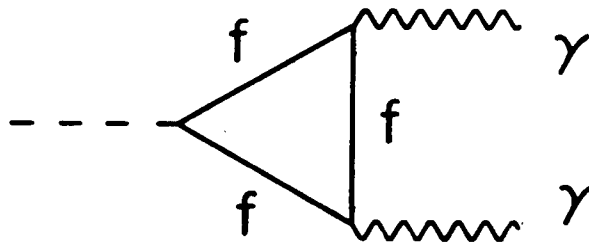


Figure 17 - Fermion Loop Contribution to Pseudoscalar 2γ -Decay

Substituting for the loop integrals C_0, C_2 and multiplying by 2 for identical photons gives

$$M_{f'}^{\mu\nu} = - \frac{e^2 e_f^2 y_f m_f}{4\pi^2} I_{-1} \epsilon^{\mu\nu\alpha\beta} k_{1\alpha} k_{2\beta} / k_1 \cdot k_2 \quad (\text{B.4.3})$$

which is the form expected.

This concludes the demonstration of the evaluation of the Feynman diagrams which contribute to the two photon decay width of Higgs bosons. The relative weights due to the coupling strengths will vary for different models, but the basic structure as shown in equations (B.1.2), (B.2.2), (B.3.1) and (B.4.2) is the same.

APPENDIX C - EVALUATION OF LOOP INTEGRALS

The one-loop Feynman diagrams which contribute to the Higgs two photon decay width contain several integrals which are evaluated in this appendix. A useful definition is

$$I_n(\lambda) \equiv - \int_0^1 dx x^n \ln \left[\frac{\lambda}{x(x-1)+\lambda} \right] \quad (C.1)$$

where $\lambda = m^2/M_H^2$ is the ratio of the loop particle mass squared over the Higgs mass squared.

First consider the integral

$$C_0 = \int \frac{d^4 q}{(2\pi)^4} \frac{1}{[q^2 - m^2][(q - k_1)^2 - m^2][(q - h)^2 - m^2]} \quad (C.2)$$

where $h = k_1 + k_2$ is the Higgs 4-momentum and k_1, k_2 are the photon 4-momenta.

Expanding with Feynman parameters gives

$$C_0 = \int \frac{d^4 q}{(2\pi)^4} \int_0^1 dx \int_0^1 dy \int_0^1 dz \frac{\Gamma(3) \delta(1-x-y-z)}{[(q^2 - m^2)x + (q^2 - 2q \cdot k_1 - m^2)y + (q^2 - 2q \cdot h + M_H^2 - m^2)z]^3} \quad (C.3)$$

Performing the integral over the loop variable q gives the result

$$C_0 = \frac{1}{16\pi^2 M_H^2} \int_0^1 dx \int_0^1 dy \frac{\theta(1-x-y)}{[x(1-x-y) - \lambda]} \quad (C.4)$$

Finally integrating over y and using definition (C.1) gives

$$C_0 = \frac{1}{16\pi^2 M_H^2} I_{-1} \quad (C.5)$$

Second consider the integral

$$C_1^\mu = \int \frac{d^4 q}{(2\pi)^4} \frac{q^\mu}{[q^2 - m^2][q^2 - k_1^2 - m^2][(q-h)^2 - m^2]} \quad (C.6)$$

Again expanding with Feynman parameters and evaluating the integral over the loop parameter q gives

$$C_1^\mu = \frac{i}{16\pi^2 M_H^2} \int_0^1 dx \int_0^1 dy \frac{[yk_1^\mu + (1-x-y)h^\mu] \theta(1-x-y)}{[x(1-x-y) - \lambda]} \quad (C.7)$$

Then integrating over y and using definition (C.1) results in

$$C_1^\mu = \frac{i}{16\pi^2 M_H^2} [k_1^\mu (I_0 - I_{-1}) - k_2^\mu I_0] \quad (C.8)$$

Third consider the integral

$$C_2^{\mu\nu} = \int \frac{d^4 q}{(2\pi)^4} \frac{q^\mu q^\nu}{[q^2 - m^2][(q-k_1)^2 - m^2][(q-h)^2 - m^2]} \quad (C.9)$$

which is expanded using Feynman parameters as before. Unlike the previous two cases, $C_2^{\mu\nu}$ is not finite and the integral over the loop variable q must be regularized. This is performed in $d=4-\epsilon$ dimensions using the method of dimensional regularization, and yields

$$C_2^{\mu\nu} = \frac{i}{16\pi^2 M_H^2} \int_0^1 dx \int_0^1 dy \frac{[yk_1^\mu + (1-x-y)h^\mu][yk_1^\nu + (1-x-y)h^\nu] \theta(1-x-y)}{[x(1-x-y) - \lambda]} \\ + \frac{i g^{\mu\nu}}{32\pi^2} \int_0^1 dx \int_0^1 dy \left\{ \bar{\Delta} + \ln \left[\frac{\lambda}{\lambda - x(1-x-y)} \right] \right\} \theta(1-x-y) \quad (C.10)$$

where $\bar{\Delta} = \frac{2}{\epsilon} + \psi(1) + \ln(4\pi u^2/m^2)$ and u is the arbitrary mass scale introduced by the regularization. The integral over y then gives

$$C_2^{\mu\nu} = \frac{i}{16\pi^2 M_H^2} \left[\left(-\frac{1}{2} + I_0 - \lambda I_{-1}\right) (k_1^\nu k_2^\mu + k_1^\mu k_2^\nu) \right] \quad (C.11)$$

$$+ \frac{i g^{\mu\nu}}{64\pi^2} \left[\bar{\Delta} + 1 - I_0 + 2\lambda I_{-1} \right] + (\text{terms} \propto k_1^\mu k_1^\nu, k_2^\mu k_2^\nu)$$

When contracting indices on $C_2^{\mu\nu}$ it must be remembered that the metric is in $4-\epsilon$ dimensions so that $g^\mu_\mu = 4-\epsilon$. Thus

$$C_2^\mu{}_\mu = \frac{i}{16\pi^2} \left[\bar{\Delta} + \lambda I_{-1} \right] \quad (C.12)$$

Next consider the integral

$$C' = \int \frac{d^4 q}{(2\pi)^4} \frac{1}{[q^2 - m^2][(q-h)^2 - m^2]} \quad (C.13)$$

Expanding with Feynman parameters gives

$$C' = \int \frac{d^4 q}{(2\pi)^4} \int_0^1 dx \int_0^1 dy \frac{\Gamma(2) \delta(1-x-y)}{[(q^2 - m^2)x + (q^2 - 2q \cdot h + M_H^2 - m^2)y]^2} \quad (C.14)$$

Again the integral over the loop parameter must be regularized giving

$$C' = \frac{i}{16\pi^2} \left[\bar{\Delta} - I_0 \right] \quad (C.15)$$

Similarly

$$C'' = \int \frac{d^4 q}{(2\pi)^4} \frac{1}{[q^2 - m^2][(q-k_1)^2 - m^2]} = \frac{i}{16\pi^2} \bar{\Delta} \quad (C.16)$$

APPENDIX D - PROPERTIES OF THE FUNCTION $I(\lambda)$

This appendix describes the function $I(\lambda)$ where

$$I(\lambda) = \int_0^1 dx \frac{1}{x} \ln\left[\frac{\lambda-x(1-x)}{\lambda}\right] \quad (\text{D.1})$$

Note that $I(\lambda)$ is just I_{-1} as defined in equation (C.1). This function appears in all of the matrix elements for spin-0 boson to two photon decay widths. Evaluating equation (D.1) gives

$$I(\lambda) = \begin{cases} -2\left[\sin^{-1}\left(\frac{1}{2\sqrt{\lambda}}\right)\right]^2 & \lambda > \frac{1}{4} \\ -\frac{\pi^2}{2} + 2\ln^2\left[\frac{1+\sqrt{1-4\lambda}}{2\sqrt{\lambda}}\right] - 2i\pi\ln\left[\frac{1+\sqrt{1-4\lambda}}{2\sqrt{\lambda}}\right] & \lambda < \frac{1}{4} \end{cases} \quad (\text{D.2})$$

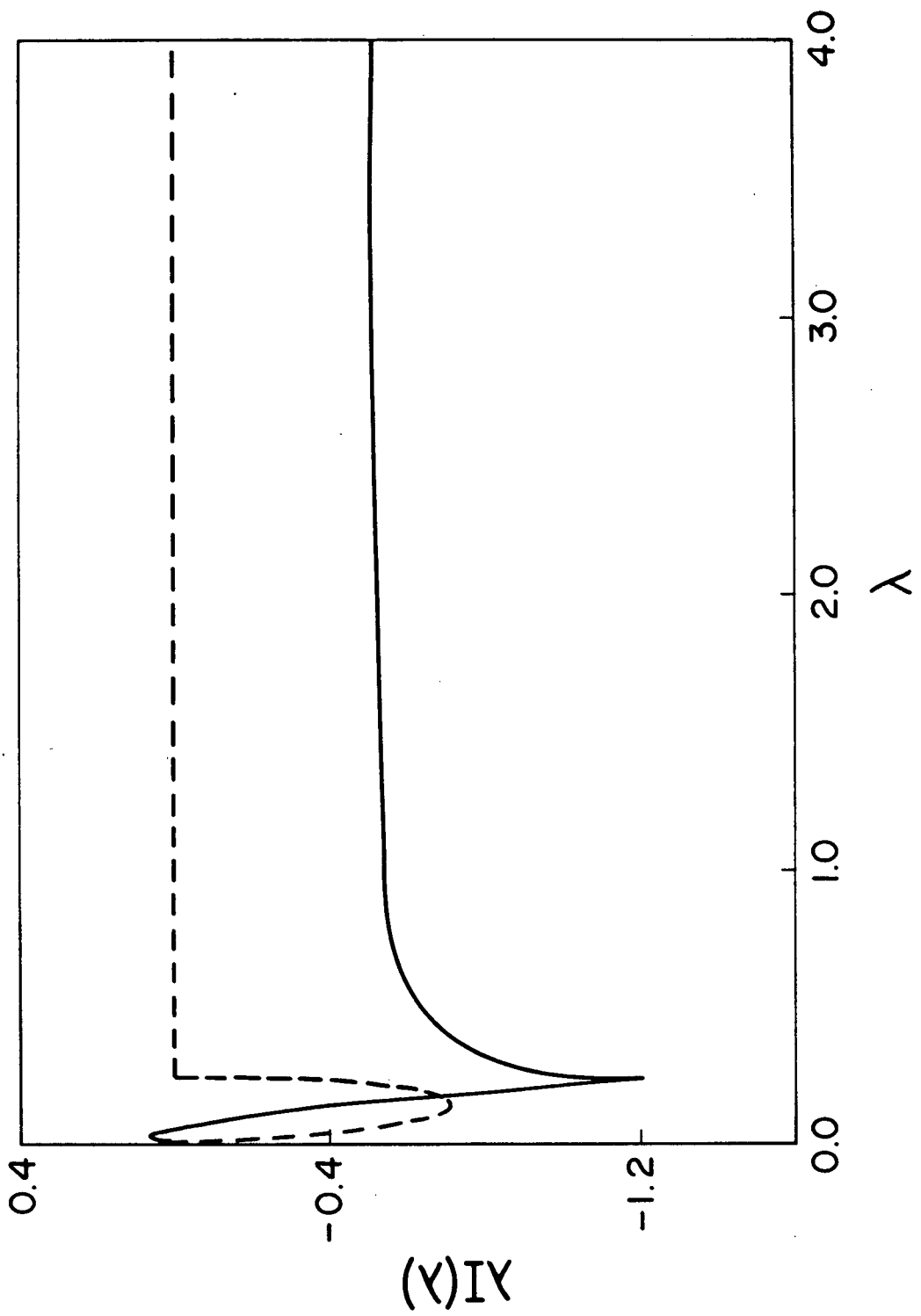
The function $\lambda I(\lambda)$ is plotted in figure 18. The real part shows a very weak dependence on λ for values of $\lambda \gg 1/4$, and there is a sharp peak at $\lambda=1/4$. The imaginary part is zero for $\lambda > 1/4$, and peaks between $0 < \lambda < 1/4$. Both the real and imaginary parts go to zero as $\lambda \rightarrow 0$.

Physically $\lambda=1/4$ corresponds to the threshold to produce a pair of real rather than virtual particles at the Higgs--loop particle vertex. Hence one should see this peaking behaviour whenever a threshold is crossed.

[In equation (B.1.3) $I(\lambda)$ is multiplied by a factor of $4\lambda-1$, and hence in this case the peak at $\lambda=1/4$ is suppressed.]

Providing that one is well below threshold, i.e. $\lambda \gg 1/4$, then equation (D.2) can be approximated by $I(\lambda) \approx \frac{1}{2}\lambda^{-1} + O(\lambda^{-2})$ which is useful in making simple comparisons. In particular $1 + 2\lambda I(\lambda) \approx O(\lambda^{-1})$, and hence the scalar loops in equation (B.2.3) will make small contributions below threshold.

Figure 18 - Plot of the Function $\lambda I(\lambda)$ vs λ



The solid (broken) curve shows the real (imaginary) part.

APPENDIX E - FEYNMAN RULES FOR MINIMAL BROKEN SUPERSYMMETRY

The effective Lagrangian for broken supersymmetric standard models is given in equation (3.1.2)-(3.1.8) in component fields. The component field content of the theory is displayed in table II. In working with component fields, the usual Wess-Zumino gauge of supersymmetry [34] is chosen. The gauge of the $SU(2) \times U(1)$ symmetry is fixed to be the 't Hooft-Feynman gauge. The Fadeev-Popov (FP) ghost is thus the same as that of the standard model [35]. Due to the mixing of the scalars all three fields H_j^0 ($j=1,2,3$) couple to the ghost field. As expected the pseudoscalars H_4^0 and H_5^0 do not couple to the FP ghosts.

The relevant couplings for the calculation of the amplitudes of $X^0 \rightarrow \gamma\gamma$ are given in different sets below. The first set involves the scalar couplings to fermions, sfermions, charged Higgs bosons H^\pm and their companion would-be Goldstone bosons, G^\pm , as well as the gauge bosons W^\pm and the FP ghosts. This is displayed in figure 19. The set of diagrams in figure 16 is gauge invariant in the standard model and in the two Higgs doublet model. Demanding that this gauge invariance holds in supersymmetry is a reasonable condition, which greatly simplified the $G^+G^-H_j^0$ vertex (and consequently the $H^+H^-H_j^0$ vertex). Figure 20 gives all the photon couplings. The mixed states of charged Higgsinos and W-gauginos, χ_1 and χ_2 , have couplings to the Higgs scalars given in figure 21. Sewing together the vertices given below gives the full set of Feynman diagrams displayed in figure 1 for H_j^0 to two photon decays.

For the pseudoscalars the couplings are simpler. Only two are relevant; namely χ_1 and χ_2 and fermion couplings are involved and these are represented in figure 22.

Figure 19 - Feynman Rules for Scalar H_j^0 Couplings

$$\begin{array}{l}
 \begin{array}{c} \text{---} \\ \text{H}_j^0 \\ \text{---} \end{array} \begin{array}{c} \nearrow f \\ \searrow f \end{array} \quad -im_f V^f \\
 \\
 \begin{array}{c} \text{---} \\ \text{H}_j^0 \\ \text{---} \end{array} \begin{array}{c} \nearrow H^+ \\ \searrow H^- \end{array} \quad \left[\frac{-igM_W + igM_j^2}{2M_W} \right] \left[\frac{v_1 U_{1j} + v_2 U_{2j}}{v} \right] -2ih^2 v_3 U_3 \\
 \\
 \begin{array}{c} \text{---} \\ \text{H}_j^0 \\ \text{---} \end{array} \begin{array}{c} \nearrow G^+ \\ \searrow G^- \end{array} \quad \frac{-igM_j^2}{2M_W} \left[\frac{v_1 U_{1j} + v_2 U_{2j}}{v} \right] \\
 \\
 \begin{array}{c} \text{---} \\ \text{H}_j^0 \\ \text{---} \end{array} \begin{array}{c} \nearrow \tilde{f}_{R/L} \\ \searrow \tilde{f}_{R/L} \end{array} \quad \frac{ig^2(v_2 U_{2j} - v_1 U_{1j})}{2\cos^2\theta_W} N_{R/L}^{\tilde{f}} - 2im_f^2 V^{\tilde{f}} \\
 \\
 \begin{array}{c} \text{---} \\ \text{H}_j^0 \\ \text{---} \end{array} \begin{array}{c} \nearrow g^\pm \\ \searrow g^\pm \end{array} \quad \frac{ig}{2} M_W \left[\frac{v_1 U_{1j} + v_2 U_{2j}}{v} \right] \\
 \\
 \begin{array}{c} \text{---} \\ \text{H}_j^0 \\ \text{---} \end{array} \begin{array}{c} \nearrow W^+ \\ \searrow W^- \end{array} \quad igM_W g_{\mu\nu} \left[\frac{v_1 U_{1j} + v_2 U_{2j}}{v} \right] \\
 \\
 \begin{array}{c} \nearrow W^\pm \\ \searrow G^\mp \end{array} \begin{array}{c} p \\ \text{---} \\ p' \end{array} \begin{array}{c} \text{---} \\ \text{H}_j^0 \\ \text{---} \end{array} \quad \mp \frac{ig(p-p')_\mu}{2} \left[\frac{v_1 U_{1j} + v_2 U_{2j}}{v} \right] \\
 \\
 \begin{array}{c} \nearrow \gamma \\ \searrow W^\pm \end{array} \begin{array}{c} \text{---} \\ \text{H}_j^0 \\ \text{---} \end{array} \begin{array}{c} \nearrow G^\mp \\ \searrow H_j^0 \end{array} \quad \frac{ieg}{2} g_{\mu\nu} \left[\frac{v_1 U_{1j} + v_2 U_{2j}}{v} \right]
 \end{array}$$

Here $j=1,2,3$ and the definitions on page 54 are used.

Figure 20 - Feynman Rules for Photon Couplings

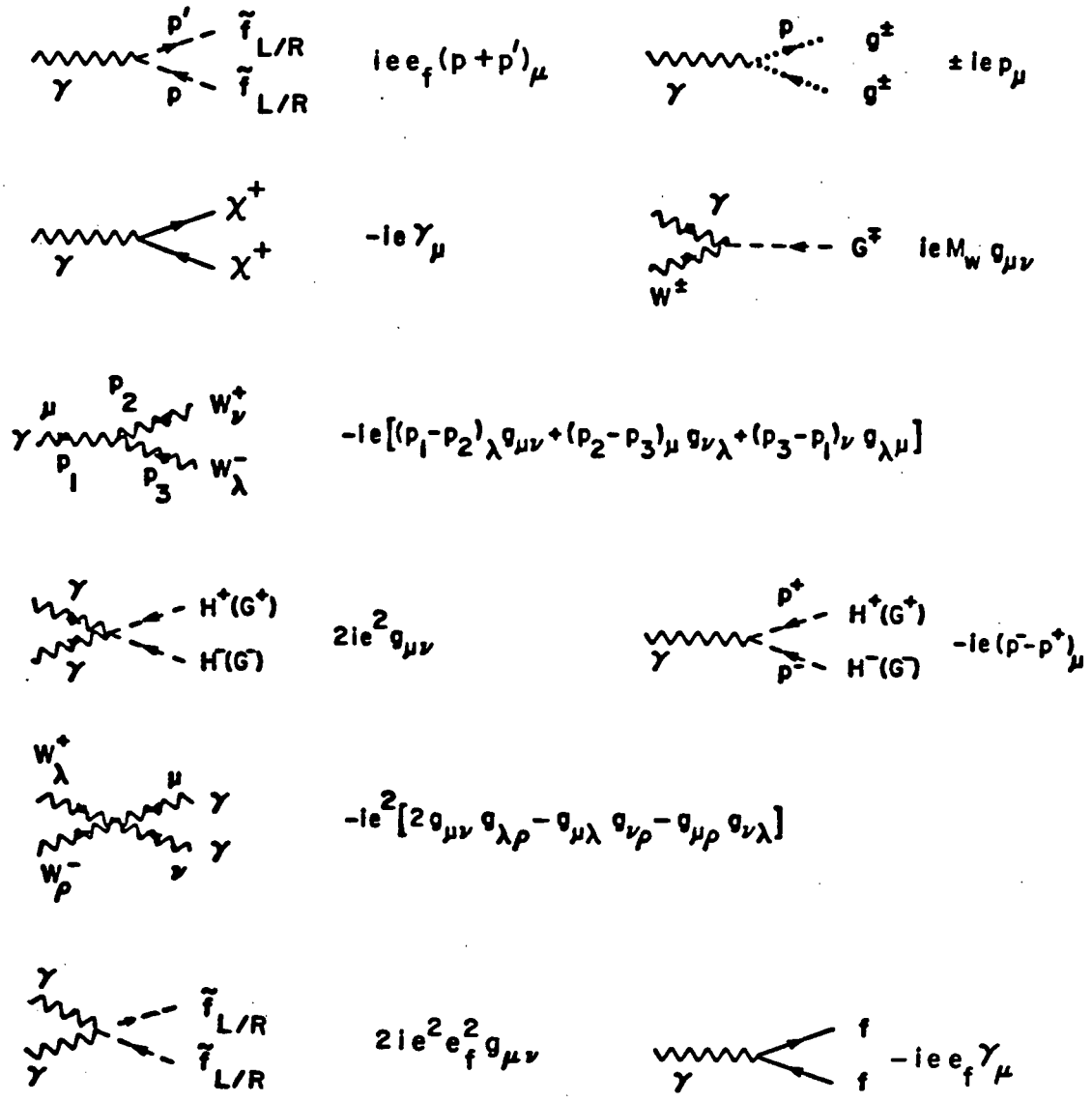
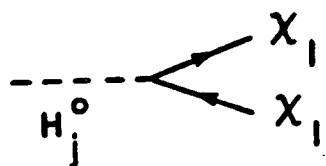
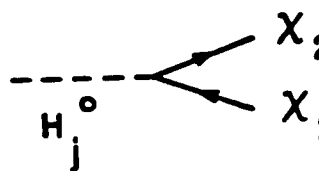


Figure 21 - Feynman Rules for Chargino-Scalar H_j^0 Couplings



A Feynman diagram showing a dashed line on the left labeled H_j^0 that splits into two solid lines on the right, both labeled X_1 . The lines have arrows pointing away from the vertex.

$$-i \frac{g}{\sqrt{2}} (S_- C_+ U_{1j} + S_+ C_- U_{2j})$$



A Feynman diagram showing a dashed line on the left labeled H_j^0 that splits into two solid lines on the right, both labeled X_2 . The lines have arrows pointing away from the vertex.

$$-i \frac{g}{\sqrt{2}} (S_+ C_- U_{1j} + S_- C_+ U_{2j})$$

Figure 22 - Feynman Rules for Chargino-Pseudoscalar H_k^0 Couplings

$$\begin{array}{c}
 \text{---} \\
 \text{H}_k^0 \\
 \text{---}
 \end{array}
 \begin{array}{c}
 \nearrow \\
 \searrow
 \end{array}
 \begin{array}{c}
 \chi_1 \\
 \chi_1
 \end{array}
 \quad \frac{g\gamma_5}{\sqrt{2}v} (v_2 S_{-C_+} + v_1 S_{+C_-}) \eta_k$$

$$\begin{array}{c}
 \text{---} \\
 \text{H}_k^0 \\
 \text{---}
 \end{array}
 \begin{array}{c}
 \nearrow \\
 \searrow
 \end{array}
 \begin{array}{c}
 \chi_2 \\
 \chi_2
 \end{array}
 \quad \frac{g\gamma_5}{\sqrt{2}v} (v_2 S_{+C_-} + v_1 S_{-C_+}) \eta_k$$

$$\begin{array}{c}
 \text{---} \\
 \text{H}_k^0 \\
 \text{---}
 \end{array}
 \begin{array}{c}
 \nearrow \\
 \searrow
 \end{array}
 \begin{array}{c}
 f \\
 f
 \end{array}
 \quad -\eta_k \frac{m_f \gamma_5}{v} \begin{bmatrix} v_1 \\ v_2 \end{bmatrix}^{\eta_f}$$

Here $k=4,5$ and $\eta_f = +1$ (-1) for up (down) type fermions. Also $\eta_k = \cos x$ ($\sin x$) for $k=4$ (5).

APPENDIX F - EQUIVALENT PHOTON APPROXIMATION

The equivalent photon approximation (EPA) [29,30] is used to simplify the calculation of the cross section for the electron-quark scattering process in figure 8b. It involves treating one of the exchange photons as a parton-like object, calculating the photon-quark cross section and then convoluting over a photon spectrum distribution to obtain the electron-quark cross section.

The photon-quark "subprocess" is depicted in figure 23. This leads to a matrix element given by

$$M = \bar{u}(q_1) [ie e_q \gamma^\mu] u(p_1) \left(\frac{-ig_{\mu\nu}}{t} \right) M^{\sigma\nu}(-p_2, -p_1+q_1) \varepsilon_\sigma(p_2) \quad (\text{F.1})$$

where $M^{\sigma\nu}(k_1, k_2)$ is the Higgs to 2γ decay width matrix element, and $\varepsilon_\sigma(p_2)$ is the polarization vector of the incoming photon. The usual Mandelstam variables will be used. The structure of $M^{\sigma\nu}(k_1, k_2)$ must be of the form

$$M^{\sigma\nu}(k_1, k_2) = F \left(g^{\sigma\nu} - \frac{k_1^\nu k_2^\sigma}{k_1 \cdot k_2} \right) \quad (\text{F.2a})$$

for a scalar Higgs, or

$$M^{\sigma\nu}(k_1, k_2) = F \left(\varepsilon^{\sigma\nu\alpha\beta} \frac{k_{1\alpha} k_{2\beta}}{k_1 \cdot k_2} \right) \quad (\text{F.2b})$$

for a pseudoscalar, as described earlier in appendix B.

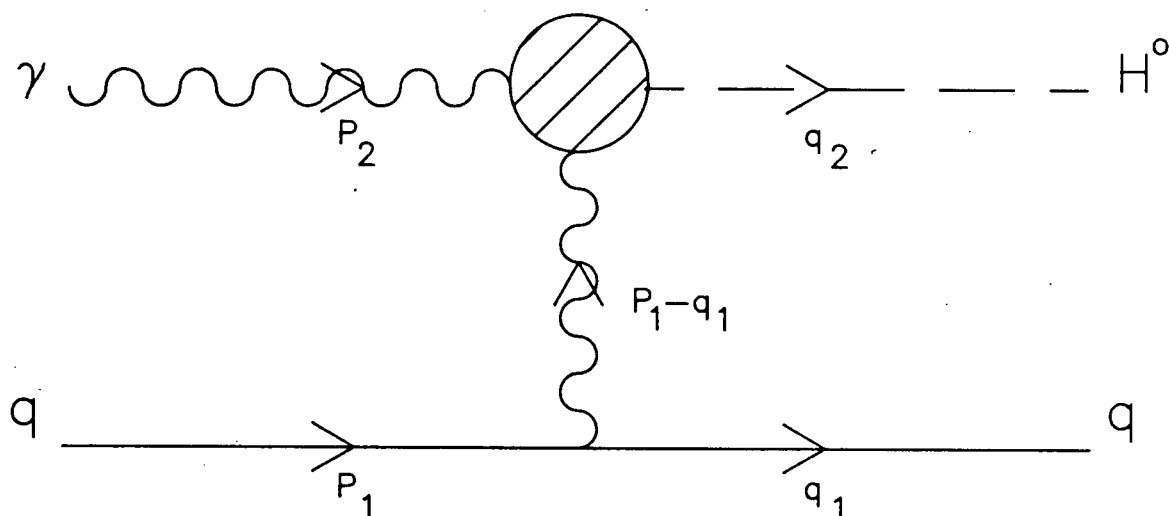


Figure 23 - Photon Quark Subprocess

Substituting these into equation (F.1) leads to photon quark cross sections of the form

$$\sigma_{\gamma q}(\text{scalar}) = \frac{\alpha e^2 F^2}{4s^2} \left\{ \ln\left[\frac{s(s-M_H^2)^2}{m_q^2 M_H^4}\right] + \frac{2s}{M_H^4} (s-M_H^2) \ln\left[\frac{(s-M_H^2)^2}{m_q^2 M_H^2}\right] - \frac{2s(s-M_H^2)}{M_H^4} \right\} \quad (\text{F.3a})$$

and

$$\sigma_{\gamma q}(\text{pseudoscalar}) = \frac{\alpha e^2 F^2}{4s^2} \left\{ \ln\left[\frac{s(s-M_H^2)^2}{m_q^2 M_H^4}\right] + \frac{2s}{M_H^4} (s-M_H^2) \ln\left[\frac{s(s-M_H^2)^2}{m_q^2 M_H^2}\right] - \frac{3(s-M_H^2)^2}{2M_H^4} \right\} \quad (\text{F.3b})$$

respectively. These are then convoluted with the photon spectrum in equation (4.1.4) to give the electron-quark scattering cross sections. The results are shown in equations (4.1.5) and (4.1.6).

Identical steps are taken to obtain electron-electron cross sections with this method, and for that matter any differential cross sections which may be needed. The main advantage in using the EPA method is that all integrals may be done analytically. It should be noted that for the electron-quark scattering process, the electron's photon must be the one treated with EPA. This is to avoid the subsequent complications which arise when the quark is convoluted over the usual parton distributions.

APPENDIX G - MONTE CARLO INTEGRATION ROUTINE

This appendix contains the FORTRAN code for numerically calculating a general 2 to N body scattering cross section. It is a generalization of a program first developed in reference [36]. All of the integration routines used were modified versions of this program. The "amplitude" which must be supplied for the given process, refers to the matrix element squared. Differential cross sections are easily obtained by using the BIN subroutine, which stores the desired variable with the appropriate weight for each event. The convergence of the routine was quite good except where noted in chapter 4. A general description of the Monte-Carlo method can be found in reference [37].

```

C-----C
C               PROGRAM MONTE.FOR               C
C-----C
C   FILE 5: INPUT FROM SOURCE
C   FILE 6: OUTPUT TO SINK
C   FILE 74: ANSWER EVERY 1000 PTS FOR DISPLAY
C   FILE 75: STORE LATEST ANSWER FOR RESTART
C   FILE 76: STORE MASSES FOR RESTART
C   FILE 77: MISCELLANEOUS FOR DISPLAY
C-----C
CC          DECLARE VARIABLES
C-----C
C   II,JJ,KK ARE ABBREVIATIONS FOR OFTEN USED INTEGER EXPRESSIONS
C   NPTS IS THE NUMBER OF POINTS TO BE USED IN THE MONTE CARLO
C   N IS THE NUMBER OF PARTICLES IN THE FINAL STATE
C   SEED IS A PARAMETER NEEDED BY RANDOM NUMBER GENERATOR GGUBFS
C   P IS THE INITIAL PARTICLE MOMENTUM IN THE LAB CM FRAME
C   M(I) IS THE MASS OF PARTICLE I
C   M2(I) IS THE SQUARE OF M(I)
C   MSUM(I) IS THE SUM OF M(J) FOR J=I TO N
C   MX(I) IS THE MASS OF THE VIRTUAL PARTICLE ABOUT TO DECAY INTO
C                                     M(I) AND MX(I+1)
C   MX2(I) IS THE SQUARE OF MX(I)
C   THE MATRIX B(4,4,I) BOOSTS THE MX(I) CM FRAME ONE BACK
C   LAMBDA(I) IS THE MAGNITUDE OF THE MOMENTUM OF PARTICLE I IN
C                                     THE MX(I) CM FRAME
C   STOT IS THE CM ENERGY SQUARED OF THE PROCESS IN LAB CM FRAME
C   X1,X2 ARE THE USUAL PARTON MOMENTUM FRACTIONS
C   S IS THE CM ENERGY SQUARED OF THE SUBPROCESS
C   V,XI ARE VELOCITY AND RAPIDITY OF ONE FRAME W.R.T. ANOTHER
C   THETA,PHI ARE THE USUAL ANGLES
C   K4V(4,I) IS THE MOMENTUM 4-VECTOR OF PARTICLE I
C   LK4V(4,I) IS K4V(4,I) AFTER BOOSTING TO LAB FRAME
C   DV1 IS A DUMMY 4-VECTOR USED FOR PROGRAMMING EASE
C   A IS THE SUBPROCESS AMPLITUDE SUPPLIED BY THE USER
C   W IS THE ELEMENT OF X-SECTION CALCULATED ON EACH LOOP PASS
C   SUMW IS THE SUM OF THE ELEMENTS W FOR ALL LOOP PASSES
C   JAC IS THE JACOBIAN FACTOR FROM THE INTEGRALS
C   INTEGRAL IS THE FINAL ANSWER
C-----C
C   INTEGER II,JJ,KK,NPTS,START,N,RAT
C   REAL*8 M(9),M2(9),MSUM(9),MX(9),MX2(9),B(4,4,9),LAMBDA(8)
C   REAL*8 SEED,P,DUMMY,STOT,X1,X2,S,V,XI,COSTHETA,THETA,PHI,PI
C   REAL*8 K4V(4,9),LK4V(4,9),DV1(4)
C   REAL*8 A,W,SUMW,JAC,FLUX,FACTOR,INTEGRAL
C   COMMON SEED
C-----C
CC          PROGRAM SETUP
C-----C
C   NEW CALCULATION OR RESTART, NUMBER OF EVENTS
C-----C
C   WRITE(6,12)
C   12  FORMAT(' NEW CALCULATION (TYPE 0) OR RESTART (TYPE 1) ? ')
C   READ(5,15)JJ
C   15  FORMAT(I1)
C   IF(JJ.NE.0.AND.JJ.NE.1) THEN
C     WRITE(6,17)
C   17  FORMAT(' YOU MUST TYPE 0 OR 1 ')
C     STOP

```

```

      END IF
      WRITE(6,18)
18  FORMAT(' ENTER NUMBER OF EVENTS DESIRED (I7)')
      READ(5,19)NPTS
19  FORMAT(I7)
-----
C      NEW: READ ENTRIES THROUGH TERMINAL
-----
      IF(JJ.EQ.0) THEN
          START=1
          SUMW=0.0
          SEED=12345.0
          WRITE(6,21)
21  FORMAT(' ENTER P (F15.8)')
          READ(5,22)P
22  FORMAT(F15.8)
          WRITE(6,23)
23  FORMAT(' ENTER NUMBER (3-9) OF PARTICLES (I1)')
          READ(5,15)N
          IF(N.LT.3.OR.N.GT.9) STOP
          DO 29 I=1,N
              WRITE(6,26)I
26  FORMAT(' ENTER M(,I1,') (F15.8)')
              READ(5,22)M(I)
              M2(I)=M(I)**2
              WRITE(76,32)M(I),M2(I)
29  CONTINUE
          END IF
-----
C      RESTART: READ ENTRIES FROM FILES
-----
      IF(JJ.EQ.1) THEN
          READ(75,31)START,N,SEED,SUMW,P,DUMMY
31  FORMAT(I7,I2,4D18.10)
          START=START+1
          IF(START.GE.NPTS) STOP
          DO 33 I=1,N
              READ(76,32)M(I),M2(I)
32  FORMAT(2D18.10)
33  CONTINUE
          END IF
-----
C      INITIALIZE VARIABLES
-----
      DO 42 I=1,N
          MSUM(I)=0.0
          DO 41 J=I,N
41  MSUM(I)=MSUM(I)+M(J)
42  CONTINUE
          KK=N-1
          II=3*N-4
          STOT=4.0*P*P
          IF((2.0*P).LE.MSUM(1)) THEN
              WRITE(6,43)
43  FORMAT(' NOT ENOUGH ENERGY FOR REACTION')
              STOP
          END IF
          PI=3.141592654
          MX(N)=M(N)
          MX2(N)=M2(N)

```

```

WRITE(6,48)
48 FORMAT(' BEGINNING MAIN MONTE CARLO LOOP',/)
C-----
C          BEGIN MAIN MONTE CARLO LOOP
C-----
      DO 999 IJ=START,NPTS
C-----
C          GENERATE X1,X2 AND CHECK IF ENOUGH ENERGY
C-----
50      X1=1.0
        X2=1.0
        S=X1*X2*STOT
        MX(1)=SQRT(S)
        MX2(1)=S
C          IF(MX(1).LE.MSUM(1)) GO TO 50
C-----
C          GENERATE VIRTUAL PARTICLE MASSES
C-----
      DO 65 I=2,KK
        MX(I)=(MX(I-1)-MSUM(I-1))*GGUBFS(SEED)+MSUM(I)
        MX2(I)=MX(I)**2
65      CONTINUE
C-----
C          FIND BOOST MATRIX FROM SUBPROCESS CM TO LAB FRAME
C-----
        V=(X1-X2)/(X1+X2)
        XI=LOG((1.0+V)/(1.0-V))/2.0
        COSTHETA=2.0*GGUBFS(SEED)-1.0
        THETA=ACOS(COSTHETA)
        PHI=2.0*PI*GGUBFS(SEED)
        CALL BOOST(B(1,1,1),XI,THETA,PHI)
C-----
C          LET THE PARTICLES DECAY, GET THE BOOST MATRICES AND 4-VECTORS
C-----
      DO 79 I=1,KK
69      CALL DECAY(MX(I),MX(I+1),M(I),K4V(1,I),B(1,1,I+1))
        K4V(1,N)=MX(KK)-K4V(1,KK)
        K4V(2,N)=-K4V(2,KK)
        K4V(3,N)=-K4V(3,KK)
        K4V(4,N)=-K4V(4,KK)
C-----
C          BOOST 4-MOMENTA TO LAB FRAME
C-----
      DO 88 I=1,N
        DO 81 K=1,4
81      DV1(K)=K4V(K,I)
        DO 84 JK=1,I
          J=I-JK+1
          IF(I.EQ.N) J=I-JK
          IF(J.EQ.O) GO TO 84
          CALL MULT(B(1,1,J),DV1,LK4V(1,I))
          DO 83 K=1,4
83      DV1(K)=LK4V(K,I)
84      CONTINUE
88      CONTINUE
C-----
C          CALL AMPLITUDE -- MUST BE LINKED TO, OR PART OF THE PROGRAM
C-----
        A=1.0
C-----

```

```

C      CALCULATE PHASE SPACE DENSITY AND ELEMENT OF INTEGRAL
C-----
      W=1.0
      DO 92 I=1, KK
        LAMBDA(I)=-4.0*M2(I)*MX2(I+1)+(MX2(I)-M2(I)-MX2(I+1))**2
        LAMBDA(I)=SQRT(LAMBDA(I))/(2.0*MX(I))
        W=W*LAMBDA(I)
92     CONTINUE
      JAC=(4.0*PI)**KK
      DO 93 I=1, KK-1
93     JAC=JAC*(MX(I)-MSUM(I))
        FLUX=1.0/(2.0*S)
        FACTOR=SQRT(S)*(2.0*PI)**II
        FACTOR=FACTOR*(2.0**N)
        W=W*A*JAC*FLUX/FACTOR
        SUMW=SUMW+W
C-----
C      WRITE OUT THE FIRST TEN EVENTS
C-----
      IF(IJ.LE.10.DR.W.LE.0) THEN
        WRITE(77,101)
101     FORMAT(' IJ      I      LK4V(1,I)',10X,'2',14X,'3',14X,'4')
        DO 103 I=1,N
          WRITE(77,102)IJ,I,LK4V(1,I),LK4V(2,I),LK4V(3,I),LK4V(4,I)
102     FORMAT(I7,1X,I2,4D15.5)
103     CONTINUE
        WRITE(77,104)
104     FORMAT(' IJ      A      W')
        WRITE(77,105)IJ,A,W
105     FORMAT(I7,2D12.4,/)
      END IF
C-----
C      STORE ANSWER EVERY 1000 EVENTS FOR RESTART IF SYSTEM CRASHES
C-----
      RAT=MOD(IJ,1000)
      IF(RAT.EQ.0) THEN
        WRITE(74,31)IJ,N,SEED,SUMW,P,SUMW/FLOAT(IJ)
        OPEN(UNIT=75)
        WRITE(75,31)IJ,N,SEED,SUMW,P,SUMW/FLOAT(IJ)
        CLOSE(UNIT=75)
        WRITE(6,112)IJ
112     FORMAT(' FINISHED ',I7,' POINTS')
      END IF
C-----
CC     END MAIN MONTE CARLO LOOP
C-----
999   CONTINUE
C-----
CC     CALCULATE THE INTEGRAL AND OUTPUT
C-----
      INTEGRAL=SUMW/FLOAT(NPTS)
      WRITE(77,113)NPTS,P
113   FORMAT(' NPTS= ',I7,4X,' P= ',D15.6)
      WRITE(77,114)INTEGRAL
114   FORMAT(' X-SECTION= ',D15.6)
      END
C-----
C----- MUST LINK TO RTNS.OBJ FOR SUBROUTINES -----
C-----

```

```

C-----C
C           RTNS.FOR CONTAINS MONTE-CARLO SUBROUTINES           C
C-----C

```

```

SUBROUTINE DECAY2(M1,M2,M3,BM2,BM3)

```

```

C-----C
C           FOR TWO CHAIN DECAY OF M1 INTO M2,M3 FIND BOOST MATRICES BACK
C-----C

```

```

REAL*8 M1,M2,M3,V2(4),V3(4),BM2(4,4),BM3(4,4)
REAL*8 COSTHETA,THETA,PHI,V,SEED,PI,XI
COMMON SEED
EXTERNAL GGUBFS,BOOST
PI=3.141592654
V3(1)=(M1*M1+M3*M3-M2*M2)/(2.0*M1)
V3(4)=DSQRT(V3(1)*V3(1)-M3*M3)
V2(1)=M1-V3(1)
V2(4)=-V3(4)
V=V2(4)/V2(1)
IF(V.EQ.-1.0) STOP
XI=DLOG((1.0+V)/(1.0-V))/2.0
COSTHETA=2.0*GGUBFS(SEED)-1.0
THETA=DACOS(COSTHETA)
PHI=2.0*PI*GGUBFS(SEED)
CALL BOOST(BM2,XI,THETA,PHI)
V=V3(4)/V3(1)
IF(V.EQ.-1.0) STOP
XI=DLOG((1.0+V)/(1.0-V))/2.0
COSTHETA=2.0*GGUBFS(SEED)-1.0
THETA=DACOS(COSTHETA)
PHI=2.0*PI*GGUBFS(SEED)
CALL BOOST(BM3,XI,THETA,PHI)
RETURN
END

```

```

SUBROUTINE BOOST(B,XI,THETA,PHI)
REAL *8 B(4,4), XI, THETA, PHI
B(1,1)= DCOSH(XI)
B(1,2)= -DSINH(XI) * DSIN(THETA)
B(1,3)= 0.
B(1,4)= DSINH(XI)*DCOS(THETA)
B(2,1)= 0.
B(2,2)= DCOS(PHI)*DCOS(THETA)
B(2,3)= -DSIN(PHI)
B(2,4)= DSIN(THETA)*DCOS(PHI)
B(3,1)= 0.
B(3,2)= DSIN(PHI)*DCOS(THETA)
B(3,3)= DCOS(PHI)
B(3,4)= DSIN(THETA)*DSIN(PHI)
B(4,1)= DSINH(XI)
B(4,2)= -DCOSH(XI)*DSIN(THETA)
B(4,3)= 0.
B(4,4)= DCOSH(XI)*DCOS(THETA)
RETURN
END

```

```

SUBROUTINE BIN(F,AR,INF,SUP, W)

```

```

C-----C
C           CLASSES F INTO ONE OF 101 BINS BETWEEN INF AND SUP AND PUT 1
C           IT INTO ARRAY AR 1
C-----C

```

```

C-----
REAL*8 F,AR(101),INF,SUP,W
INTEGER POS
POS = DINT(100. * (F - INF)/(SUP - INF)) + 1
IF (POS .GT. 101) POS = 101
IF (POS .LT. 1) POS=1
AR(POS) = AR(POS) + W
RETURN
END

SUBROUTINE SCALP3(V1,V2,VSV)
REAL*8 V1(4), V2(4), VSV
VSV = V1(2)*V2(2) + V1(3)*V2(3) + V1(4)*V2(4)
RETURN
END

SUBROUTINE MULT(B,V1,V2)
C-----
C          CALCULATES THE PRODUCT BETWEEN THE MATRIX B AND      1
C          VECTOR V1 AND PUTS RESULT INTO V2                      1
C-----
REAL*8 B(4,4), V1(4), V2(4), PH
DO 300 I=1,4
PH=0.
DO 301 J=1,4
301  PH = B(I,J) * V1(J) + PH
V2(I) = PH
300  CONTINUE
RETURN
END

SUBROUTINE DECAY(M1,M2,M3,V3,M)
C-----
C  FOR DECAY OF M1 INTO M2 AND M3, CALCULATE THE 4-VECTOR V3
C  OF PARTICLE 3 IN M1 REST FRAME, THEN CALCULATE BOOST MATRIX
C  FROM M2 TO M1 REST FRAME
C-----
REAL*8 M1,M2,M3,V3(4),M(4,4),COSTHETA,THETA,PHI,V,SEED,PI,XI
COMMON SEED
EXTERNAL GGUBFS,BOOST
PI= 3.141592654
V3(1) = (M1*M1+M3*M3-M2*M2)/(2.*M1)
V3(2) = 0.
V3(3) = 0.
V3(4) = DSQRT(V3(1) *V3(1) - M3*M3)
PX2 = -V3(4)
EX2 = M1 - V3(1)
C-----
C          COMPOSE BOOST MATRIX BETWEEN QUARKS CM AND X CM
C-----
V = PX2/EX2
IF(V .NE. -1.) XI= DLOG((1. + V)/(1. - V))/2.
IF(V .EQ. -1.) RETURN
COSTHETA = 2.* GGUBFS(SEED)-1.
THETA = DACOS(COSTHETA)
PHI = 2. * PI* GGUBFS(SEED)
CALL BOOST(M, XI, THETA, PHI)
RETURN
END

SUBROUTINE SCALP(V1,V2,S)
C-----
C  TAKE THE SCALAR PRODUCT OF THE TWO 4-VECTORS V1
C  AND V2 AND PUT THE RESULT INTO S
C-----
REAL*8 V1(4),V2(4),S
S = V1(1)*V2(1) - V1(2)*V2(2) - V1(3)*V2(3) - V1(4)*V2(4)
RETURN
END

```

APPENDIX H - GLOSSARY

chargino: This charged superparticle is a fermion. Its mass eigenstate is actually a mixture of the superpartners for the W-boson and the Higgs.

chiral symmetry: A symmetry which preserves the handedness of massless fermions. Technically this means a γ_5 invariance.

electroweak breaking scale: Energy scale at which the electromagnetic and weak forces are unified. Experimentally established as being ≈ 246 GeV.

Faddeev-Popov ghosts: Mathematical constructs known as ghosts are introduced in addition to the physical fields to preserve gauge invariance. These are simply a convenient technical invention which allow us to express the complex mathematics of a physical process in a simple graphical form.

Goldstone boson: Massless particle which results whenever a continuous global symmetry is spontaneously broken.

Higgs mechanism: Process through which gauge bosons acquire mass, where a Goldstone boson becomes the longitudinal component of the gauge boson.

loops, loop diagram, loop particle: Physical processes can be represented graphically, with particles represented by a line and their interactions by a vertex. The diagrams for higher order processes will involve loops formed by the particles.

one-loop approximation: Used with the graphical representation of a physical process, where only diagrams with one loop are included.

renormalization: Procedure in which divergent quantities that arise from higher order corrections are absorbed into a redefinition of parameters, thereby making a perturbative expansion convergent.

spontaneous symmetry breaking: The ground state of the system does not respect the same symmetry as the Lagrangian which is used to describe it.

superparticles, superpartners: The supersymmetric partners to the usual standard model particles, which differ by $1/2$ integer unit of quantum spin.

two photon fusion mechanism: Any process in which the final state is produced by the interaction of two initial photons. In this case used to describe a method of producing Higgs bosons during the exchange of a photon between colliding particles.

vacuum expectation value (VEV): The value which the scalar field acquires in its ground state.

would-be Goldstone boson: This refers to the degree of freedom which would normally be a Goldstone boson, but is instead absorbed via the Higgs mechanism as the longitudinal component of a gauge boson.

Yukawa interaction: The interaction between scalars (or pseudoscalars) and fermions. In our case it is the Higgs boson-fermion interaction.